UNIVERSIDADE FEDERAL DO CEARÁ

CENTRO DE TECNOLOGIA

DEPARTAMENTO DE ENGENHARIA DE TELEINFORMÁTICA

PROGRAMA DE PÓS-GRADUAÇÃO EM ENGENHARIA DE TELEINFORMÁTICA

THIAGO AZEVEDO DE VASCONCELOS

MATCHING STRATEGIES FOR MULTI-ANTENNA ARRAYS IN SINGLE AND MULTIUSER SCENARIOS

FORTALEZA

2020

THIAGO AZEVEDO DE VASCONCELOS

MATCHING STRATEGIES FOR MULTI-ANTENNA ARRAYS IN SINGLE AND MULTIUSER SCENARIOS

Dissertação apresentada à coordenação do Programa de Pós-Graduação em Engenharia de Teleinformática do Centro de Tecnologia da Universidade Federal do Ceará, como requisito parcial à obtenção do título de Mestre em Engenharia de Teleinformática. Área de Concentração: Sinais e Sistemas.

Orientador: Prof. Dr. techn. Dr. h.c. Josef Anton Nossek

FORTALEZA

2020

Dados Internacionais de Catalogação na Publicação
Universidade Federal do Ceará
Biblioteca Universitária
Gerada automaticamente pelo módulo Catalog, mediante os dados fornecidos pelo(a) autor(a)

V451m Vasconcelos, Thiago Azevedo de.
Matching strategies for multi-antenna arrays in single and multiuser scenarios / Thiago Azevedo de Vasconcelos. – 2020.
111 f. : il. color.

Dissertação (mestrado) – Universidade Federal do Ceará, Centro de Tecnologia, Programa de Pós-Graduação em Engenharia de Teleinformática, Fortaleza, 2020.
Orientação: Prof. Dr. Josef Anton Nossek.

1. Decoupling and matching networks. 2. Mutual coupling. 3. Ergodic capacity. 4. Multi-antenna arrays. I. Título.

CDD 621.38

THIAGO AZEVEDO DE VASCONCELOS

MATCHING STRATEGIES FOR MULTI-ANTENNA ARRAYS IN SINGLE AND MULTIUSER SCENARIOS

Dissertação apresentada à coordenação do Programa de Pós-Graduação em Engenharia de Teleinformática do Centro de Tecnologia da Universidade Federal do Ceará, como requisito parcial à obtenção do título de Mestre em Engenharia de Teleinformática. Área de Concentração: Sinais e Sistemas.

Aprovada em: 20 de novembro de 2020.

BANCA EXAMINADORA

Prof. Dr. techn. Dr. h.c. Josef Anton Nossek (Orientador)
Universidade Federal do Ceará (UFC)

Prof. Dr. André Lima Férrer de Almeida
Universidade Federal do Ceará (UFC)

Prof. Dr. -Ing. Tarcísio Ferreira Maciel
Universidade Federal do Ceará (UFC)

Prof. Dr. -Ing. Amine Mezghani
University of Manitoba, Winnipeg, Canada

To my family, to Marina and to Christ.

ACKNOWLEDGEMENTS

In many ways God, Our Father, has given me support to the extent I can't even comprehend. To Him, I offer this work and all of the happiness and hardships I felt during the master's program.

I would like to thank Professor Josef A. Nossek, with whom I have had the opportunity to work in exciting new topics. Thank you for the insightful and enjoyable technical and personal conversations, which have inspired me scientifically.

I want to thank Tobias Laas for all of his contributions to this research. I thank Professors André de Almeida, Tarcísio Maciel and Amine Mezghani for being part of the examination board and for the valuable reviews of this thesis.

I thank the staff and the professors whose work is present everyday in the Federal University of Ceará and in the Teleinformatics Engineering Department. I also thank CAPES and the Department for the scholarship bestowed upon me, giving me financial support during my master's program.

I would like to thank my dear girlfriend, Marina, who has cheered for my accomplishments and has been a great listener with whom I shared many feelings of my scientific life. To my friends, particularly those from the Department, I am grateful for making life lighter.

For my family I give thanks, for I can always count on you. To my parents, Guilherme and Solange, and to my brother, Felipe, I give my gratitude for all of the close support in my private life. Thank you for the familiar environment you have provided, which has always been crucial to the privileged education you gave me.

Fortaleza, December 2020,
Thiago Azevedo.

Do everything for Love. Thus there will be no little things: everything will be big. Perseverance in little things for Love is heroism.

(Saint Josemaría Escrivá)

RESUMO

Em sistemas de comunicações móveis modernos, arranjos de muitas antenas, espaçadas por centímetros ou milímetros, são visados para alcançar metas ambiciosas. Entretanto, as interações eletromagnéticas entre antenas pouco espaçadas num mesmo arranjo não são comumente consideradas na literatura, levando a modelos de sistemas de comunicação fisicamente inconsistentes. Nesse cenário, esta dissertação apresenta a teoria e a pesquisa por trás da computação das taxas e capacidades ergódicas de sistemas de comunicação multi-antena considerando o acoplamento mútuo entre as antenas. Para isso, a Multiport Communication Theory foi usada como o referencial teórico para modelar os sistemas de comunicação com multiportas da teoria de circuitos, as quais encapsulam os efeitos do acoplamento mútuo. Considerando esse efeito, dois sistemas foram modelados: um concebido empregando estratégias de desacoplamento e de casamento ótimas, por meio do uso de circuitos especializados, conectando amplificadores de alta potência e amplificadores de baixo ruído aos seus respectivos arranjos de antena, e outro concebido com uma estratégia sem desacoplamento e com casamentos sub-ótimos, usando uma conexão direta entre amplificadores e as antenas. Apesar de capazes de prover performance a nível da teoria da informação ao sistema com eles, circuitos de desacoplamento e de casamento têm grandes desvantagens ligadas à quantidade de elementos, todos reativos, compondo-os. Esses podem causar grandes perdas ôhmicas e limitações de banda em grandes números. Para a análise desses circuitos, as taxas e capacidades dos sistemas são investigadas em casos de banda estreita e larga. No primeiro, considera-se que os circuitos e as antenas operam na sua frequência de design e, assim, o potencial desses circuitos pode ser destacado comparado ao sistema sem eles. No último, os circuitos e as antenas operam em frequências diferentes da sua de design, destacando os efeitos da variação de frequência nas suas performances e no acoplamento mútuo. A partir esses casos, as taxas totais ergódicas dentro de diferentes bandas são calculadas para um sistema exemplar, a fim de introduzir os conceitos de bandas ótima e crítica, figuras de mérito que podem ajudar a determinar se o ganho de capacidade trazido pelos circuitos de desacoplamento e de casamento compensa a sua complexidade e tudo o que acarreta em termos de limitações (efeitos parasíticos). Em última análise, um dos objetivos principais desta dissertação é invocar a importância de considerar o acoplamento mútuo entre antenas pouco espaçadas.

Palavras-chave: Circuitos de desacoplamento e de casamento. Acoplamento mútuo. Capacidade ergódica. Arranjos de multi-antenas.

ABSTRACT

In modern mobile communication systems, arrays of many antennas, spaced in centimeters or millimeters, are sought to reach ambitious goals. However, the electromagnetic interactions between closely spaced antennas in the same array are usually not taken into consideration in the literature, leading to physically inconsistent communications systems models. In this scenario, this thesis presents the theory and the research behind the computation of the ergodic rates and capacities of multi-antenna communication systems accounting for the mutual coupling between the antenna elements. For this end, the Multiport Communication Theory was used as the theoretical framework to model the communication systems with circuit theoretic multiports, which encapsulate the effects of mutual coupling. Considering this effect, two systems were modelled: one conceived employing optimal decoupling and matching strategies through the use of specialized networks connecting high-power amplifiers and low-noise amplifiers to their respective antenna arrays, and the other conceived with no decoupling and a sub-optimal matching strategy using a direct connection between amplifiers and the antennas. Although capable of providing information theoretic level of performance to the system with them, decoupling and matching networks have major disadvantages related to the quantity of elements, all reactive, composing them. The elements can cause big Ohmic losses and frequency band limitations for large numbers of them. For the analysis of these networks, the systems' rates and capacities are investigated in narrow and wideband cases. In the former, the networks and the antenna elements are considered to operate at their design frequency and, as such, the potential of these networks can be highlighted compared to the system without them. In the latter, the networks and the antenna elements operate in a frequency different from their design frequency, highlighting the effects of frequency variation in their performance and in the mutual coupling. Following these simulation cases, the total ergodic rates inside different bands of frequency are computed for one exemplary system to introduce the concept of optimal and critical bands, figures of merit that can help to determine whether or not the capacity gain brought by decoupling and matching networks is worth their complexity and everything it entails in terms of limitations (parasitics). Ultimately, one of the main goals of this thesis is to invoke on the importance of taking the mutual coupling between closely spaced antennas into account.

Keywords: Decoupling and matching networks. Mutual coupling. Ergodic capacity. Multi-antenna arrays.

LIST OF FIGURES

LIST OF ALGORITHMS

LIST OF ABBREVIATIONS

bpcu	bits per channel-use
BS	base station
CMS	canonical minimum-scattering
DMN	decoupling and matching network
EVD	eigenvalue decomposition
HPA	high-power amplifier
i.i.d.	independent and identically distributed
LNA	low-noise amplifier
MCT	Multiport Communication Theory
MIMO	multiple-input-multiple-output
MISO	multiple-input-single-output
MU	multi-user
RF	radio-frequency
Rx	receive
SIMO	single-input-multiple-output
SNR	signal-to-noise ratio
SU	single-user
Tx	transmit
UCA	uniform circular array

LIST OF SYMBOLS

$\mathbf{0}_N$	The all-zeros vector in $\mathbb{R}^N$
$\mathbf{0}_{N\times M}$	The all-zeros matrix in $\mathbb{R}^{N\times M}$
$\mathbf{1}_N$	The all-ones vector in $\mathbb{R}^N$
$\mathbf{1}_{N\times M}$	The all-ones matrix in $\mathbb{R}^{N\times M}$
$\boldsymbol{I}_N$	The identity matrix in $\mathbb{R}^{N\times N}$
$\mathcal{N}_C(\boldsymbol{\mu}, \boldsymbol{R})$	A circularly symmetric complex Gaussian distribution with mean $\boldsymbol{\mu}$ and covariance $\boldsymbol{R}$

TABLE OF CONTENTS

1 INTRODUCTION

In the novel generation of cellular mobile communication networks, the fifth generation (5G), high demands are imposed over the systems to support large data rates, low-latency and low energy consumption. To meet these ambitious goals, multi-antenna arrays are often regarded as a key technology (MARZETTA, 2010), (LARSSON *et al.*, 2014), (RUSEK *et al.*, 2013).

Despite all of the advantages and positive features of these arrays, usually considered in the literature, they also have an important effect always present: the mutual-coupling, which is usually not taken into consideration. This effect is responsible to make the excitation of one antenna create fields which influence all the other antennas in the array. As antenna arrays become increasingly more compact, it is expected that the mutual-coupling also becomes stronger.

For a multi-antenna array in the transmit side, this can lead to the signals generated and then radiated by one antenna influencing the transmission of the signals on the other antennas. On the receive side, a similar effect can take place among the receive signals and also on the propagation of the noise in the circuitry of one antenna to the circuitry of the other antennas.

Not to consider the mutual-coupling leads to physical inconsistencies of the signal and information theoretic model (IVRLAČ; NOSSEK, 2010) in multi-antenna arrays. This has negative impacts on features as array gain and diversity (IVRLAČ; NOSSEK, 2014), energy efficiency for bits-transfer (IVRLAČ; NOSSEK, 2016), capacity for MIMO systems (WALLACE; JENSEN, 2004), reciprocity in TDD systems (LAAS *et al.*, 2017), among other problems.

This effect raises an important challenge, which is to make an efficient connection between the high-power amplifiers in the transmit side and the low-noise amplifiers in the receive side with the antennas in their respective arrays. This problem has already been discussed in (IVRLAČ; NOSSEK, 2010) and (IVRLAČ; NOSSEK, 2014).

In these publications, Ivrlač and Nossek proposed networks capable of addressing the problem of mutual-coupling in antenna arrays by decoupling and matching the antenna ports at the output of the high-power amplifiers and at the input of the low-noise amplifiers. These are the decoupling and matching networks, multiports designed within the theoretical framework of the multiport communication theory and correspond to the first matching strategy in this thesis.

Decoupling and matching networks are conceived to be lossless, thus they consist only of lumped reactive elements. Unfortunately, to compose such networks, a very large number of reactive elements (inductors and capacitors) may be necessary, depending on the number of antennas in the array. As it was proven in (NIE *et al.*, 2014), the smallest number of elements

needed is $N^2 + N$, which represents a quadratic growth with the number of antennas N.

If the number of antennas is large, as sometimes it is expected to be in the literature (e.g., 100 antennas), the implementation of a decoupling and matching network becomes impractical or even unfeasible, due to the increased layout complexity of the network. In addition, the large number of reactive elements may bring many parasitics.

Decoupling and matching networks are designed to guarantee decoupled ports for the transmitter and for the receiver, while also achieving power matching on the transmit side and noise matching on the receive side. This is, however, granted only when the elements are lossless and operate at the single-frequency for which they were designed.

Thus, networks with large number of elements may present bandwidth limitations, because for frequencies too different from the single design frequency, the impedance matrices of the networks can change considerably. Having a large number of elements also generates large losses, since real world reactive elements are not ideally lossless, but lossy.

These disadvantages of the decoupling and matching networks lead to the second, and last, strategy adopted: to make direct connections from the high-power amplifiers to the transmit antennas and from the receive antennas to the low-noise amplifiers. In (IVRLAČ; NOSSEK, 2014), this is called the canonical model and since it has no decoupling and matching network, it is not subject to the frequency limitations and ohmic losses of these multiports.

To analyse these two matching strategies, rates and capacity computations are performed for both systems, with and without decoupling and matching networks, considering lossless and lossy situations, narrow and wideband cases and, finally, single and multiuser scenarios. This thesis reproduces the analysis and results in (VASCONCELOS *et al.*, 2020), which considered only single-user scenarios and extend them for multiuser ones.

In Chapter 2, the background necessary on the multiport communication theory is explored to build on the knowledge of the equations of the physically consistent modelling. Following, it is included the generalization of the models considering losses and frequency dependency. In the sequence of the presentation of the theoretical background, the different capacity equations in multi-antenna systems in Chapter 3 are presented.

In Chapter 4, the simulations, their parameters and their results are displayed following their cases: ergodic rates analysis in narrow and wideband cases, always comparing the efficacy of the two matching strategies. Finally, Chapter 5 is dedicated for the conclusions on the use of each strategy and for considerations of the importance of physically consistent modelling.

2 THE MULTIPORT COMMUNICATION THEORY

The multiport communication theory bridges the electrodynamics and the signal and information theory together using the circuit theory as the theoretical framework. The theories and equations of these domains are developed in this chapter for the two models representing the matching strategies for the multi-antenna systems.

The theoretical development begins with the electromagnetic model, describing and explaining the antenna elements adopted, their array geometry and the interactions between themselves, i.e. the electromagnetic coupling. This will lead to an impedance matrix which will be encapsulated into the circuit theoretic models in order to account for the mutually coupled antennas in packed small antenna arrays.

Following this, the system with DMNs is presented, making the circuit theoretic modeling of the system and deriving its equations. After this part, the information theoretic equations for a communication system are written down and the mapping of the circuit and information models' variables is made. To conclude the description of the system with DMNs, the architectures of these networks, in terms of mathematical modelling and layout, used in the research of this thesis are presented.

A similar theoretical procedure is made, but for the system without DMNs, including the development of all of the equations necessary for the comprehension and simulation of this system. Up to this point, both systems are considered ideal, i.e. lossless and operating at a single frequency.

In the sequence, these systems' descriptions are generalized to include losses and frequency dependency. It is due to the non-idealities that the limitations of the DMNs strategy, compared to the non-use of them, are highlighted. This becomes clear in the simulations results in Chapter 4.

2.1 The Uniform Circular Array

When antenna elements are packed in arrays, they become susceptible to the electromagnetic effect of the mutual coupling (ALLEN; DIAMOND, 1966). As each of them is powered by a voltage generator, currents flow through them producing electromagnetic fields immediately radiated, which excite the other antennas in the array. This excitation leads to the creation of electrical currents flowing through the latter, which in turn are excited and end up

producing new electromagnetic fields, called scatter fields.

These response fields excite the first antennas, through which, now, will flow new electrical currents, restarting this process of "resonant"excitation repeatedly, resulting in the arising of the mutual coupling. This process was described in (SCHELKUNOFF; FRIIS, 1952) to calculate the mutual-impedance and mutual-admittance of a pair of antenna dipoles.

The mutual coupling effect can be brought to the Multiport Communication Theory (MCT) via the characterization of the impedance matrix of an antenna array consisting of self- and mutual-impedance elements. The array impedance matrix is, then, used as a part of a multiport's impedance matrix in the circuit theoretic model, as done in Sections 2.2 and in 2.3.

The systems have N transmit and M receive antennas packed in arrays–for N, M or both larger than one, else the antenna stands by-itself. The geometry of the arrays adopted is composed of antenna elements positioned in a circle and equally spaced from each neighbouring element. This is known as a uniform circular array (UCA).

This geometry is interesting due to its spatial symmetry in the plane where it sits (IOANNIDES; BALANIS, 2005). This symmetry offers, according to the authors, great advantages for arrays of smart-antennas, among them the ability to electronically rotate directional patterns in the plane of the array causing negligible changes and the ability to compensate the mutual coupling.

The antennas in this work are half-wavelength ($\lambda/2$) dipoles, elements composed of two straight arms of length $\frac{\lambda}{4}$ and separated by a very small distance, such that the total length of the elements is close to $\frac{\lambda}{2}$. λ is a fixed value corresponding to a specific wavelength after which the dipoles are modelled. It would be expected that this is the center frequency's wavelength of the bandwidth in which the dipoles will operate.

A big advantage of these elements is that they can be considered canonical minimum-scattering (CMS) antennas (WASYLKIWSKYJ; KAHN, 1970b). In this publication, the authors state that such an approximation is possible for "antennas that are small in terms of wavelength". Thus, short dipoles as the $\lambda/2$-dipole can be included in this approximation.

CMS antennas, according to (KAHN; KURSS, 1965), become invisible when their ports are open-circuited, i.e. no current is flowing through them. Still in this publication, the authors state that arrays of such antennas display two interesting properties: the fields radiated by one antenna in the array are the same as if this antenna was isolated and the computation of the open circuit voltage of the other antennas of this array under these fields is the same as if these

antennas were isolated.

Using this, Wasylkiwskyj and Kahn in (WASYLKIWSKYJ; KAHN, 1970a) compute the mutual-impedance between two elementary dipoles, taking their scattering matrices when isolated in free space and their power radiation patterns. They compute it for multiple radiating modes, each mode being generated by a port, and isolating the mutual-impedance computation for one specific mode by open-circuiting the ports corresponding to the other modes.

This strategy for computing the mutual coupling impedance matrix is again used by the same authors in (WASYLKIWSKYJ; KAHN, 1970b), but now for any CMS antenna and considering that the same procedure of open-circuiting the radiating modes' ports can be done for the antennas' ports in case of multiple antennas.

Thus, to use $\lambda/2$-dipoles allows one to compute the impedance matrix of an array of such antennas with the analytic equations of the self- and mutual-impedance of these elements, considering, respectively, the antennas individually and in pairs, as done in (IVRLAČ; NOSSEK, 2010) and (LAAS *et al.*, 2017).

Exemplary schematics of an array of $N = 9$ antenna elements and of a $\lambda/2$-dipole are shown in Fig. 1. Not only is $N = 9$ used for examples in this section, as further, in Chapter 3, 9 is the number of antennas on the base station (BS) for all of the scenarios considered in this work.

In this figure, s is the antenna spacing of the array, i.e. the distance between neighbouring elements, $d_{y,x}$ is the distance between the dipoles $\lambda/2$-d_y and $\lambda/2$-d_x, r_{array} is the radius of the array and l is the length of the $\lambda/2$-dipoles' arms.

For an N antenna elements UCA, the abstract impedance matrix has the form:

$$\boldsymbol{Z}_{\text{array}} = \begin{bmatrix} Z_{1,1} & Z_{1,2} & \cdots & Z_{1,N} \\ Z_{2,1} & Z_{2,2} & \cdots & Z_{2,N} \\ \vdots & \vdots & \ddots & \vdots \\ Z_{N,1} & Z_{N,2} & \cdots & Z_{N,N} \end{bmatrix}. \tag{2.1}$$

where $Z_{i,i}$ represents the self-impedance (the same as the input impedance) of the antenna $\lambda/2$-d_i when all of the other antennas are open-circuited on their ports, whereas $Z_{i,j}$, $i \neq j$ is the mutual-impedance between the elements $\lambda/2$-d_i and $\lambda/2$-d_j when all of the other antennas are open-circuited. According to (RUSSER, 2006) and (BALANIS, 1982), the self-impedance can

Figure 1 – The UCA of 8 $\lambda/2$-dipoles (left) and the $\lambda/2$-dipole schematic (right)

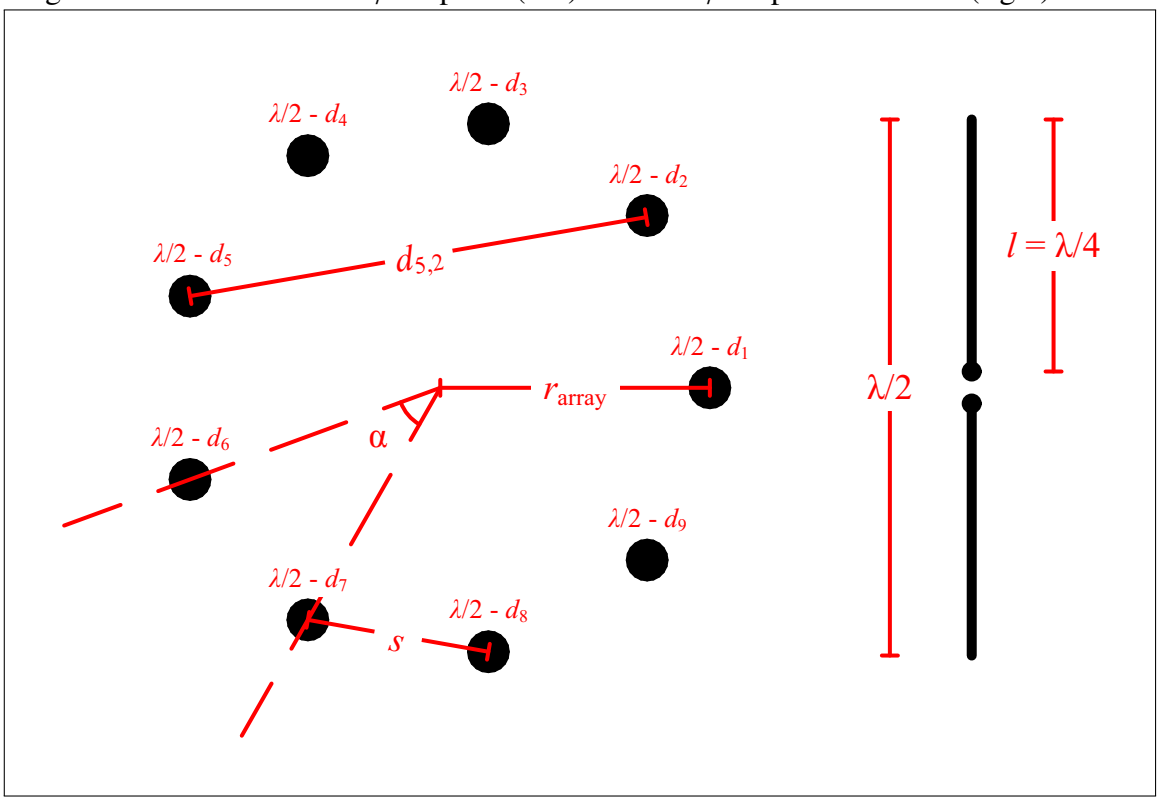

Source: The author.

be calculated by (2.4),

$$R_{\mathrm{A}} = \frac{Z_0}{4\pi \sin^2(kl)}\Big\{2\mathrm{Cin}(2kl) + \sin(2kl)[\mathrm{Si}(4kl) - \mathrm{Si}(2kl)] + \\ + \cos(2kl)[\mathrm{Ci}(4kl) - 2\mathrm{Ci}(2kl) + \gamma + \ln(kl)]\Big\} \tag{2.2}$$

$$X_{\mathrm{A}} = \frac{Z_0}{4\pi \sin^2(kl)}\Big\{2\mathrm{Si}(2kl) + \cos(2kl)[\mathrm{Si}(2kl) - \mathrm{Si}(4kl)] + \\ + \sin(2kl)[\mathrm{Ci}(4kl) - 2\mathrm{Ci}(2kl) + \mathrm{Ci}(ka^2l^{-1})]\Big\} \tag{2.3}$$

$$Z_{\mathrm{A}} = R_{\mathrm{A}} + jX_{\mathrm{A}}, \tag{2.4}$$

where Z_0 is the impedance of the free-space, $k = \dfrac{2\pi}{\lambda}$ is the wavenumber (λ being the wavelength of the impinging wave), $\mathrm{Si}(x) = \displaystyle\int_0^x \frac{\sin t}{t} dt$ is the sine integral, $\mathrm{Cin}(x) = \displaystyle\int_0^x \frac{1-\cos t}{t} dt$, $\mathrm{Ci}(x) = \gamma + \ln(x) - \mathrm{Cin}(x)$ is the cosine integral and γ is the Euler-Mascheroni constant and a is the width of the dipole's arms.

Figure 2 – Two parallel $\lambda/2$-dipoles

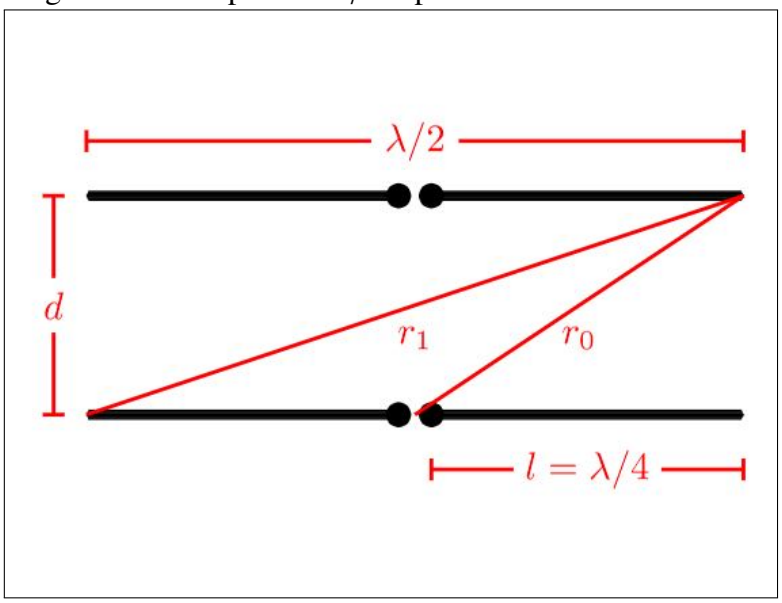

Source: The author, adapted from (SCHELKUNOFF; FRIIS, 1952).

For the mutual-impedance, consider Fig. 2, where there are 2 new space parameters for two parallel $\lambda/2$-dipoles: r_1 is the distance between one of the dipole's extremity to the other dipole's opposite extremity and r_0 is the distance from the center of a dipole to any extremity of the other. With these new space parameters in addition, it is possible to compute the values of the mutual-impedance using the equations derived in (SCHELKUNOFF; FRIIS, 1952)

$$
\begin{aligned}
R_{\mathrm{m}} = \frac{Z_0}{4\pi \sin^2(kl)} \Bigg\{ & 2[2\mathrm{Ci}(2kd) - \mathrm{Ci}(k(r_0+l)) - \mathrm{Ci}(k(r_0-l))] + \\
& + \cos(2kl) \Big[2\mathrm{Ci}(2kd) - 2\mathrm{Ci}(k(r_0+l)) - 2\mathrm{Ci}(k(r_0-l)) + \\
& \qquad + \mathrm{Ci}(k(r_1+2l)) + \mathrm{Ci}(k(r_1-2l)) \Big] + \\
& + \sin(2kl) \Big[2\mathrm{Si}(k(r_0-l)) - 2\mathrm{Si}(k(r_0+l)) + \mathrm{Si}(k(r_1+2l)) + \\
& \qquad - \mathrm{Si}(k(r_1-2l)) \Big] \Bigg\}
\end{aligned}
\tag{2.5}
$$

$$X_{\mathrm{m}} = \frac{Z_0}{4\pi \sin^2(kl)} \Bigg\{ 2[\mathrm{Si}(k(r_0+l)) + \mathrm{Si}(k(r_0-l)) - 2\mathrm{Si}(2kd)] + \\ + \cos(2kl) \Big[2\mathrm{Si}(k(r_0+l)) + 2\mathrm{Si}(k(r_0-l)) - 2\mathrm{Si}(2kd) + \\ - \mathrm{Si}(k(r_1+2l)) - \mathrm{Si}(k(r_1-2l)) \Big] + \\ + \sin(2kl) \Big[2\mathrm{Ci}(k(r_0-l)) - 2\mathrm{Ci}(k(r_0+l)) + \mathrm{Ci}(k(r_1+2l)) + \\ - \mathrm{Ci}(k(r_1-2l)) \Big] \Bigg\} \tag{2.6}$$

$$Z_{\mathrm{m}} = R_{\mathrm{m}} + jX_{\mathrm{m}} \tag{2.7}$$

To compute the self- and the mutual-resistances, reactances and impedances, to fill the matrix $\boldsymbol{Z}_{\mathrm{array}}$ in (2.1), only four fixed parameters need to be established for each of these entries: λ_{c}, a and d, and one additional variable determined by the impinging wave's frequency point: λ.

λ_{c} is the center frequency of the transmission (and reception) bandwidth. This value determines the value of the $\lambda/2$-dipoles' arms length, equal to $\frac{\lambda_{\mathrm{c}}}{4}$. It is important not to mistake the "$\lambda/2$" in "$\lambda/2$-dipole" as half the value of the impinging wave's wavelength.

When a wave impinges on the array, it has a wavelength, which varies depending on the wave's frequency inside the transmission bandwidth. Thus, for a given bandwidth, λ and, consequently, k have different values for every frequency. In a simulation environment, different λ are used to compute the different wavenumbers in the self- and mutual-impedance equations.

The second fixed parameter, a, may be an arbitrary (up to a certain degree of freedom) value, limited by the manufacturing realizability of the dipoles for a given material and, possibly, treated as a subject of an optimization.

It is worth to note that in (2.3), for a half-wavelength dipole's self-reactance, the width of the dipole modifies the reactance when the impinging wave is not at the center frequency. This effect for other frequencies was not considered in (SCHELKUNOFF; FRIIS, 1952), where the analytical formula of the self-impedance is written only for the frequency equivalent to the wavelength determining the length of the dipole.

Finally, d, the distance between two dipoles, may be equal to the UCA antenna spacing for two neighbouring antennas or larger for two dipoles not standing side-by-side in the

UCA. In any case, (2.8) computes the distance $d_{y,x}$ for any two dipoles $\lambda/2$-d_y and $\lambda/2$-d_x (as in Fig. 1), $y \neq x$, in the array,

$$d_{y,x} = s\frac{\sin(\alpha_{y,x}/2)}{\sin(\alpha/2)}, \tag{2.8}$$

$\alpha_{y,x}$ being the angular distance between dipoles $\lambda/2$-d_y and $\lambda/2$-d_x, and α the angular separation between neighbouring dipoles. As it can be seen, for any two neighbouring antennas: $d = s$.

The spatial parameters of the UCA may be determined in different ways, depending on the priority of the antenna design. If the objective is to make a compact antenna array, the most important spatial parameter might be the radius r_{array} of the UCA. Using the radius and the number of antennas N, it is possible to determine the value of the antenna spacing.

$$s = 2r_{\text{array}}\sin(\alpha/2). \tag{2.9}$$

It is worth, sometimes, to express the antenna spacing in terms of the wavelength of the center frequency λ_c, i.e. as a multiple of λ_c. Defining a multiplicative factor κ for the spacing

$$s = \kappa\lambda_c \implies r_{\text{array}} = \frac{\kappa}{2\sin(\pi/N)}\lambda_c, \tag{2.10}$$

leads to the definition of the radius in terms of the wavelength, which is useful for arrays and antenna elements of sizes and spatial dimensions comparable to a wavelength.

Using (2.2) to (2.7) the impedance matrix in (2.1) can be filled for any number of elements, given the three fixed values $\{\lambda_c, a, r_{\text{array}}\}$ and the frequency points to have the different λ. To compute the impedance matrices $\boldsymbol{Z}_{\text{array}}$ of both transmit and receive arrays gives all of the mathematical representation necessary to encapsulate the mutual coupling effects into the Circuit Theoretic model to be described in Sections 2.2 and 2.3.

2.2 System with Decoupling and Matching Networks

To model a communication system using a Circuit Theoretic approach, the elements playing major roles in intrinsic interactions and effects in a communication link must be represented by circuit elements, each reproducing, in the Circuit Theory framework, the behavior of the original element.

Figure 3 – MCT model of the system with DMNs.

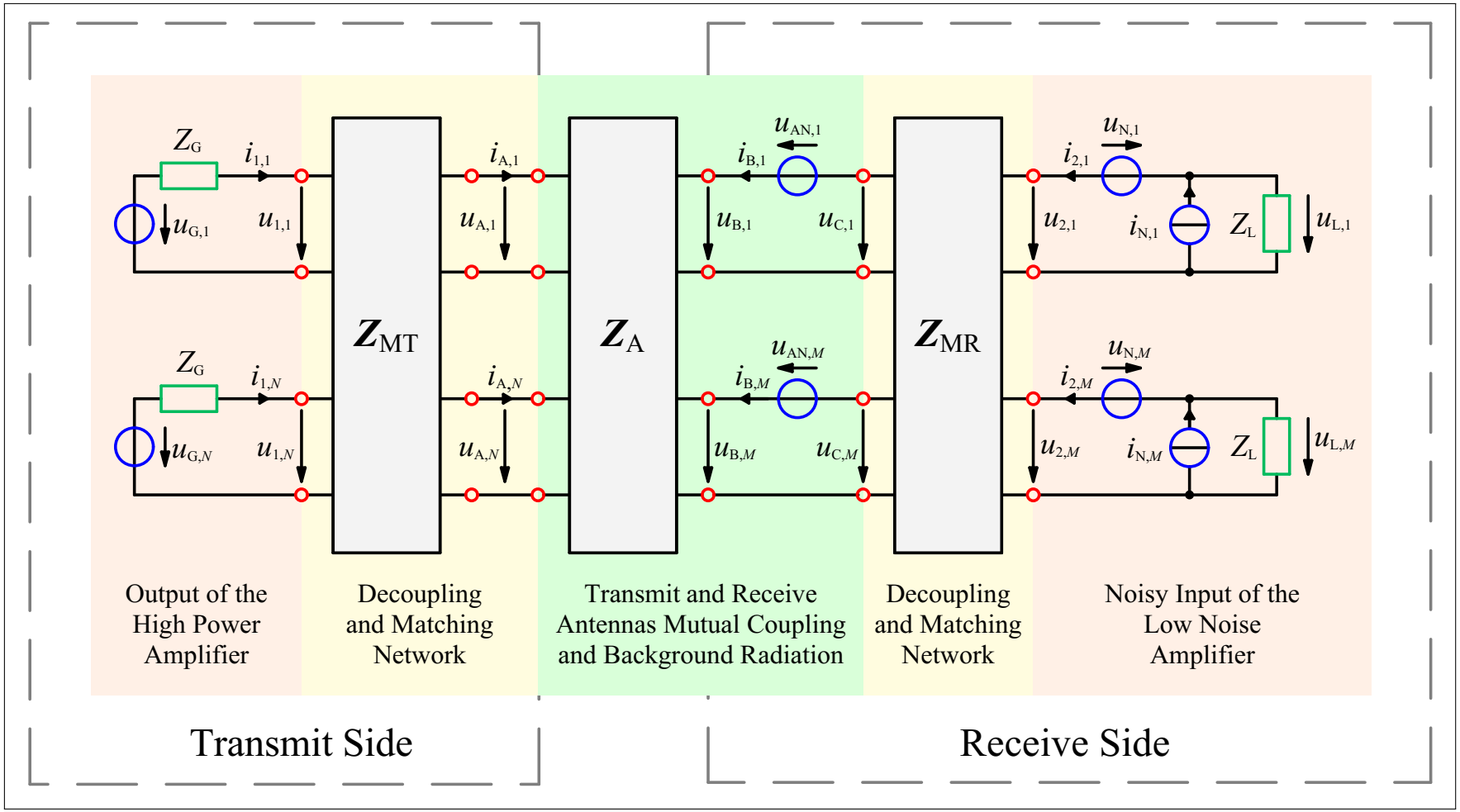

Source: The author, adapted from (IVRLAČ; NOSSEK, 2014)

The modeling and the elements used in this work were proposed in (IVRLAČ; NOSSEK, 2010) and (IVRLAČ; NOSSEK, 2014). The mathematical formulation of the equations are inspired from (LAAS *et al.*, 2017). Finally, the theoretical development of the equations is based on (IVRLAČ, 2017), in which the theory is thoroughly explained.

The system model in Fig. 3 may represent the downlink or the uplink of a communication link, the theoretical development of this chapter is valid for both. Still it can be better visualized from the downlink perspective in a scenario where the transmitter is a base station and the receiver(s) is(are) mobile terminal(s), as it was considered in (LAAS *et al.*, 2017).

On one side, the transmitter has the voltage sources $\boldsymbol{u}_\mathrm{G} \in \mathbb{C}^{N\times 1}\mathrm{V}$ and its series impedances $Z_\mathrm{G} \in \mathbb{C}^{N\times 1}\Omega$, the $\boldsymbol{Z}_\mathrm{MT} \in \mathbb{C}^{2N\times 2N}\Omega$ block and part of the $\boldsymbol{Z}_\mathrm{A} \in \mathbb{C}^{(N+M)\times(N+M)}\Omega$ block. On the other side, the receiver has part of the $\boldsymbol{Z}_\mathrm{A}$ block, the $\boldsymbol{Z}_\mathrm{MR} \in \mathbb{C}^{2M\times 2M}\Omega$ block, two sets of voltage sources: $\boldsymbol{u}_\mathrm{AN} \in \mathbb{C}^{M\times 1}\mathrm{V}$ and $\boldsymbol{u}_\mathrm{N} \in \mathbb{C}^{M\times 1}\mathrm{V}$, current sources $\boldsymbol{i}_\mathrm{N} \in \mathbb{C}^{M\times 1}\mathrm{A}$ and load impedances $\boldsymbol{Z}_\mathrm{L} \in \mathbb{C}^{M\times 1}\Omega$.

Following again (LAAS *et al.*, 2017), all of the voltages and currents in the models in this thesis represent root mean square values of complex phasors of the respective quantities.

The transmitter has N $\lambda/2$-dipoles arranged in an UCA. Each of the antennas is connected to a radio-frequency (RF) chain of electronic components–digital processors, modulators, quantizers, up-converters and more. One of these elements is the high-power amplifier (HPA), which sits on the end of the RF chain and raises the power level of the transmit signal. Anything before the HPA is not important to this circuits model, so it begins by voltage generators with series impedances, representing the output of the HPAs.

Still in the transmit (Tx) side, the $\boldsymbol{Z}_\mathrm{MT}$ block represents the Tx-DMN. The concept behind the DMNs is to make efficient use of the mutual coupling between the antenna elements, providing to the output of the HPAs the desired input impedance on the $\boldsymbol{u}_1$ and $\boldsymbol{i}_1$ ports while also providing the desired output impedance to the antenna elements connected to the $\boldsymbol{u}_\mathrm{A}$ and $\boldsymbol{i}_\mathrm{A}$ ports–one antenna per port. What is meant by "desired" will be explained further.

The Tx-UCA is represented by its impedance matrix $\boldsymbol{Z}_\mathrm{AT} \in \mathbb{C}^{N\times N}\Omega$ inside $\boldsymbol{Z}_\mathrm{A}$

$$\boldsymbol{Z}_A = \begin{bmatrix} \boldsymbol{Z}_\mathrm{AT} & \boldsymbol{Z}_\mathrm{ATR} \\ \boldsymbol{Z}_\mathrm{ART} & \boldsymbol{Z}_\mathrm{AR} \end{bmatrix}, \tag{2.11}$$

since the antenna arrays are reciprocal, then $\boldsymbol{Z}_\mathrm{AT} = \boldsymbol{Z}_\mathrm{AT}^\mathrm{T}$, $\boldsymbol{Z}_\mathrm{AR} = \boldsymbol{Z}_\mathrm{AR}^\mathrm{T}$ and $\boldsymbol{Z}_\mathrm{ART} = \boldsymbol{Z}_\mathrm{ATR}^\mathrm{T}$, implying that $\boldsymbol{Z}_A = \boldsymbol{Z}_A^\mathrm{T}$ as well.

$\boldsymbol{Z}_{\mathrm{ATR}} \in \mathbb{C}^{N\times M}\Omega$ is the impedance matrix which translates the influence of the receive (Rx)-UCA on the Tx-UCA whereas the $\boldsymbol{Z}_{\mathrm{ART}} \in \mathbb{C}^{M\times N}\Omega$ impedance matrix translates the influence of the Tx-UCA on the Rx-UCA. In essence, those two matrices are responsible for the connections between transmitter and receiver and $\boldsymbol{Z}_{\mathrm{ART}}$ is the physical communication channel from transmitter to receiver.

Although $\boldsymbol{Z}_{\mathrm{ATR}}$ exists and, indeed, means that the receiver may exert an influence on the transmitter, it can be neglected according to the Unilateral Approximation described in (IVRLAČ; NOSSEK, 2010). The currents $\boldsymbol{i}_{\mathrm{B}}$ on the receive side are not strong enough to produce fields that can cause any noticeable influence on the transmitter.

Besides being a reasonable intuition, it has an actual mathematical condition to be met: $\|\boldsymbol{Z}_{\mathrm{ATR}}\|_{\mathrm{F}} = \|\boldsymbol{Z}_{\mathrm{ART}}\|_{\mathrm{F}} \ll \|\boldsymbol{Z}_{\mathrm{AT}}\|_{\mathrm{F}}$. Fortunately, this is often the case for practical mobile communication systems and is considered in this work as well.

$\boldsymbol{Z}_{\mathrm{AR}} \in \mathbb{C}^{M\times M}\Omega$ is the Rx-UCA impedance matrix and is the first part of the receive side in Fig. 3, representing the electromagnetic interactions of the M $\lambda/2$-dipoles arranged in the receive UCA. The antennas are connected, individually, to other RF chains, whose first element is the low-noise amplifier (LNA).

The LNA role is to amplify the weak signal received from a far-field transmission, after it has lost most of its power in the travelled path–due to, e.g. path loss, fading effects, reflections–and add the least amount of noise, intrinsic to the equipment itself, as possible. Its objective is to increase the power while avoiding to reduce the signal-to-noise ratio (SNR).

Everything that may come after the LNA in the RF chain is ignored. The receivers also have voltage sources $\boldsymbol{u}_{\mathrm{AN}} \in \mathbb{C}^{M\times 1}\mathrm{V}$ and $\boldsymbol{u}_{\mathrm{N}} \in \mathbb{C}^{M\times 1}\mathrm{V}$, a current source $\boldsymbol{i}_{\mathrm{N}} \in \mathbb{C}^{M\times 1}\mathrm{V}$ and load impedances $\boldsymbol{Z}_{\mathrm{L}} \in \mathbb{C}^{M\times 1}\Omega$.

The sources $\boldsymbol{u}_{\mathrm{N}}$ and $\boldsymbol{i}_{\mathrm{N}}$ are stochastic sources which account for the noise produced by the circuitry of the LNAs, called the intrinsic noise. The noise sources of an LNA (on one port) are uncorrelated to the noise sources of another LNA (on another port), even though they might be on the same receiver. Their circuit modelling as two-port elements and statistical description were first developed in (ROTHE; DAHLKE, 1956) and in (HAUS *et al.*, 1960).

Following the model in Fig. 3, the statistical properties of the LNA intrinsic noise sources are

$$\mathbb{E}\left[u^*_{N,i}u_{N,j}\right] = \mathbb{E}\left[u^*_{N,i}i_{N,j}\right] = \mathbb{E}\left[i^*_{N,i}i_{N,j}\right] = 0,\ i \neq j, \tag{2.12}$$

for the cross-correlation of sources of different ports (i.e. different LNAs) and

$$\begin{aligned}
&\mathbb{E}\left[u_{N,i}^{*}u_{N,i}\right] = \mathbb{E}\left[|u_{N,i}|^2\right] = \sigma_u^2, \\
&\mathbb{E}\left[i_{N,i}^{*}i_{N,i}\right] = \mathbb{E}\left[|i_{N,i}|^2\right] = \sigma_i^2, \\
&\rho = \mathrm{Re}(\rho) + j\mathrm{Im}(\rho) = \frac{\mathbb{E}\left[u_{N,i}i_{N,i}^{*}\right]}{\sqrt{\mathbb{E}\left[|u_{N,i}|^2\right]\mathbb{E}\left[|i_{N,i}|^2\right]}},
\end{aligned} \tag{2.13}$$

for the correlations of noise sources in the same port (i.e. in the same LNA), where $\mathbb{E}\left[|u_{N,i}|^2\right]$ and $\mathbb{E}\left[|i_{N,i}|^2\right]$ are the variances of the voltage and current noise sources, respectively, and ρ is the complex correlation coefficient of a voltage and a current noise source in the same port.

The statistical values $\mathbb{E}\left[|u_{N,i}|^2\right]$, $\mathbb{E}\left[|i_{N,i}|^2\right]$, $\mathrm{Re}(\rho)$ and $\mathrm{Im}(\rho)$ can either be provided by the LNAs' manufacturer or characterized using the port measurements routines proposed by (LEHMEYER *et al.*, 2017), in which only a set of impedances and a tunable power meter, whose noise bandwidth is known, are enough to proceed with the measurements, without the necessity of using advanced equipment.

The $\boldsymbol{u}_{\mathrm{AN}}$ are also stochastic sources and are used as the circuit model for the thermal equilibrium noise of the receive antennas due to background radiation. This phenomenon was first discovered and measured by Johnson was formally presented in (JOHNSON, 1928) and was later explained by Nyquist (NYQUIST, 1928). The main statistical property follows in (2.14) as the Johnson-Nyquist formula

$$\mathbb{E}\left[u_{AN,i}u_{AN,j}^{*}\right] = 4kT\Delta_f \mathrm{Re}\left((\boldsymbol{Z}_{\mathrm{AR}})_{i,j}\right), \forall j, i, \tag{2.14}$$

where k is the Boltzmann constant, T is the temperature in Kelvin, Δ_f is the noise bandwidth and $\mathrm{Re}\left((\boldsymbol{Z}_{\mathrm{AR}})_{i,j}\right)$ is the real part of the mutual-impedance between the i-th and the j-th antenna dipole. It is also worth to make it clear that the extrinsic noise is uncorrelated to the intrinsic noise, even in the same port, i.e.

$$\mathbb{E}\left[u_{AN,i}^{*}u_{N,j}\right] = \mathbb{E}\left[u_{AN,i}^{*}i_{N,j}\right] = 0, \ \forall i, j. \tag{2.15}$$

Formally, it would be necessary to add noise sources on the transmit side as well. However, since the power levels of intrinsic and extrinsic noise sources are so small if compared

to the power level attained by the HPA output signals that they can be ignored. When transmitted this weak noise signal will simply be highly attenuated as the electromagnetic waves travel from the transmitter to the receiver and become negligible in face of the message carrying signal.

At last, the Rx-DMN has the similar role as the Tx-DMN: to present to the input of the LNAs a desired output impedance at its $\boldsymbol{u}_2$ ports and to the output of the Rx-antennas the desired input impedance at the $\boldsymbol{u}_\mathrm{B}$ ports. The difference between the Tx-DMNs and the Rx-DMNs is the kind of ports matching that is aimed by each. This will be discussed later.

2.2.1 Circuit Theoretic Model of the System With DMNs

In the circuit theoretic model, it makes sense to start describing the decoupling and matching multiports $\boldsymbol{Z}_\mathrm{MT}$ and $\boldsymbol{Z}_\mathrm{MR}$ and the antenna multiport $\boldsymbol{Z}_\mathrm{A}$ matrix equations.

$$\begin{bmatrix} \boldsymbol{u}_1 \\ \boldsymbol{u}_\mathrm{A} \end{bmatrix} = \begin{bmatrix} \boldsymbol{Z}_{\mathrm{MT}_{1,1}} & \boldsymbol{Z}_{\mathrm{MT}_{1,2}} \\ \boldsymbol{Z}_{\mathrm{MT}_{2,1}} & \boldsymbol{Z}_{\mathrm{MT}_{2,2}} \end{bmatrix} \begin{bmatrix} \boldsymbol{i}_1 \\ -\boldsymbol{i}_\mathrm{A} \end{bmatrix} \tag{2.16}$$

$$\begin{bmatrix} \boldsymbol{u}_\mathrm{A} \\ \boldsymbol{u}_\mathrm{B} \end{bmatrix} = \begin{bmatrix} \boldsymbol{Z}_\mathrm{AT} & \boldsymbol{Z}_\mathrm{ATR} \\ \boldsymbol{Z}_\mathrm{ART} & \boldsymbol{Z}_\mathrm{AR} \end{bmatrix} \begin{bmatrix} \boldsymbol{i}_\mathrm{A} \\ \boldsymbol{i}_\mathrm{B} \end{bmatrix} \tag{2.17}$$

$$\begin{bmatrix} \boldsymbol{u}_2 \\ \boldsymbol{u}_\mathrm{C} \end{bmatrix} = \begin{bmatrix} \boldsymbol{Z}_{\mathrm{MR}_{1,1}} & \boldsymbol{Z}_{\mathrm{MR}_{1,2}} \\ \boldsymbol{Z}_{\mathrm{MR}_{2,1}} & \boldsymbol{Z}_{\mathrm{MR}_{2,2}} \end{bmatrix} \begin{bmatrix} \boldsymbol{i}_2 \\ -\boldsymbol{i}_\mathrm{B} \end{bmatrix} \tag{2.18}$$

All of these matrices represent reciprocal systems and for the design of the lossless DMNs $\boldsymbol{Z}_\mathrm{MT}$ and $\boldsymbol{Z}_\mathrm{MR}$ are required to be imaginary. For a generic lossless multiport equality $\boldsymbol{u} = \boldsymbol{Z}\boldsymbol{i}$, the following holds:

$$\mathbb{E}\left[\sum_k \mathrm{Re}\left(u_k^* i_k\right)\right] = \mathbb{E}\left[\mathrm{Re}\left(\boldsymbol{u}^\mathrm{H}\boldsymbol{i}\right)\right] = \mathbb{E}\left[\frac{1}{2}(\boldsymbol{u}^\mathrm{H}\boldsymbol{i} + \boldsymbol{i}^\mathrm{H}\boldsymbol{u})\right] = \frac{1}{2}\mathbb{E}\left[\boldsymbol{i}^\mathrm{H}(\boldsymbol{Z}^\mathrm{H} + \boldsymbol{Z})\boldsymbol{i}\right] = 0, \tag{2.19}$$

which implies that $\boldsymbol{Z} = -\boldsymbol{Z}^\mathrm{H}$. Together with the fact that the $\boldsymbol{Z}$ matrix represents a reciprocal multiport, i.e. $\boldsymbol{Z} = \boldsymbol{Z}^\mathrm{T}$, $\boldsymbol{Z} = -\boldsymbol{Z}^*$ holds. This result is valid for both $\boldsymbol{Z}_\mathrm{MT}$ and $\boldsymbol{Z}_\mathrm{MR}$, meaning that $\boldsymbol{Z}_\mathrm{MT} \in j \cdot \Omega\,\mathbb{R}^{2N\times 2N}$ and $\boldsymbol{Z}_\mathrm{MR} \in j \cdot \Omega\,\mathbb{R}^{2M\times 2M}$. This is a mathematical proof of what is expected by the theory: all of the elements constituting a DMN must be reactive in order to guarantee that this multiport is theoretically lossless–or, in practice, has minimal losses.

Finally, the last important multiport system description emphasises the transmit signals at the output of the Tx-HPAs and the receive signals at the input of the Rx-LNAs. This is the decoupling and matching perspective of the multiport system which encompasses the three multiports $\boldsymbol{Z}_{\mathrm{MT}}$, $\boldsymbol{Z}_{\mathrm{A}}$ and $\boldsymbol{Z}_{\mathrm{MR}}$ into one and after which the DMNs' architecture will be designed.

$$\begin{bmatrix} \boldsymbol{u}_1 \\ \boldsymbol{u}_2 \end{bmatrix} = \begin{bmatrix} \boldsymbol{Z}_{\mathrm{T}} & \boldsymbol{Z}_{\mathrm{TR}} \\ \boldsymbol{Z}_{\mathrm{RT}} & \boldsymbol{Z}_{\mathrm{R}} \end{bmatrix} \begin{bmatrix} \boldsymbol{i}_1 \\ \boldsymbol{i}_2 \end{bmatrix}. \tag{2.20}$$

This important description allows for a better understanding of the decoupling and matching effects of the multiport networks $\boldsymbol{Z}_{\mathrm{MT}}$ and $\boldsymbol{Z}_{\mathrm{MR}}$, since these two capabilities are operated over the ports from the perspectives of the Tx-HPAs and of the Rx-LNAs.

Now, the objective is to have an equation capable of describing $\boldsymbol{u}_{\mathrm{L}}$ in terms of all of the sources variables in Fig. 3, i.e.

$$\begin{aligned} &\boldsymbol{u}_{\mathrm{L}} = f(\boldsymbol{u}_{\mathrm{G}}, \boldsymbol{u}_{\mathrm{AN}}, \boldsymbol{u}_{\mathrm{N}}, \boldsymbol{i}_{\mathrm{N}}), \\ &f(\boldsymbol{u}_{\mathrm{G}}, \boldsymbol{u}_{\mathrm{AN}}, \boldsymbol{u}_{\mathrm{N}}, \boldsymbol{i}_{\mathrm{N}}) = f_1(\boldsymbol{u}_{\mathrm{G}}) + f_2(\boldsymbol{u}_{\mathrm{AN}}) + f_3(\boldsymbol{u}_{\mathrm{N}}) + f_4(\boldsymbol{i}_{\mathrm{N}}). \end{aligned} \tag{2.21}$$

To do so, the principle of the superposition is applied and, step-by-step, $\boldsymbol{u}_{\mathrm{L}}$ is computed in terms of one of the sources $\{\boldsymbol{u}_{\mathrm{G}}, \boldsymbol{u}_{\mathrm{AN}}, \boldsymbol{u}_{\mathrm{N}}, \boldsymbol{i}_{\mathrm{N}}\}$ while the others are considered equal to short (for $\boldsymbol{u}_{\mathrm{G}}$, $\boldsymbol{u}_{\mathrm{AN}}$ or $\boldsymbol{u}_{\mathrm{N}}$) or open circuits (for $\boldsymbol{i}_{\mathrm{N}}$). Then, the final result of the superposition is the sum all of the individual results, leading to (2.21).

2.2.1.1 Superposition Step 1: $\boldsymbol{u}_{\mathrm{AN}} = \boldsymbol{u}_{\mathrm{N}} = \boldsymbol{0}_M$ V *and* $\boldsymbol{i}_{\mathrm{N}} = \boldsymbol{0}_M$ A

The first step consists on letting only $\boldsymbol{u}_{\mathrm{G}}$ to be different of $\boldsymbol{0}_N$ V and calculating $\boldsymbol{u}_{\mathrm{L}} = f_1(\boldsymbol{u}_{\mathrm{G}})$. For this, the Unilateral Approximation described before is applied in (2.17) to make $\boldsymbol{Z}_{\mathrm{ATR}} = \boldsymbol{0}_{N,M}\,\Omega$, which gives $\boldsymbol{u}_{\mathrm{A}} = \boldsymbol{Z}_{\mathrm{AT}}\boldsymbol{i}_{\mathrm{A}}$. Together with (2.16) it holds

$$\boldsymbol{u}_{\mathrm{A}} = \boldsymbol{Z}_{\mathrm{MT}_{2,1}}\boldsymbol{i}_1 - \boldsymbol{Z}_{\mathrm{MT}_{2,2}}\boldsymbol{i}_{\mathrm{A}} = \boldsymbol{Z}_{\mathrm{AT}}\boldsymbol{i}_{\mathrm{A}} \implies \boldsymbol{i}_{\mathrm{A}} = (\boldsymbol{Z}_{\mathrm{AT}} + \boldsymbol{Z}_{\mathrm{MT}_{2,2}})^{-1}\boldsymbol{Z}_{\mathrm{MT}_{2,1}}\boldsymbol{i}_1, \tag{2.22}$$

$$\boldsymbol{u}_1 = \boldsymbol{Z}_{\mathrm{MT}_{1,1}}\boldsymbol{i}_1 - \boldsymbol{Z}_{\mathrm{MT}_{1,2}}\boldsymbol{i}_{\mathrm{A}} \implies \boldsymbol{u}_1 = [\boldsymbol{Z}_{\mathrm{MT}_{1,1}} - \boldsymbol{Z}_{\mathrm{MT}_{1,2}}(\boldsymbol{Z}_{\mathrm{AT}} + \boldsymbol{Z}_{\mathrm{MT}_{2,2}})^{-1}\boldsymbol{Z}_{\mathrm{MT}_{2,1}}]\boldsymbol{i}_1. \tag{2.23}$$

Using (2.20) and the Unilateral Approximation, $\boldsymbol{Z}_{\mathrm{TR}} = \boldsymbol{0}_{N,M}\,\Omega$ also holds. The outcome of this is

$$\boldsymbol{Z}_{\mathrm{T}} = \boldsymbol{Z}_{\mathrm{MT}_{1,1}} - \boldsymbol{Z}_{\mathrm{MT}_{1,2}}(\boldsymbol{Z}_{\mathrm{AT}} + \boldsymbol{Z}_{\mathrm{MT}_{2,2}})^{-1}\boldsymbol{Z}_{\mathrm{MT}_{2,1}}. \tag{2.24}$$

From the receive side of Fig. 3, (2.18) and (2.17),

$$\begin{aligned}
&\boldsymbol{u}_{\mathrm{C}} = \boldsymbol{u}_{\mathrm{B}} + \boldsymbol{u}_{\mathrm{AN}},\ \boldsymbol{u}_{\mathrm{AN}} = \boldsymbol{0}_M\mathrm{V} \\
&\boldsymbol{u}_{\mathrm{B}} = \boldsymbol{u}_{\mathrm{C}} = \boldsymbol{Z}_{\mathrm{MR}_{2,1}}\boldsymbol{i}_2 - \boldsymbol{Z}_{\mathrm{MR}_{2,2}}\boldsymbol{i}_{\mathrm{B}}, \qquad (2.25) \\
&\boldsymbol{u}_{\mathrm{B}} = \boldsymbol{Z}_{\mathrm{ART}}\boldsymbol{i}_{\mathrm{A}} + \boldsymbol{Z}_{\mathrm{AR}}\boldsymbol{i}_{\mathrm{B}} = \boldsymbol{Z}_{\mathrm{ART}}(\boldsymbol{Z}_{\mathrm{AT}} + \boldsymbol{Z}_{\mathrm{MT}_{2,2}})^{-1}\boldsymbol{Z}_{\mathrm{MT}_{2,1}}\boldsymbol{i}_1 + \boldsymbol{Z}_{\mathrm{AR}}\boldsymbol{i}_{\mathrm{B}}, \qquad (2.26)
\end{aligned}$$

where (2.22) in (2.26) were inserted to obtain its final format. Now an equality sign can be inserted between both equations to produce

$$\boldsymbol{i}_{\mathrm{B}} = (\boldsymbol{Z}_{\mathrm{AR}} + \boldsymbol{Z}_{\mathrm{MR}_{2,2}})^{-1}[-\boldsymbol{Z}_{\mathrm{ART}}(\boldsymbol{Z}_{\mathrm{AT}} + \boldsymbol{Z}_{\mathrm{MT}_{2,2}})^{-1}\boldsymbol{Z}_{\mathrm{MT}_{2,1}}\boldsymbol{i}_1 + \boldsymbol{Z}_{\mathrm{MR}_{2,1}}\boldsymbol{i}_2]. \tag{2.27}$$

Finally, the relation between $\boldsymbol{u}_2$ and $\boldsymbol{i}_1$ and $\boldsymbol{i}_2$ is obtained.

$$\begin{aligned}
\boldsymbol{u}_2 =&[\boldsymbol{Z}_{\mathrm{MR}_{1,2}}(\boldsymbol{Z}_{\mathrm{AR}} + \boldsymbol{Z}_{\mathrm{MR}_{2,2}})^{-1}\boldsymbol{Z}_{\mathrm{ART}}(\boldsymbol{Z}_{\mathrm{AT}} + \boldsymbol{Z}_{\mathrm{MT}_{2,2}})^{-1}\boldsymbol{Z}_{\mathrm{MT}_{2,1}}]\boldsymbol{i}_1 + \\
&+ [\boldsymbol{Z}_{\mathrm{MR}_{1,1}} - \boldsymbol{Z}_{\mathrm{MR}_{1,2}}(\boldsymbol{Z}_{\mathrm{AR}} + \boldsymbol{Z}_{\mathrm{MR}_{2,2}})^{-1}\boldsymbol{Z}_{\mathrm{MR}_{2,1}}]\boldsymbol{i}_2.
\end{aligned} \tag{2.28}$$

Again, using (2.20) to identify $\boldsymbol{Z}_{\mathrm{RT}}$ and of $\boldsymbol{Z}_{\mathrm{R}}$ it follows that

$$\begin{aligned}
&\boldsymbol{u}_2 = \boldsymbol{Z}_{\mathrm{RT}}\boldsymbol{i}_1 + \boldsymbol{Z}_{\mathrm{R}}\boldsymbol{i}_2, \\
&\boldsymbol{Z}_{\mathrm{RT}} = \boldsymbol{Z}_{\mathrm{MR}_{1,2}}(\boldsymbol{Z}_{\mathrm{AR}} + \boldsymbol{Z}_{\mathrm{MR}_{2,2}})^{-1}\boldsymbol{Z}_{\mathrm{ART}}(\boldsymbol{Z}_{\mathrm{AT}} + \boldsymbol{Z}_{\mathrm{MT}_{2,2}})^{-1}\boldsymbol{Z}_{\mathrm{MT}_{2,1}}, \qquad (2.29) \\
&\boldsymbol{Z}_{\mathrm{R}} = \boldsymbol{Z}_{\mathrm{MR}_{1,1}} - \boldsymbol{Z}_{\mathrm{MR}_{1,2}}(\boldsymbol{Z}_{\mathrm{AR}} + \boldsymbol{Z}_{\mathrm{MR}_{2,2}})^{-1}\boldsymbol{Z}_{\mathrm{MR}_{2,1}}.
\end{aligned}$$

Since in this first step of the superposition oriented circuit analysis $\boldsymbol{u}_{\mathrm{AN}} = \boldsymbol{u}_{\mathrm{N}} = \boldsymbol{0}_M\mathrm{V}$ and $\boldsymbol{i}_{\mathrm{N}} = \boldsymbol{0}_M\mathrm{A}$, $\boldsymbol{u}_{\mathrm{L}} = \boldsymbol{u}_2$, thus making possible to find an equality between $\boldsymbol{u}_{\mathrm{L}}$ and $\boldsymbol{u}_1$. However, $\boldsymbol{u}_{\mathrm{L}} = f_1(\boldsymbol{u}_{\mathrm{G}})$ is needed and, for such, the circuit analysis on Fig. 3 gives

$$\begin{aligned}
&\boldsymbol{u}_{\mathrm{G}} = Z_{\mathrm{G}}\boldsymbol{i}_1 + \boldsymbol{u}_1 = (Z_{\mathrm{G}}\boldsymbol{I}_N + \boldsymbol{Z}_{\mathrm{T}})\boldsymbol{i}_1 \implies \boldsymbol{i}_1 = (Z_{\mathrm{G}}\boldsymbol{I}_N + \boldsymbol{Z}_{\mathrm{T}})^{-1}\boldsymbol{u}_{\mathrm{G}}, \qquad (2.30) \\
&\boldsymbol{u}_{\mathrm{L}} = -Z_{\mathrm{L}}\boldsymbol{i}_2 \implies \boldsymbol{i}_2 = -\frac{1}{Z_{\mathrm{L}}}\boldsymbol{u}_{\mathrm{L}}, \qquad (2.31)
\end{aligned}$$

both of which can be plugged back in (2.29) to obtain

$$\begin{aligned}
&\boldsymbol{u}_{\mathrm{L}} = Z_{\mathrm{L}}(Z_{\mathrm{L}}\boldsymbol{I}_M + \boldsymbol{Z}_{\mathrm{R}})^{-1}\boldsymbol{Z}_{\mathrm{RT}}(Z_{\mathrm{G}}\boldsymbol{I}_N + \boldsymbol{Z}_{\mathrm{T}})^{-1}\boldsymbol{u}_{\mathrm{G}}, \\
&\boldsymbol{u}_{\mathrm{L}} = f_1(\boldsymbol{u}_{\mathrm{G}}) = \boldsymbol{D}\boldsymbol{u}_{\mathrm{G}} \implies \boldsymbol{D} = Z_{\mathrm{L}}(Z_{\mathrm{L}}\boldsymbol{I}_M + \boldsymbol{Z}_{\mathrm{R}})^{-1}\boldsymbol{Z}_{\mathrm{RT}}(Z_{\mathrm{G}}\boldsymbol{I}_N + \boldsymbol{Z}_{\mathrm{T}})^{-1}.
\end{aligned} \tag{2.32}$$

2.2.1.2 *Superposition Step 2:* $\boldsymbol{u}_\mathrm{G} = \mathbf{0}_N$ V, $\boldsymbol{u}_\mathrm{N} = \mathbf{0}_M$ V *and* $\boldsymbol{i}_\mathrm{N} = \mathbf{0}_M$ A

In the second step, $\boldsymbol{u}_\mathrm{AN}$ is activated and $\boldsymbol{u}_\mathrm{G}$ is substituted by a short circuit. If $\boldsymbol{u}_\mathrm{G} = \mathbf{0}_N$ V, then by (2.30) and (2.22), $\boldsymbol{i}_\mathrm{A} = \mathbf{0}_N$ A is obtained. Using this in (2.17) and in (2.18), reproduced here for convenience, the following holds

$$\begin{bmatrix} \boldsymbol{u}_\mathrm{A} \\ \boldsymbol{u}_\mathrm{B} \end{bmatrix} = \begin{bmatrix} \boldsymbol{Z}_\mathrm{AT} & \boldsymbol{Z}_\mathrm{ATR} \\ \boldsymbol{Z}_\mathrm{ART} & \boldsymbol{Z}_\mathrm{AR} \end{bmatrix} \begin{bmatrix} \boldsymbol{i}_\mathrm{A} \\ \boldsymbol{i}_\mathrm{B} \end{bmatrix}, \; \boldsymbol{u}_\mathrm{B} = \boldsymbol{Z}_\mathrm{AR}\boldsymbol{i}_\mathrm{B}, \tag{2.33}$$

$$\begin{bmatrix} \boldsymbol{u}_2 \\ \boldsymbol{u}_\mathrm{C} \end{bmatrix} = \begin{bmatrix} \boldsymbol{Z}_{\mathrm{MR}_{1,1}} & \boldsymbol{Z}_{\mathrm{MR}_{1,2}} \\ \boldsymbol{Z}_{\mathrm{MR}_{2,1}} & \boldsymbol{Z}_{\mathrm{MR}_{2,2}} \end{bmatrix} \begin{bmatrix} \boldsymbol{i}_2 \\ -\boldsymbol{i}_\mathrm{B} \end{bmatrix}, \; \boldsymbol{u}_\mathrm{C} = \boldsymbol{u}_\mathrm{B} + \boldsymbol{u}_\mathrm{AN}, \tag{2.34}$$

$$\begin{aligned} &\boldsymbol{u}_\mathrm{B} = \boldsymbol{Z}_{\mathrm{MR}_{2,1}}\boldsymbol{i}_2 - \boldsymbol{Z}_{\mathrm{MR}_{2,2}}\boldsymbol{i}_\mathrm{B} - \boldsymbol{u}_\mathrm{AN} \implies \boldsymbol{i}_\mathrm{B} = (\boldsymbol{Z}_\mathrm{AR} + \boldsymbol{Z}_{\mathrm{MR}_{2,2}})^{-1}(\boldsymbol{Z}_{\mathrm{MR}_{2,1}}\boldsymbol{i}_2 - \boldsymbol{u}_\mathrm{AN}), \\ &\boldsymbol{u}_2 = \boldsymbol{Z}_{\mathrm{MR}_{1,1}}\boldsymbol{i}_2 - \boldsymbol{Z}_{\mathrm{MR}_{1,2}}(\boldsymbol{Z}_\mathrm{AR} + \boldsymbol{Z}_{\mathrm{MR}_{2,2}})^{-1}(\boldsymbol{Z}_{\mathrm{MR}_{2,1}}\boldsymbol{i}_2 - \boldsymbol{u}_\mathrm{AN}). \end{aligned} \tag{2.35}$$

Taking again the relation $\boldsymbol{i}_2 = -\dfrac{1}{Z_\mathrm{L}}\boldsymbol{u}_\mathrm{L} = -\dfrac{1}{Z_\mathrm{L}}\boldsymbol{u}_2$,

$$\begin{aligned} \boldsymbol{u}_2 = \boldsymbol{u}_\mathrm{L} = &[\boldsymbol{Z}_{\mathrm{MR}_{1,1}} - \boldsymbol{Z}_{\mathrm{MR}_{1,2}}(\boldsymbol{Z}_\mathrm{AR} + \boldsymbol{Z}_{\mathrm{MR}_{2,2}})^{-1}\boldsymbol{Z}_{\mathrm{MR}_{2,1}}]\left(-\frac{1}{Z_\mathrm{L}}\right)\boldsymbol{u}_\mathrm{L} + \\ &+ \boldsymbol{Z}_{\mathrm{MR}_{1,2}}(\boldsymbol{Z}_\mathrm{AR} + \boldsymbol{Z}_{\mathrm{MR}_{2,2}})^{-1}\boldsymbol{u}_\mathrm{AN} \\ Z_\mathrm{L}\boldsymbol{u}_\mathrm{L} = &-\boldsymbol{Z}_\mathrm{R}\boldsymbol{u}_\mathrm{L} + Z_\mathrm{L}\boldsymbol{F}_\mathrm{R}\boldsymbol{u}_\mathrm{AN} \end{aligned} \tag{2.36}$$

which directly leads to the sought relation between $\boldsymbol{u}_\mathrm{AN}$ and $\boldsymbol{u}_\mathrm{L}$

$$\begin{aligned} &\boldsymbol{u}_\mathrm{L} = f_2(\boldsymbol{u}_\mathrm{AN}) = \boldsymbol{Q}\boldsymbol{F}_\mathrm{R}\boldsymbol{u}_\mathrm{AN}, \\ &\boldsymbol{F}_\mathrm{R} = \boldsymbol{Z}_{\mathrm{MR}_{1,2}}(\boldsymbol{Z}_\mathrm{AR} + \boldsymbol{Z}_{\mathrm{MR}_{2,2}})^{-1}, \\ &\boldsymbol{Q} = Z_\mathrm{L}(Z_\mathrm{L}\boldsymbol{I}_M + \boldsymbol{Z}_\mathrm{R})^{-1} = Z_\mathrm{L}[Z_\mathrm{L}\boldsymbol{I}_M + (\boldsymbol{Z}_{\mathrm{MR}_{1,1}} - \boldsymbol{F}_\mathrm{R}\boldsymbol{Z}_{\mathrm{MR}_{2,1}})]^{-1}. \end{aligned} \tag{2.37}$$

2.2.1.3 *Superposition Step 3:* $\boldsymbol{u}_\mathrm{G} = \mathbf{0}_N$ V, $\boldsymbol{u}_\mathrm{AN} = \mathbf{0}_M$ V *and* $\boldsymbol{i}_\mathrm{N} = \mathbf{0}_M$ A

For this third step, $\boldsymbol{u}_\mathrm{N}$ is activated and all of the other sources are deactivated to compute $\boldsymbol{u}_\mathrm{L} = f_3(\boldsymbol{u}_\mathrm{N})$. As in the previous superposition step, because of $\boldsymbol{i}_\mathrm{A} = \mathbf{0}_N$ A, (2.33) holds again. Now, with $\boldsymbol{u}_\mathrm{AN} = \mathbf{0}_M$ V and (2.34) we get

$$\begin{aligned}
&\boldsymbol{u}_\mathrm{B} = \boldsymbol{u}_\mathrm{C} = \boldsymbol{Z}_{\mathrm{MR}_{2,1}}\boldsymbol{i}_2 - \boldsymbol{Z}_{\mathrm{MR}_{2,2}}\boldsymbol{i}_\mathrm{B},\\
&\boldsymbol{u}_\mathrm{B} = \boldsymbol{Z}_\mathrm{AR}\boldsymbol{i}_\mathrm{B} \implies \boldsymbol{i}_\mathrm{B} = (\boldsymbol{Z}_\mathrm{AR} + \boldsymbol{Z}_{\mathrm{MR}_{2,2}})^{-1}\boldsymbol{Z}_{\mathrm{MR}_{2,1}}\boldsymbol{i}_2.
\end{aligned} \tag{2.38}$$

Taking this result and applying it in the same multiport (2.34)

$$\begin{aligned}
&\boldsymbol{u}_2 = [\boldsymbol{Z}_{\mathrm{MR}_{1,1}} - \boldsymbol{Z}_{\mathrm{MR}_{1,2}}(\boldsymbol{Z}_\mathrm{AR} + \boldsymbol{Z}_{\mathrm{MR}_{2,2}})^{-1}\boldsymbol{Z}_{\mathrm{MR}_{2,1}}]\boldsymbol{i}_2,\\
&\boldsymbol{u}_2 = \boldsymbol{u}_\mathrm{L} + \boldsymbol{u}_\mathrm{N},\ \boldsymbol{i}_2 = -\frac{1}{Z_\mathrm{L}}\boldsymbol{u}_\mathrm{L},\\
&\boldsymbol{u}_\mathrm{L} + \boldsymbol{u}_\mathrm{N} = [\boldsymbol{Z}_{\mathrm{MR}_{1,1}} - \boldsymbol{Z}_{\mathrm{MR}_{1,2}}(\boldsymbol{Z}_\mathrm{AR} + \boldsymbol{Z}_{\mathrm{MR}_{2,2}})^{-1}\boldsymbol{Z}_{\mathrm{MR}_{2,1}}]\left(-\frac{1}{Z_\mathrm{L}}\right)\boldsymbol{u}_\mathrm{L} = -\frac{1}{Z_\mathrm{L}}\boldsymbol{Z}_\mathrm{R}\boldsymbol{u}_\mathrm{L},\\
&Z_\mathrm{L}\boldsymbol{u}_\mathrm{N} = -(Z_\mathrm{L}\boldsymbol{I}_M + \boldsymbol{Z}_\mathrm{R})\boldsymbol{u}_\mathrm{L} \implies \boldsymbol{u}_\mathrm{L} = -Z_\mathrm{L}(Z_\mathrm{L}\boldsymbol{I}_M + \boldsymbol{Z}_\mathrm{R})^{-1}\boldsymbol{u}_\mathrm{N},
\end{aligned} \tag{2.39}$$

which concludes the third step of the superposition

$$\begin{aligned}
&\boldsymbol{u}_\mathrm{L} = f_3(\boldsymbol{u}_\mathrm{N}) = -\boldsymbol{Q}\boldsymbol{u}_\mathrm{AN},\\
&\boldsymbol{Q} = Z_\mathrm{L}(Z_\mathrm{L}\boldsymbol{I}_M + \boldsymbol{Z}_\mathrm{R})^{-1}.
\end{aligned} \tag{2.40}$$

2.2.1.4 Superposition Step 4: $\boldsymbol{u}_\mathrm{G} = \boldsymbol{0}_N$ V *and* $\boldsymbol{u}_\mathrm{N} = \boldsymbol{u}_\mathrm{AN} = \boldsymbol{0}_M$ V

From the equations in (2.29) $\boldsymbol{u}_2 = \boldsymbol{Z}_\mathrm{R}\boldsymbol{i}_2$, because $\boldsymbol{u}_\mathrm{G} = \boldsymbol{0}_{N,1}\mathrm{V} \implies \boldsymbol{i}_1 = \boldsymbol{0}_{N,1}\mathrm{A}$ (from (2.23)). The nodal current analysis at the node just above $\boldsymbol{i}_\mathrm{N}$ in Fig. 3 gives $\boldsymbol{u}_\mathrm{L} = f_4(\boldsymbol{i}_\mathrm{N})$

$$\begin{aligned}
&\boldsymbol{i}_\mathrm{N} = \boldsymbol{i}_2 + \frac{1}{Z_\mathrm{L}}\boldsymbol{u}_\mathrm{L} \implies \boldsymbol{i}_2 = \frac{1}{Z_\mathrm{L}}\boldsymbol{u}_\mathrm{L} - \boldsymbol{i}_\mathrm{N},\\
&\boldsymbol{u}_2 = \boldsymbol{u}_\mathrm{L} = \boldsymbol{Z}_\mathrm{R}\boldsymbol{i}_2 = \boldsymbol{Z}_\mathrm{R}(\frac{1}{Z_\mathrm{L}}\boldsymbol{u}_\mathrm{L} - \boldsymbol{i}_\mathrm{N}),\\
&\boldsymbol{u}_\mathrm{L} = f_4(\boldsymbol{i}_\mathrm{N}) = Z_\mathrm{L}(Z_\mathrm{L}\boldsymbol{I}_M + \boldsymbol{Z}_\mathrm{R})^{-1}\boldsymbol{Z}_\mathrm{R}\boldsymbol{i}_\mathrm{N} = \boldsymbol{Q}\boldsymbol{Z}_\mathrm{AR}\boldsymbol{i}_\mathrm{N}.
\end{aligned} \tag{2.41}$$

An alternative way to arrive at this result is to use the Helmholtz-Thévenin theorem, according to (JOHNSON, 2003), and transform the $\boldsymbol{i}_\mathrm{N}$ current source into the $\boldsymbol{Z}_\mathrm{R}\boldsymbol{i}_\mathrm{N}$ voltage source connected in series with Z_L. Thus, it would be similar to the superposition principle for $\boldsymbol{u}_\mathrm{AN}$ and for $\boldsymbol{u}_\mathrm{N}$, yielding the same $\boldsymbol{u}_\mathrm{L} = \boldsymbol{Q}(\boldsymbol{Z}_\mathrm{R}\boldsymbol{i}_\mathrm{N})$ result.

2.2.1.5 *Superposition Final Step:* $f = f_1 + f_2 + f_3 + f_4$

Now it is possible to develop (2.21) applying (2.32), (2.37), (2.40) and (2.41) and get the complete relation between the loads $\boldsymbol{u}_{\mathrm{L}}$ receive port-voltages, the generators $\boldsymbol{u}_{\mathrm{G}}$ transmit port-voltages and the main noise contributions $\{\boldsymbol{u}_{\mathrm{AN}}, \boldsymbol{u}_{\mathrm{N}}, \boldsymbol{i}_{\mathrm{N}}\}$.

$$
\begin{aligned}
f_1(\boldsymbol{u}_{\mathrm{G}}) &= \boldsymbol{D}\boldsymbol{u}_{\mathrm{G}} = [Z_{\mathrm{L}}(Z_{\mathrm{L}}\boldsymbol{I}_M + \boldsymbol{Z}_{\mathrm{R}})^{-1}\boldsymbol{Z}_{\mathrm{RT}}(Z_{\mathrm{G}}\boldsymbol{I}_N + \boldsymbol{Z}_{\mathrm{T}})^{-1}]\boldsymbol{u}_{\mathrm{G}},\\
f_2(\boldsymbol{u}_{\mathrm{AN}}) &= \boldsymbol{Q}\boldsymbol{F}_{\mathrm{R}}\boldsymbol{u}_{\mathrm{AN}} = Z_{\mathrm{L}}(Z_{\mathrm{L}}\boldsymbol{I}_M + \boldsymbol{Z}_{\mathrm{R}})^{-1}\boldsymbol{F}_{\mathrm{R}}\boldsymbol{u}_{\mathrm{AN}},\\
f_3(\boldsymbol{u}_{\mathrm{N}}) &= -\boldsymbol{Q}\boldsymbol{u}_{\mathrm{N}} = -Z_{\mathrm{L}}(Z_{\mathrm{L}}\boldsymbol{I}_M + \boldsymbol{Z}_{\mathrm{R}})^{-1}\boldsymbol{u}_{\mathrm{N}},\\
f_4(\boldsymbol{i}_{\mathrm{N}}) &= \boldsymbol{Q}\boldsymbol{Z}_{\mathrm{R}}\boldsymbol{i}_{\mathrm{N}} = Z_{\mathrm{L}}(Z_{\mathrm{L}}\boldsymbol{I}_M + \boldsymbol{Z}_{\mathrm{R}})^{-1}\boldsymbol{Z}_{\mathrm{R}}\boldsymbol{i}_{\mathrm{N}},\\
f(\boldsymbol{u}_{\mathrm{G}}, \boldsymbol{u}_{\mathrm{AN}}, \boldsymbol{u}_{\mathrm{N}}, \boldsymbol{i}_{\mathrm{N}}) &= f_1(\boldsymbol{u}_{\mathrm{G}}) + f_2(\boldsymbol{u}_{\mathrm{AN}}) + f_3(\boldsymbol{u}_{\mathrm{N}}) + f_4(\boldsymbol{i}_{\mathrm{N}}),
\end{aligned}
\tag{2.42}
$$

$$
\boldsymbol{u}_{\mathrm{L}} = \boldsymbol{D}\boldsymbol{u}_{\mathrm{G}} + \boldsymbol{Q}(\boldsymbol{F}_{\mathrm{R}}\boldsymbol{u}_{\mathrm{AN}} - \boldsymbol{u}_{\mathrm{N}} + \boldsymbol{Z}_{\mathrm{R}}\boldsymbol{i}_{\mathrm{N}}). \tag{2.43}
$$

Equation (2.43) is the straight result of the superposition principle, however it is not in its best formulation. For this purpose, explained later in 2.2.2.3, $\boldsymbol{u}_{\mathrm{L}}$ can be written according to

$$
\boldsymbol{u}_{\mathrm{L}} = \boldsymbol{D}\boldsymbol{u}_{\mathrm{G}} + \sqrt{R_{\mathrm{L}}}\boldsymbol{\eta}, \tag{2.44}
$$

where $R_{\mathrm{L}} = \mathrm{Re}(Z_{\mathrm{L}})$ is the real part of the load impedances.

2.2.2 *Information Theoretic Model for the System with DMNs*

As stated before, on the one hand of the MCT there is the physical part of the communication systems given by the Tx- and Rx-antenna arrays coupling effects–inside and between themselves. On the other hand, there is the mathematical part of the communication systems given by Information Theory and, finally, connecting these two parts there is the Circuit Theoretic framework.

The circuit theoretic equation (2.44) relating the transmit and the receive voltages was obtained and it encapsulates the coupling effects of the antennas interactions. Then, what is left is to map this equation's variables into the classic Information Theoretic equation

$$
\boldsymbol{y} = \boldsymbol{H}\boldsymbol{x} + \boldsymbol{\nu}, \tag{2.45}
$$

where $\boldsymbol{y}$ and $\boldsymbol{x}$ are, respectively, the receive and transmit signals, $\boldsymbol{H}$ represents the communications channel and $\boldsymbol{\nu}$ is the additive noise.

From a first look, it might be tempting to make a straight-forward mapping of (2.44) to (2.45) (e.g. $\boldsymbol{x} = \boldsymbol{u}_\mathrm{G}$ and $\boldsymbol{H} = \boldsymbol{D}$), but that would be a mistake, since it would not keep the physical meaning of the variables properly. For instance, the transmit power, computed with $\mathbb{E}\left[\|\boldsymbol{x}\|_2^2\right] \in \mathbb{R}^N\mathrm{V}^2$, would have no unit of power. Thus, the mapping must be oriented by the necessary physical quantities.

To do so, the analysis of the transmit power and of the noise covariance from the Circuit Theoretic perspective is made and, then, these quantities are mapped to the transmit power and noise covariance of the Information Theoretic model, leading, finally, to the mapping of each variable in (2.45).

2.2.2.1 Circuit Theoretic Transmit Power

The transmit power is calculated taking the expectation of the sum of the real parts of the N Tx-antennas input ports variables product. Since the antennas are considered lossless for the theory development, all of the input power is radiated by the antennas.

$$P_\mathrm{T} = \mathbb{E}\left[\sum_{n=1}^{N} \mathrm{Re}\left(i_{\mathrm{A},n}^{*} u_{\mathrm{A},n}\right)\right] = \mathbb{E}\left[\mathrm{Re}\left(\boldsymbol{i}_\mathrm{A}^\mathrm{H}\boldsymbol{u}_\mathrm{A}\right)\right] = \frac{1}{2}\mathbb{E}\left[\boldsymbol{i}_\mathrm{A}^\mathrm{H}\boldsymbol{u}_\mathrm{A} + \boldsymbol{u}_\mathrm{A}^\mathrm{H}\boldsymbol{i}_\mathrm{A}\right]. \tag{2.46}$$

To further develop this equation $\boldsymbol{u}_\mathrm{A} = \boldsymbol{Z}_\mathrm{AT}\boldsymbol{i}_\mathrm{A}$, (2.22) and (2.30) can be plugged in to write the transmit power in terms of the generators voltages.

$$P_\mathrm{T} = \frac{1}{2}\mathbb{E}\left[\boldsymbol{i}_\mathrm{A}^\mathrm{H}(\boldsymbol{Z}_\mathrm{AT} + \boldsymbol{Z}_\mathrm{AT}^\mathrm{H})\boldsymbol{i}_\mathrm{A}\right] = \mathbb{E}[\boldsymbol{i}_\mathrm{A}^\mathrm{H}\,\mathrm{Re}(\boldsymbol{Z}_\mathrm{AT})\boldsymbol{i}_\mathrm{A}], \tag{2.47}$$

$$\begin{aligned} P_\mathrm{T} = \mathbb{E}\Big[&\boldsymbol{u}_\mathrm{G}^\mathrm{H}[(Z_\mathrm{G}\boldsymbol{I}_N + \boldsymbol{Z}_\mathrm{T})^{-\mathrm{H}}\boldsymbol{Z}_{\mathrm{MT}_{2,1}}^\mathrm{H}(\boldsymbol{Z}_\mathrm{AT} + \boldsymbol{Z}_{\mathrm{MT}_{2,2}})^{-\mathrm{H}}]\,\mathrm{Re}(\boldsymbol{Z}_\mathrm{AT}) \\ &[(\boldsymbol{Z}_\mathrm{AT} + \boldsymbol{Z}_{\mathrm{MT}_{2,2}})^{-1}\boldsymbol{Z}_{\mathrm{MT}_{2,1}}(Z_\mathrm{G}\boldsymbol{I}_N + \boldsymbol{Z}_\mathrm{T})^{-1}]\boldsymbol{u}_\mathrm{G}\Big] \end{aligned} \tag{2.48}$$

$$\begin{aligned} \boldsymbol{B} = 4R_\mathrm{G}[&(Z_\mathrm{G}\boldsymbol{I}_N + \boldsymbol{Z}_\mathrm{T})^{-\mathrm{H}}\boldsymbol{Z}_{\mathrm{MT}_{2,1}}^\mathrm{H}(\boldsymbol{Z}_\mathrm{AT} + \boldsymbol{Z}_{\mathrm{MT}_{2,2}})^{-\mathrm{H}}]\,\mathrm{Re}(\boldsymbol{Z}_\mathrm{AT}) \\ &[(\boldsymbol{Z}_\mathrm{AT} + \boldsymbol{Z}_{\mathrm{MT}_{2,2}})^{-1}\boldsymbol{Z}_{\mathrm{MT}_{2,1}}(Z_\mathrm{G}\boldsymbol{I}_N + \boldsymbol{Z}_\mathrm{T})^{-1}], \end{aligned} \tag{2.49}$$

$$P_{\mathrm{T}} = \frac{1}{4R_{\mathrm{G}}}\mathbb{E}\left[\boldsymbol{u}_{\mathrm{G}}^{\mathrm{H}}\boldsymbol{B}\boldsymbol{u}_{\mathrm{G}}\right]. \tag{2.50}$$

The $\boldsymbol{B}$ matrix is called the power coupling matrix and it is defined with a factor of $4R_{\mathrm{G}} = 4\mathrm{Re}(Z_{\mathrm{G}})$, four times the real part of the series impedance of the generators voltage sources. This definition of the $\boldsymbol{B}$ matrix is meant to make it more mathematically tractable, while also considering the physical units involved.

2.2.2.2 Circuit Theoretic Noise Covariance

The second physical quantity of interest is the $\boldsymbol{R}_{\boldsymbol{\eta}}$ noise covariance matrix

$$\boldsymbol{\eta} = \frac{1}{\sqrt{R_L}}\boldsymbol{Q}\boldsymbol{F}_{\mathrm{R}}(\boldsymbol{u}_{\mathrm{AN}} - \boldsymbol{u}_{\mathrm{N}} + \boldsymbol{Z}_{\mathrm{R}}\boldsymbol{i}_{\mathrm{N}}), \tag{2.51}$$

$$\begin{aligned}\boldsymbol{R}_{\boldsymbol{\eta}} = \mathbb{E}\left[\boldsymbol{\eta}\boldsymbol{\eta}^{\mathrm{H}}\right] = \mathbb{E}\Bigg[&\frac{1}{\sqrt{R_L}}\boldsymbol{Q}(\boldsymbol{F}_{\mathrm{R}}\boldsymbol{u}_{\mathrm{AN}} - \boldsymbol{u}_{\mathrm{N}} + \boldsymbol{Z}_{\mathrm{R}}\boldsymbol{i}_{\mathrm{N}}) \\ &(\boldsymbol{F}_{\mathrm{R}}\boldsymbol{u}_{\mathrm{AN}} - \boldsymbol{u}_{\mathrm{N}} + \boldsymbol{Z}_{\mathrm{R}}\boldsymbol{i}_{\mathrm{N}})^{\mathrm{H}}\boldsymbol{Q}^{\mathrm{H}}\left(\frac{1}{\sqrt{R_L}}\right)^{*}\Bigg], \\ \boldsymbol{R}_{\boldsymbol{\eta}} = \frac{1}{R_L}\boldsymbol{Q}\Big\{&\boldsymbol{F}_{\mathrm{R}}\mathbb{E}\left[\boldsymbol{u}_{\mathrm{AN}}\boldsymbol{u}_{\mathrm{AN}}^{\mathrm{H}}\right]\boldsymbol{F}_{\mathrm{R}}^{\mathrm{H}} + \mathbb{E}\left[\boldsymbol{u}_{\mathrm{N}}\boldsymbol{u}_{\mathrm{N}}^{\mathrm{H}}\right] + \boldsymbol{Z}_{\mathrm{R}}\mathbb{E}\left[\boldsymbol{i}_{\mathrm{N}}\boldsymbol{i}_{\mathrm{N}}^{\mathrm{H}}\right]\boldsymbol{Z}_{\mathrm{R}}^{\mathrm{H}} + \\ &- 2\,\mathrm{Re}[\mathbb{E}(\boldsymbol{u}_{\mathrm{N}}\boldsymbol{i}_{\mathrm{N}}^{\mathrm{H}})\boldsymbol{Z}_{\mathrm{R}}^{\mathrm{H}}] - 2\,\mathrm{Re}[\boldsymbol{F}_{\mathrm{R}}\mathbb{E}(\boldsymbol{u}_{\mathrm{AN}}\boldsymbol{u}_{\mathrm{N}}^{\mathrm{H}})] + 2\,\mathrm{Re}[\boldsymbol{F}_{\mathrm{R}}\mathbb{E}(\boldsymbol{u}_{\mathrm{AN}}\boldsymbol{i}_{\mathrm{N}}^{\mathrm{H}})\boldsymbol{Z}_{\mathrm{R}}]\Big\}\boldsymbol{Q}^{\mathrm{H}}.\end{aligned} \tag{2.52}$$

To compute (2.52), the noise vectors statistics described in (2.12), (2.13), (2.14) and (2.15) need to be applied in the equation. Additionally, the substitution $\boldsymbol{Q} = Z_{\mathrm{L}}(Z_{\mathrm{L}}\boldsymbol{I}_M + \boldsymbol{Z}_{\mathrm{R}})^{-1}$ is made and it follows that

$$\begin{aligned}\boldsymbol{R}_{\boldsymbol{\eta}} = \frac{|Z_{\mathrm{L}}|^2}{R_L}(Z_{\mathrm{L}}\boldsymbol{I}_M + \boldsymbol{Z}_{\mathrm{R}})^{-1}\Big[&4kT\Delta_f\boldsymbol{F}_{\mathrm{R}}\,\mathrm{Re}(\boldsymbol{Z}_{\mathrm{AR}})\boldsymbol{F}_{\mathrm{R}}^{\mathrm{H}} + \sigma_u^2\boldsymbol{I}_M + \\ &+ \sigma_i^2\boldsymbol{Z}_{\mathrm{R}}\boldsymbol{Z}_{\mathrm{R}}^{\mathrm{H}} - 2\sigma_u\sigma_i\,\mathrm{Re}(\rho\boldsymbol{Z}_{\mathrm{R}}^{\mathrm{H}})\Big](Z_{\mathrm{L}}\boldsymbol{I}_M + \boldsymbol{Z}_{\mathrm{R}})^{-\mathrm{H}},\end{aligned} \tag{2.53}$$

where the identity matrices come from the fact that, according to the equations mentioned above, for different ports intrinsic and extrinsic noise sources are uncorrelated. For, e.g. $\boldsymbol{u}_{\mathrm{N}}$ and $\boldsymbol{i}_{\mathrm{N}}$ the following holds

$$\mathbb{E}\left[\boldsymbol{u}_{\mathrm{N}}\boldsymbol{i}_{\mathrm{N}}^{\mathrm{H}}\right]\boldsymbol{Z}_{\mathrm{R}}^{\mathrm{H}} = \mathbb{E}\left\{\begin{bmatrix} u_{\mathrm{N},1} \\ \vdots \\ u_{\mathrm{N},M} \end{bmatrix}\left[i_{\mathrm{N},1}^{*}\cdots i_{\mathrm{N},M}^{*}\right]\right\}\boldsymbol{Z}_{\mathrm{R}}^{\mathrm{H}},$$

$$\mathbb{E}\left[\boldsymbol{u}_{\mathrm{N}}\boldsymbol{i}_{\mathrm{N}}^{\mathrm{H}}\right]\boldsymbol{Z}_{\mathrm{R}}^{\mathrm{H}} = \begin{bmatrix} \mathbb{E}(u_{\mathrm{N},1}i_{\mathrm{N},1}^{*}) & \mathbb{E}(u_{\mathrm{N},1}i_{\mathrm{N},2}^{*}) & \cdots & \mathbb{E}(u_{\mathrm{N},1}i_{\mathrm{N},M}^{*}) \\ \mathbb{E}(u_{\mathrm{N},2}i_{\mathrm{N},1}^{*}) & \mathbb{E}(u_{\mathrm{N},2}i_{\mathrm{N},2}^{*}) & \cdots & \mathbb{E}(u_{\mathrm{N},2}i_{\mathrm{N},M}^{*}) \\ \vdots & \vdots & \vdots & \vdots \\ \mathbb{E}(u_{\mathrm{N},M}i_{\mathrm{N},1}^{*}) & \mathbb{E}(u_{\mathrm{N},M}i_{\mathrm{N},2}^{*}) & \cdots & \mathbb{E}(u_{\mathrm{N},M}i_{\mathrm{N},M}^{*}) \end{bmatrix}\boldsymbol{Z}_{\mathrm{R}}^{\mathrm{H}}, \tag{2.54}$$

$$\mathbb{E}\left[\boldsymbol{u}_{\mathrm{N}}\boldsymbol{i}_{\mathrm{N}}^{\mathrm{H}}\right]\boldsymbol{Z}_{\mathrm{R}}^{\mathrm{H}} = \begin{bmatrix} \rho\sigma_u\sigma_i & 0 & \cdots & 0 \\ 0 & \rho\sigma_u\sigma_i & \cdots & 0 \\ \vdots & \vdots & \vdots & \vdots \\ 0 & 0 & \cdots & \rho\sigma_u\sigma_i \end{bmatrix}\boldsymbol{Z}_{\mathrm{R}}^{\mathrm{H}} = \rho\sigma_u\sigma_i\boldsymbol{I}_M\boldsymbol{Z}_{\mathrm{R}}^{\mathrm{H}} = \rho\sigma_u\sigma_i\boldsymbol{Z}_{\mathrm{R}}^{\mathrm{H}}.$$

2.2.2.3 The Channel Matrix

The transmit power and the noise covariance matrix were computed from the circuit theoretic perspective of the model in Fig. 3 and, thus, their physical units is in Watts. In the case of the transmit power, in which the power coupling matrix $\boldsymbol{B}$ is defined with a specific choice of the scaling factor–$4R_{\mathrm{L}}$ in (2.49)–, its units remain always in Watts.

However, in the case of the noise covariance matrix, the units in Watts were made possible by the definition of $\boldsymbol{\eta}$ in (2.44). An analysis of the variables in $\boldsymbol{Q}(\boldsymbol{F}_{\mathrm{R}}\boldsymbol{u}_{\mathrm{AN}} - \boldsymbol{u}_{\mathrm{N}} + \boldsymbol{Z}_{\mathrm{R}}\boldsymbol{i}_{\mathrm{N}})$ shows that this quantity is in volts, but $\eta = \frac{1}{\sqrt{R_{\mathrm{L}}}}\boldsymbol{Q}(\boldsymbol{F}_{\mathrm{R}}\boldsymbol{u}_{\mathrm{AN}} - \boldsymbol{u}_{\mathrm{N}} + \boldsymbol{Z}_{\mathrm{R}}\boldsymbol{i}_{\mathrm{N}})$ is in $\mathrm{V}/\sqrt{\Omega}$, which allows $\boldsymbol{R}_{\boldsymbol{\eta}}$ to be in Watts.

It is through these two quantities that the links between the physical circuit theoretic model and the mathematical information theoretical model are made. In the scope of the latter, (2.45) (rewritten here for convenience)

$$\boldsymbol{y} = \boldsymbol{H}\boldsymbol{x} + \boldsymbol{\nu},$$

bears the variable $\boldsymbol{x}$ from which the transmit power $\mathbb{E}\left[||\boldsymbol{x}||_2^2\right]$ can be calculated. In order to keep

the physical consistency of this variable, which is the objective of the MCT, this power needs to be in Watts. The transmit power according to (2.50) and to the Information Theory can be related by

$$P_{\mathrm{T}} = \mathbb{E}\left[||\boldsymbol{x}||_2^2\right] = \frac{1}{4R_{\mathrm{G}}}\mathbb{E}\left[\boldsymbol{u}_{\mathrm{G}}^{\mathrm{H}}\boldsymbol{B}\boldsymbol{u}_{\mathrm{G}}\right] = \mathbb{E}\left[\frac{1}{4R_{\mathrm{G}}}\boldsymbol{u}_{\mathrm{G}}^{\mathrm{H}}\boldsymbol{B}\boldsymbol{u}_{\mathrm{G}}\right] = \mathbb{E}\left[\frac{1}{4R_{\mathrm{G}}}\boldsymbol{u}_{\mathrm{G}}^{\mathrm{H}}\boldsymbol{B}^{1/2}\boldsymbol{B}^{\mathrm{H}/2}\boldsymbol{u}_{\mathrm{G}}\right], \tag{2.55}$$

leading to the equation of $\boldsymbol{x}$ and $\boldsymbol{u}_{\mathrm{G}}$

$$\boldsymbol{x} = \frac{1}{2\sqrt{R_{\mathrm{G}}}}\boldsymbol{B}^{\mathrm{H}/2}\boldsymbol{u}_{\mathrm{G}}. \tag{2.56}$$

For this equation, $\boldsymbol{B}^{\mathrm{H}/2}$ is determined using the definition adopted by (LAAS *et al.*, 2017) of the square root of positive semi-definite matrices,

$$\begin{aligned}
&\boldsymbol{B} = \boldsymbol{B}^{1/2}\boldsymbol{B}^{\mathrm{H}/2},\\
&\boldsymbol{B}^{1/2} = 2\sqrt{R_{\mathrm{G}}}[(Z_{\mathrm{G}}\boldsymbol{I}_N + \boldsymbol{Z}_{\mathrm{T}})^{-\mathrm{H}}\boldsymbol{Z}_{\mathrm{MT}_{2,1}}^{\mathrm{H}}(\boldsymbol{Z}_{\mathrm{AT}} + \boldsymbol{Z}_{\mathrm{MT}_{2,2}})^{-\mathrm{H}}]\,\mathrm{Re}(\boldsymbol{Z}_{\mathrm{AT}})^{\mathrm{H}/2},\\
&\boldsymbol{B}^{\mathrm{H}/2} = 2\sqrt{R_{\mathrm{G}}}\,\mathrm{Re}(\boldsymbol{Z}_{\mathrm{AT}})^{1/2}[(\boldsymbol{Z}_{\mathrm{AT}} + \boldsymbol{Z}_{\mathrm{MT}_{2,2}})^{-1}\boldsymbol{Z}_{\mathrm{MT}_{2,1}}(Z_{\mathrm{G}}\boldsymbol{I}_N + \boldsymbol{Z}_{\mathrm{T}})^{-1}],
\end{aligned} \tag{2.57}$$

valid for $\boldsymbol{B}$ because it is a positive definite matrix, according to (IVRLAČ; NOSSEK, 2010). Still according to the authors, because $\boldsymbol{B}$ is a Hermitian positive definite matrix, $\boldsymbol{B}^{\mathrm{H}/2}$ is also. This implies that $\boldsymbol{x} = \boldsymbol{0}_N \iff \boldsymbol{u}_{\mathrm{G}} = \boldsymbol{0}_N$ V.

Still following (2.45), the statistical covariance matrix of $\boldsymbol{y}$ can be written as

$$\mathbb{E}\left[\boldsymbol{y}\boldsymbol{y}^{\mathrm{H}}\right] = \mathbb{E}\left[\boldsymbol{H}\boldsymbol{x}\boldsymbol{x}^{\mathrm{H}}\boldsymbol{H}^{\mathrm{H}}\right] + \mathbb{E}\left[\boldsymbol{\nu}\boldsymbol{\nu}^{\mathrm{H}}\right], \tag{2.58}$$

which is important for making the link with the other important physical quantity, the noise covariance matrix.

$$\begin{aligned}
&\boldsymbol{u}_{\mathrm{L}} = \boldsymbol{D}\boldsymbol{u}_{\mathrm{G}} + \sqrt{R_{\mathrm{L}}}\boldsymbol{\eta},\\
&\boldsymbol{y} = \boldsymbol{A}\boldsymbol{u}_{\mathrm{L}} = \boldsymbol{A}(\boldsymbol{D}\boldsymbol{u}_{\mathrm{G}} + \sqrt{R_{\mathrm{L}}}\boldsymbol{\eta}) \implies \boldsymbol{A}\boldsymbol{D}\boldsymbol{u}_{\mathrm{G}} + \sqrt{R_{\mathrm{L}}}\boldsymbol{A}\boldsymbol{\eta} = \boldsymbol{H}\boldsymbol{x} + \boldsymbol{\nu},
\end{aligned} \tag{2.59}$$

$$\mathbb{E}\left[\boldsymbol{\nu}\boldsymbol{\nu}^{\mathrm{H}}\right] = \mathbb{E}\left[\boldsymbol{y}\boldsymbol{y}^{\mathrm{H}} \mid \boldsymbol{x} = \boldsymbol{0}\right] \implies \mathbb{E}\left[\boldsymbol{\nu}\boldsymbol{\nu}^{\mathrm{H}}\right] = \mathbb{E}\left[\boldsymbol{y}\boldsymbol{y}^{\mathrm{H}}\right]\Big|_{\boldsymbol{u}_{\mathrm{G}}=\boldsymbol{0}\,\mathrm{V}} = R_{\mathrm{L}}\boldsymbol{A}\mathbb{E}\left[\boldsymbol{\eta}\boldsymbol{\eta}^{\mathrm{H}}\right]\boldsymbol{A}^{\mathrm{H}}. \tag{2.60}$$

One assumption is made before continuing any further: the physical noise sources produce Gaussian noise. This is the same assumption adopted in (IVRLAČ, 2017), because only when $\boldsymbol{\eta}$ is Gaussian can $\boldsymbol{\nu}$ also be Gaussian.

$$\begin{aligned}
&\mathbb{E}\left[\boldsymbol{\nu}\boldsymbol{\nu}^{\mathrm{H}}\right] = \sigma_{\nu}^{2}\boldsymbol{I}_{M} = R_{\mathrm{L}}\boldsymbol{A}\mathbb{E}\left[\boldsymbol{\eta}\boldsymbol{\eta}^{\mathrm{H}}\right]\boldsymbol{A}^{\mathrm{H}},\\
&\boldsymbol{A}\boldsymbol{R}_{\boldsymbol{\eta}}^{1/2} = \frac{\sigma_{\nu}}{\sqrt{R_{\mathrm{L}}}}\boldsymbol{I}_{M} \implies \boldsymbol{A} = \frac{\sigma_{\nu}}{\sqrt{R_{\mathrm{L}}}}\boldsymbol{R}_{\boldsymbol{\eta}}^{-1/2},
\end{aligned} \tag{2.61}$$

where the sum of the noise powers must be physically consistent, requiring that:

$$\mathbb{E}\left[\boldsymbol{\nu}^{\mathrm{H}}\boldsymbol{\nu}\right] = \mathbb{E}\left[\boldsymbol{\eta}^{\mathrm{H}}\boldsymbol{\eta}\right] \implies \sigma_{\nu}^{2} = \frac{\mathrm{Tr}(\boldsymbol{R}_{\boldsymbol{\eta}})}{M}. \tag{2.62}$$

The linear mappings from $\boldsymbol{\eta}$ to $\boldsymbol{\nu}$ and $\boldsymbol{u}_{\mathrm{L}}$ to $\boldsymbol{y}$ are obtained using, respectively, $\boldsymbol{\nu} = \boldsymbol{A}(\sqrt{R_{\mathrm{L}}}\boldsymbol{\eta})$ and $\boldsymbol{y} = \boldsymbol{A}\boldsymbol{u}_{\mathrm{L}}$

$$\boldsymbol{\nu} = \sigma_{\nu}\boldsymbol{R}_{\boldsymbol{\eta}}^{-1/2}\boldsymbol{\eta}, \tag{2.63}$$

$$\boldsymbol{y} = \sqrt{\frac{\sigma_{\nu}^{2}}{R_{\mathrm{L}}}}\boldsymbol{R}_{\boldsymbol{\eta}}^{-1/2}\boldsymbol{u}_{\mathrm{L}}, \tag{2.64}$$

where it is necessary to compute the $\boldsymbol{R}_{\boldsymbol{\eta}}^{-1/2}$ matrix. This can be done using the definition of $\boldsymbol{R}_{\boldsymbol{\eta}}^{1/2}$, adopted from (LAAS *et al.*, 2017),

$$\begin{aligned}
&\boldsymbol{R}_{\boldsymbol{\eta}} = \frac{|Z_{\mathrm{L}}|^{2}}{R_{L}}(Z_{\mathrm{L}}\boldsymbol{I}_{M} + \boldsymbol{Z}_{\mathrm{R}})^{-1}\boldsymbol{N}^{1/2}\boldsymbol{N}^{\mathrm{H}/2}(Z_{\mathrm{L}}\boldsymbol{I}_{M} + \boldsymbol{Z}_{\mathrm{R}})^{-\mathrm{H}}\\
&\boldsymbol{N} = 4kT\Delta_{f}\boldsymbol{F}_{\mathrm{R}}\,\mathrm{Re}(\boldsymbol{Z}_{\mathrm{AR}})\boldsymbol{F}_{\mathrm{R}}^{\mathrm{H}} + \sigma_{u}^{2}\boldsymbol{I}_{M} + \sigma_{i}^{2}\boldsymbol{Z}_{\mathrm{R}}\boldsymbol{Z}_{\mathrm{R}}^{\mathrm{H}} - 2\sigma_{u}\sigma_{i}\,\mathrm{Re}(\rho\boldsymbol{Z}_{\mathrm{R}}^{\mathrm{H}}),\\
&\boldsymbol{R}_{\boldsymbol{\eta}}^{1/2} = \frac{Z_{\mathrm{L}}}{R_{L}}(Z_{\mathrm{L}}\boldsymbol{I}_{M} + \boldsymbol{Z}_{\mathrm{R}})^{-1}\boldsymbol{N}^{1/2}.
\end{aligned} \tag{2.65}$$

Now it is possible to write an equality for the channel matrix using (2.45) and the mappings in (2.56), (2.63) and (2.64)

$$\sqrt{\frac{\sigma_\nu^2}{R_\mathrm{L}}}\boldsymbol{R}_\eta^{-1/2}\boldsymbol{u}_\mathrm{L} = \boldsymbol{H}\frac{1}{2\sqrt{R_\mathrm{G}}}\boldsymbol{B}^{\mathrm{H}/2}\boldsymbol{u}_\mathrm{G} + \sigma_\nu\boldsymbol{R}_\eta^{-1/2}\boldsymbol{\eta},$$
$$\sqrt{\frac{\sigma_\nu^2}{R_\mathrm{L}}}\boldsymbol{R}_\eta^{-1/2}\boldsymbol{D}\boldsymbol{u}_\mathrm{G} + \sqrt{\frac{\sigma_\nu^2}{R_\mathrm{L}}}\boldsymbol{R}_\eta^{-1/2}\sqrt{R_\mathrm{L}}\boldsymbol{\eta} = \boldsymbol{H}\frac{1}{2\sqrt{R_\mathrm{G}}}\boldsymbol{B}^{\mathrm{H}/2}\boldsymbol{u}_\mathrm{G} + \sigma_\nu\boldsymbol{R}_\eta^{-1/2}\boldsymbol{\eta},$$
$$\sqrt{\frac{\sigma_\nu^2}{R_\mathrm{L}}}\boldsymbol{R}_\eta^{-1/2}\boldsymbol{D}\boldsymbol{u}_\mathrm{G} = \frac{1}{2\sqrt{R_\mathrm{G}}}\boldsymbol{H}\boldsymbol{B}^{\mathrm{H}/2}\boldsymbol{u}_\mathrm{G} \implies \sqrt{\frac{\sigma_\nu^2}{R_\mathrm{L}}}\boldsymbol{R}_\eta^{-1/2}\boldsymbol{D} = \frac{1}{2\sqrt{R_\mathrm{G}}}\boldsymbol{H}\boldsymbol{B}^{\mathrm{H}/2},$$
$$\boldsymbol{H} = 2\sigma_\nu\sqrt{\frac{R_\mathrm{G}}{R_\mathrm{L}}}\boldsymbol{R}_\eta^{-1/2}\boldsymbol{D}\boldsymbol{B}^{-\mathrm{H}/2}. \tag{2.66}$$

And, thus, this completes all the mappings from the circuit theoretic model to the information theoretic model. In such a way, the variables usually used in Information, Coding and Signal theories bear, now, consistent physical meanings for the system in Fig. 3. However, there is still more to consider, regarding the structures of $\boldsymbol{D}$, $\boldsymbol{B}$ and $\boldsymbol{R}_\eta$ to be able to fully apply assumptions usually made over communications systems.

2.2.3 The Architectures of the Decoupling and Matching Networks

Up to now, the DMNs have been computed in the equations in a fairly generic manner. Beyond the reciprocity and losslessness of these multiports, no other aspect of the DMNs has been discussed and, thus, it is not possible to determine the precise structures of the matrices $\boldsymbol{D}$, $\boldsymbol{B}$ and $\boldsymbol{R}_\eta$. To do so, it is necessary prior knowledge of the DMNs impedance matrices' structures, which are dependent on their architectures.

The DMNs, as the name suggests, decouple and match the transmit and receive ports of the multiport system, according to the perspective summarized by (2.20). Their architectures is determined by the objective of achieving these two effects.

The decoupling effect is intended to make the impedance matrices $\boldsymbol{Z}_\mathrm{T}$ and $\boldsymbol{Z}_\mathrm{R}$ not only diagonal, but scaled identities.

For the Tx-DMN, this means that every HPA is terminated by Z_G^*. It is important to mention that the DMNs are not intended to cancel the mutual coupling present in the antenna arrays, but rather to take it into consideration for providing decoupled ports for the transmitter and for the receiver. The Rx-DMN provides decoupled ports to the input of the Rx-LNAs.

The impedances which are presented to the elements on the decoupled ports depend also on the DMNs architectures and can be chosen, based on these elements' impedances, to take the best performance out of the system with DMNs. According to the MCT (IVRLAČ; NOSSEK,

2014), the way to achieve this best performance is to aim for power and noise matching in the transmitter and in the receiver, respectively.

2.2.3.1 Transmit DMN: Power Matching

The strategy sought on the transmit side is to transfer the most power possible from the output of the HPAs to the input of the antenna elements, leading to energy efficient transmission of data. As defined in (FRIIS, 1944), the maximum power that can be drawn from the output of the HPAs is called available power. The additional consideration that the antennas are lossless gives that all of the available power can be, then, radiated.

Figure 4 – Transmit side of the system with DMNs with power matching for the output of the HPAs.

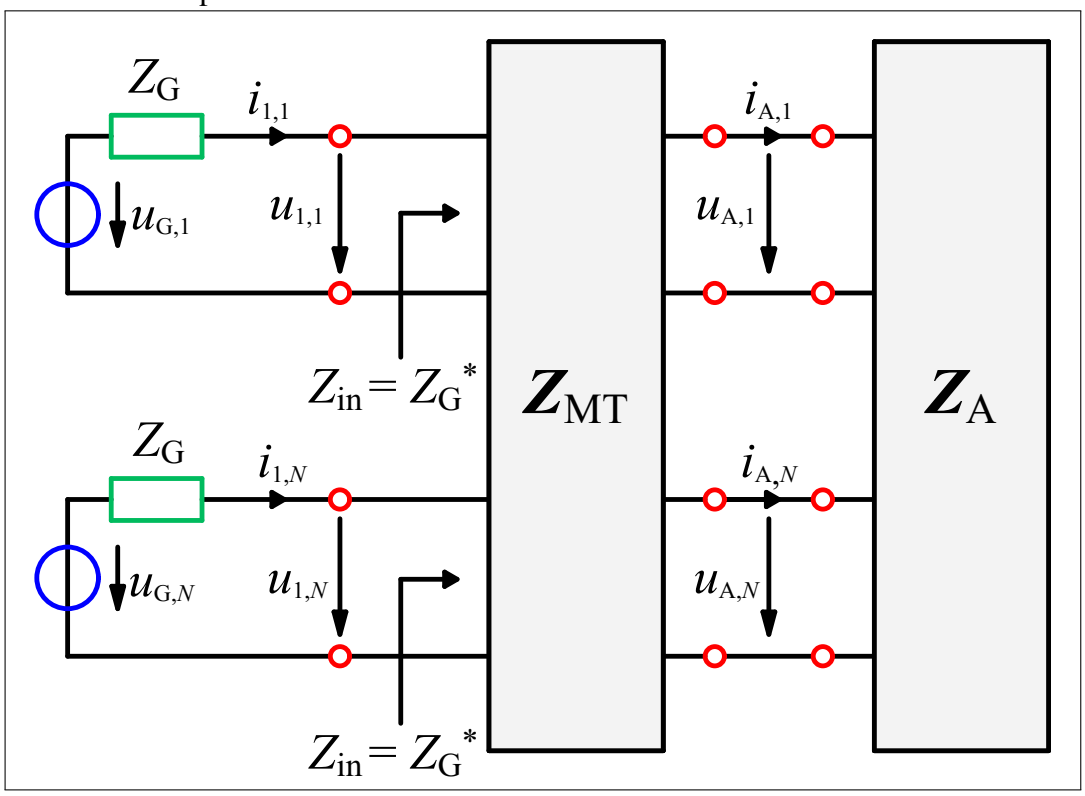

Source: The author.

The goal of the transmit DMN, thus, is to transform the decoupled antennas ports' impedances seen from the output of the HPAs, granting power matching for any impedance. In the simplified system model in Fig. 4, it does so by presenting, on each port individually, a power

matched DMN input port impedance to the Z_{G} series impedance of the amplifiers

$$\begin{aligned} u_{1,1} &= Z_{\mathrm{G}}^{*} i_{1,1}, \\ u_{1,2} &= Z_{\mathrm{G}}^{*} i_{1,2}, \\ &\vdots \\ u_{1,N} &= Z_{\mathrm{G}}^{*} i_{1,N}, \end{aligned} \tag{2.67}$$

which results in the matrix form

$$\begin{bmatrix} u_{1,1} \\ u_{1,2} \\ \vdots \\ u_{1,N} \end{bmatrix} = \begin{bmatrix} Z_{\mathrm{G}}^{*} & 0 & \cdots & 0 \\ 0 & Z_{\mathrm{G}}^{*} & \cdots & 0 \\ \vdots & \vdots & \vdots & \vdots \\ 0 & 0 & \cdots & Z_{\mathrm{G}}^{*} \end{bmatrix} \begin{bmatrix} i_{1,1} \\ i_{1,2} \\ \vdots \\ i_{1,N} \end{bmatrix}. \tag{2.68}$$

Together with the multiport (2.20) and the Unilateral Approximation, the value of the $\boldsymbol{Z}_{\mathrm{T}}$ matrix can be determined

$$\begin{aligned} \boldsymbol{u}_1 &= \boldsymbol{Z}_{\mathrm{T}} \boldsymbol{i}_1 = Z_{\mathrm{G}}^{*} \boldsymbol{i}_1, \\ \boldsymbol{Z}_{\mathrm{T}} &= Z_{\mathrm{G}}^{*} \boldsymbol{I}_N. \end{aligned} \tag{2.69}$$

According to (2.24), the structure of $\boldsymbol{Z}_{\mathrm{T}}$ is determined by the transmit antenna array and DMN impedance matrices. The impedance matrix elements of the Tx-DMN are, thus, designed to guarantee $\boldsymbol{Z}_{\mathrm{T}} = Z_{\mathrm{G}}^{*} \boldsymbol{I}_N$ given the Tx-UCA impedance matrix. There is a degree of freedom for the design of these elements, and one is not limited by the choice made in this thesis. The design is inspired from (IVRLAČ; NOSSEK, 2010) and slightly modified from the original

$$\boldsymbol{Z}_{\mathrm{MT}} = \begin{bmatrix} \boldsymbol{Z}_{\mathrm{MT}_{1,1}} & \boldsymbol{Z}_{\mathrm{MT}_{1,2}} \\ \boldsymbol{Z}_{\mathrm{MT}_{2,1}} & \boldsymbol{Z}_{\mathrm{MT}_{2,2}} \end{bmatrix} = \begin{bmatrix} -j\mathrm{Im}(Z_{\mathrm{G}})\boldsymbol{I}_N & -j\sqrt{\mathrm{Re}(Z_{\mathrm{G}})}\mathrm{Re}(\boldsymbol{Z}_{\mathrm{AT}})^{1/2} \\ -j\sqrt{\mathrm{Re}(Z_{\mathrm{G}})}\mathrm{Re}(\boldsymbol{Z}_{\mathrm{AT}})^{1/2} & -j\mathrm{Im}(\boldsymbol{Z}_{\mathrm{AT}}) \end{bmatrix}, \tag{2.70}$$

a structure that allows for decoupling the $\boldsymbol{u}_1$ and $\boldsymbol{i}_1$ transmit ports and power matching with the

output of the HPAs. From (2.24), the power matching on the transmit side holds as follows

$$\begin{aligned}
\boldsymbol{Z}_{\mathrm{T}} &= \boldsymbol{Z}_{\mathrm{MT}_{1,1}} - \boldsymbol{Z}_{\mathrm{MT}_{1,2}}(\boldsymbol{Z}_{\mathrm{AT}} + \boldsymbol{Z}_{\mathrm{MT}_{2,2}})^{-1}\boldsymbol{Z}_{\mathrm{MT}_{2,1}}, \\
\boldsymbol{Z}_{\mathrm{T}} &= -j\mathrm{Im}(Z_{\mathrm{G}})\boldsymbol{I}_N - [-j\sqrt{R_{\mathrm{G}}}\,\mathrm{Re}(\boldsymbol{Z}_{\mathrm{AT}})^{1/2}][\boldsymbol{Z}_{\mathrm{AT}} - j\,\mathrm{Im}(\boldsymbol{Z}_{\mathrm{AT}})]^{-1}[-j\sqrt{R_{\mathrm{G}}}\,\mathrm{Re}(\boldsymbol{Z}_{\mathrm{AT}})^{1/2}], \\
\boldsymbol{Z}_{\mathrm{T}} &= -j\mathrm{Im}(Z_{\mathrm{G}})\boldsymbol{I}_N + \sqrt{R_{\mathrm{G}}}\mathrm{Re}(\boldsymbol{Z}_{\mathrm{AT}})^{1/2}\mathrm{Re}(\boldsymbol{Z}_{\mathrm{AT}})^{-1}\mathrm{Re}(\boldsymbol{Z}_{\mathrm{AT}})^{1/2}\sqrt{R_{\mathrm{G}}}, \\
\boldsymbol{Z}_{\mathrm{T}} &= (R_{\mathrm{G}} - j\mathrm{Im}(Z_{\mathrm{G}}))\boldsymbol{I}_N = Z_{\mathrm{G}}^{*}\boldsymbol{I}_N.
\end{aligned} \tag{2.71}$$

Not only has now $\boldsymbol{Z}_{\mathrm{T}}$ an specific value, as do also $\boldsymbol{B}$, by making the substitution of the $\boldsymbol{Z}_{\mathrm{MT}}$ impedance matrix elements in its defining (2.49)

$$\begin{aligned}
\boldsymbol{B} &= 4R_{\mathrm{G}}[(Z_{\mathrm{G}}\boldsymbol{I}_N + \boldsymbol{Z}_{\mathrm{T}})^{-\mathrm{H}}\boldsymbol{Z}_{\mathrm{MT}_{2,1}}^{\mathrm{H}}(\boldsymbol{Z}_{\mathrm{AT}} + \boldsymbol{Z}_{\mathrm{MT}_{2,2}})^{-\mathrm{H}}]\,\mathrm{Re}(\boldsymbol{Z}_{\mathrm{AT}}) \\
&\qquad\qquad [(\boldsymbol{Z}_{\mathrm{AT}} + \boldsymbol{Z}_{\mathrm{MT}_{2,2}})^{-1}\boldsymbol{Z}_{\mathrm{MT}_{2,1}}(Z_{\mathrm{G}}\boldsymbol{I}_N + \boldsymbol{Z}_{\mathrm{T}})^{-1}], \\
\boldsymbol{B} &= 4R_{\mathrm{G}}\{[Z_{\mathrm{G}}\boldsymbol{I}_N + Z_{\mathrm{G}}^{*}\boldsymbol{I}_N]^{-\mathrm{H}}[-j\sqrt{R_{\mathrm{G}}}\,\mathrm{Re}(\boldsymbol{Z}_{\mathrm{AT}})^{1/2}]^{\mathrm{H}}[\boldsymbol{Z}_{\mathrm{AT}} - j\,\mathrm{Im}(\boldsymbol{Z}_{\mathrm{AT}})]^{-\mathrm{H}}\} \\
&\qquad \mathrm{Re}(\boldsymbol{Z}_{\mathrm{AT}})\{(\boldsymbol{Z}_{\mathrm{AT}} - j\,\mathrm{Im}(\boldsymbol{Z}_{\mathrm{AT}})]^{-1}[-j\sqrt{R_{\mathrm{G}}}\,\mathrm{Re}(\boldsymbol{Z}_{\mathrm{AT}})^{1/2}][Z_{\mathrm{G}}\boldsymbol{I}_N + Z_{\mathrm{G}}^{*}\boldsymbol{I}_N]^{-1}\}, \\
\boldsymbol{B} &= 4R_{\mathrm{G}}\left[\left(\frac{1}{2R_{\mathrm{G}}}\right)^{*}\left(\sqrt{R_{\mathrm{G}}}\right)^{*}\mathrm{Re}(\boldsymbol{Z}_{\mathrm{AT}})^{-\mathrm{H}/2}\right]\mathrm{Re}(\boldsymbol{Z}_{\mathrm{AT}})\left[\mathrm{Re}(\boldsymbol{Z}_{\mathrm{AT}})^{-1/2}\sqrt{R_{\mathrm{G}}}\frac{1}{2R_{\mathrm{G}}}\right], \\
\boldsymbol{B} &= \frac{1}{R_{\mathrm{G}}}\left(\sqrt{R_{\mathrm{G}}}\right)^{*}\sqrt{R_{\mathrm{G}}}\,\mathrm{Re}(\boldsymbol{Z}_{\mathrm{AT}})^{-\mathrm{H}/2}\,\mathrm{Re}(\boldsymbol{Z}_{\mathrm{AT}})\,\mathrm{Re}(\boldsymbol{Z}_{\mathrm{AT}})^{-1/2}.
\end{aligned} \tag{2.72}$$

The antenna arrays are reciprocal, so their impedance matrices remain invariant under transposition, meaning that the real part of the array impedance matrix is equal to its Hermitian

$$\mathrm{Re}(\boldsymbol{Z}_{\mathrm{AT}}) = \mathrm{Re}(\boldsymbol{Z}_{\mathrm{AT}})^{*} = \mathrm{Re}\left(\boldsymbol{Z}_{\mathrm{AT}}^{\mathrm{T}}\right)^{*} = \mathrm{Re}(\boldsymbol{Z}_{\mathrm{AT}})^{\mathrm{H}}, \tag{2.73}$$

which can simplify the $\boldsymbol{B}$ matrix still further to

$$\boldsymbol{B} = \mathrm{Re}(\boldsymbol{Z}_{\mathrm{AT}})^{-1/2}\,\mathrm{Re}(\boldsymbol{Z}_{\mathrm{AT}})\,\mathrm{Re}(\boldsymbol{Z}_{\mathrm{AT}})^{-1/2} = \boldsymbol{I}_N. \tag{2.74}$$

This is a very important result to proceed with the power matching analysis, as this is the power coupling matrix and it can be interpreted as a degree of how much the HPAs' output voltages are coupled from the transmit power perspective. This concept becomes clearer when analysing the available and the transmit powers together.

The available power, whose concept was introduced above, is all of the power available to be drawn from the output of the HPAs. As such, it is related to the currents $\boldsymbol{i}_1$ and voltages $\boldsymbol{u}_1$ supplied by these elements to the input ports of the Tx-DMN, as in Fig. 4, can be formulated as the active power P_A

$$P_\mathrm{A} = \mathbb{E}\left[\mathrm{Re}\left(\boldsymbol{i}_1^\mathrm{H}\boldsymbol{u}_1\right)\right] = \frac{1}{2}\mathbb{E}\left[\boldsymbol{i}_1^\mathrm{H}\boldsymbol{u}_1 + \boldsymbol{u}_1^\mathrm{H}\boldsymbol{i}_1\right], \tag{2.75}$$

and can be developed further using (2.30), reproduced below, and the power matching

$$\begin{aligned}
&\boldsymbol{u}_\mathrm{G} = Z_\mathrm{G}\boldsymbol{i}_1 + \boldsymbol{Z}_\mathrm{T}\boldsymbol{i}_1 = (Z_\mathrm{G} + Z_\mathrm{G}^*)\boldsymbol{i}_1 = 2\mathrm{Re}(Z_\mathrm{G})\boldsymbol{i}_1 = 2R_\mathrm{G}\boldsymbol{i}_1 = 2\boldsymbol{u}_1,\\
&P_\mathrm{A} = \frac{1}{2}\mathbb{E}\left[\left(\frac{1}{2R_\mathrm{G}}\boldsymbol{u}_\mathrm{G}\right)^\mathrm{H}\left(\frac{1}{2}\boldsymbol{u}_\mathrm{G}\right) + \left(\frac{1}{2}\boldsymbol{u}_\mathrm{G}\right)^\mathrm{H}\left(\frac{1}{2R_\mathrm{G}}\boldsymbol{u}_\mathrm{G}\right)\right] = \frac{1}{4R_\mathrm{G}}\mathbb{E}\left[\|\boldsymbol{u}_\mathrm{G}\|_2^2\right].
\end{aligned} \tag{2.76}$$

Being the power coupling matrix $\boldsymbol{B}$ equal to an identity matrix in (2.50)

$$P_\mathrm{T} = \frac{1}{4R_\mathrm{G}}\mathbb{E}\left[\boldsymbol{u}_\mathrm{G}^\mathrm{H}\boldsymbol{B}\boldsymbol{u}_\mathrm{G}\right] = \frac{1}{4R_\mathrm{G}}\mathbb{E}\left[\boldsymbol{u}_\mathrm{G}^\mathrm{H}\boldsymbol{I}_N\boldsymbol{u}_\mathrm{G}\right] = \frac{1}{4R_\mathrm{G}}\mathbb{E}\left[\|\boldsymbol{u}_\mathrm{G}\|_2^2\right] = P_\mathrm{A}, \tag{2.77}$$

the transmit power becomes equal to the available power, i.e. all of the power that can be drawn from the HPAs is transmitted. Now, not only from the individual perspective of each HPA, as in (2.68), but from all of the transmit ports as a whole, the achievement of the power matching by the Tx-DMN can be perceived.

As to $\boldsymbol{D}$ and to $\boldsymbol{R}_{\boldsymbol{\eta}}$, they cannot yet be fully determined because they depend on the Rx-DMN architecture.

2.2.3.2 Receive DMN: Noise Matching

The power matching is a well known and commonly employed matching strategy. In addition, designing an architecture to grant power matching ensures an energy efficient functioning of the system. It would, then, be only natural to adopt it again for the receiver.

One can, indeed, do it, but as it turns out, it would not be the best choice for the receiver. The transmitter amplifies the transmit signal to increase the capacity of information transmission and to avoid the signal decaying, before arriving at the receiver, to a level at which it cannot be distinguished from noise. This amplification makes the transmit signal higher than the noise to a degree that the latter becomes negligible.

For this case, the power matching makes sense because the system then becomes the most energy efficient for making the best use of the amplified power. On the receiver, however, if the receive signal is simply amplified by an equipment similar or equal to a HPA, the noise from the environment will be also indiscriminately augmented.

Capacity, from the Information Theory point of view, is a measure dependent on the SNR, the higher the better capacity the system will have. The SNR, in its turn, is a ratio of the signal power to the noise power. So, more importantly than strictly aiming for a high signal power, is to aim for a high ratio of the signal to the noise power.

Thus, not only are LNAs (equipments with minimal intrinsic noise from the circuitry) used instead of HPAs on the receive side, as is also power matching not used. Instead, the strategy adopted aims to match the input impedance of the LNAs with the receive antennas ensuring that the SNR will be the highest by reducing the noise figure (FRIIS, 1944) to the minimum.

In (WARNICK; JENSEN, 2007), an optimal noise matching multiport concept for receivers with mutually coupled arrays is developed and proved to be optimal. The concept of the optimal design is to provide noise matching for each LNA in the multiport system individually, through the use of a network which presents to the LNAs decoupled antenna ports with matched optimal impedance, according to the receive side schematic of the system with DMNs in Fig. 5.

Figure 5 – Receive side of the system with DMNs with noise matching for the input of the LNAs.

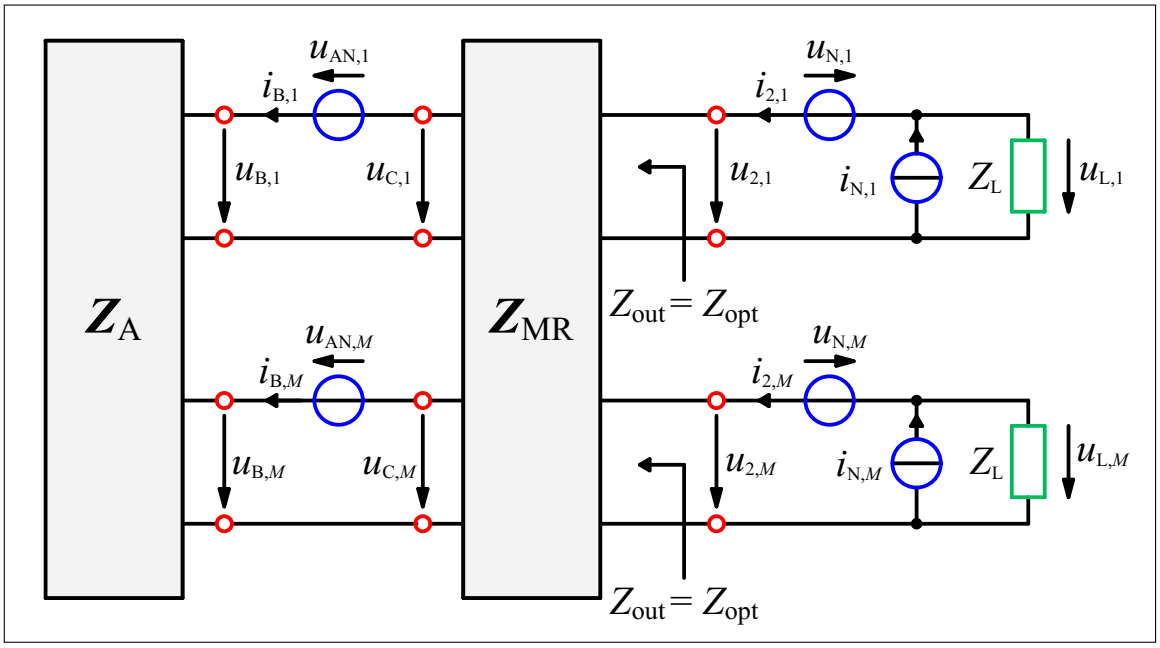

Source: The author.

$$\boldsymbol{u}_2 = \boldsymbol{Z}_{\mathrm{RT}}\boldsymbol{i}_1 + \boldsymbol{Z}_{\mathrm{R}}\boldsymbol{i}_2,$$
$$\boldsymbol{u}_2 = \boldsymbol{Z}_{\mathrm{RT}}\boldsymbol{i}_1 + Z_{\mathrm{opt}}\boldsymbol{i}_2 \implies \boldsymbol{Z}_{\mathrm{R}} = Z_{\mathrm{opt}}\boldsymbol{I}_M. \tag{2.78}$$

This is also important because, due to mutual coupling in the Rx-UCA, if the antenna ports are not decoupled for the LNAs, the intrinsic noise in one port will be radiated to the others.

The key for achieving noise matching is to find the Z_{opt} optimal impedance considering a single antenna receiver and, then, to extend it to the multi-antenna scenario, using the identity of the $\boldsymbol{Z}_{\mathrm{R}}$ matrix in (2.78). After obtaining $\boldsymbol{Z}_{\mathrm{R}}$, using (2.29), the elements of $\boldsymbol{Z}_{\mathrm{MR}}$ and, consequently, the architecture of the Rx-DMN can be determined.

At first, the model in Fig. 3 is simplified to comprise only one antenna on the receive side, producing Fig. 6, a multiple-input-single-output (MISO) system. The Helmholtz-Thévenin theorem (JOHNSON, 2003) is applied to this model to simplify it even further in order to substitute the $\boldsymbol{Z}_{\mathrm{A}}$ block and everything preceding it by a voltage source and a series impedance connected to the output port of $\boldsymbol{Z}_{\mathrm{A}}$.

To compute this equivalent model, the voltage source must have the same electromotive force as the open-circuit voltage of the circuit to be simplified. The latter produces u_{B}, which does not have any particular value, so the equivalent voltage source is called u_{S} to stand for the signals received by the receive antenna.

The next step of the Helmholtz-Thévenin theorem is to substitute every voltage and current sources by short- and open-circuits, respectively, in order to compute the output impedance of the $\boldsymbol{Z}_{\mathrm{A}}$ impedance matrix. Considering $\boldsymbol{u}_{\mathrm{G}} = \boldsymbol{0}_N$ V (short-circuits now) and letting the current i_{B} flow, from (2.17)

$$\begin{aligned} &u_{\mathrm{B}} = \boldsymbol{Z}_{\mathrm{ART}}\boldsymbol{i}_{\mathrm{A}} + Z_{\mathrm{AR}}i_{\mathrm{B}},\ \boldsymbol{i}_{\mathrm{A}} = \boldsymbol{0}\,\mathrm{A}, \\ &u_{\mathrm{B}} = Z_{\mathrm{AR}}i_{\mathrm{B}} \implies (\boldsymbol{Z}_{\mathrm{A}})_{\mathrm{out}} = \frac{u_{\mathrm{B}}}{i_{\mathrm{B}}} = Z_{\mathrm{AR}}, \end{aligned} \tag{2.79}$$

the output impedance, whose value is the same of the Helmholtz-Thévenin equivalent impedance, is obtained. The equivalent receive side model is, then, represented in Fig. 7.

Figure 6 – Model of the MISO system.

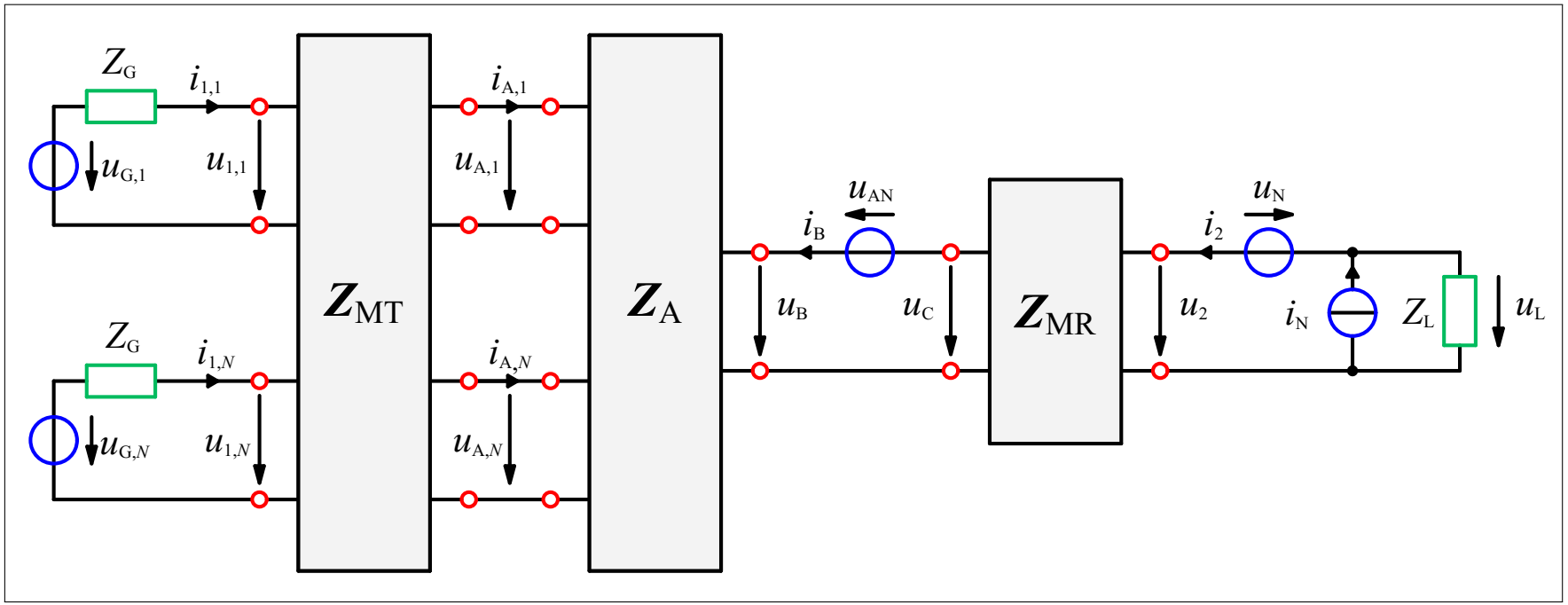

Source: The author.

Figure 7 – Model of the single-antenna receiver.

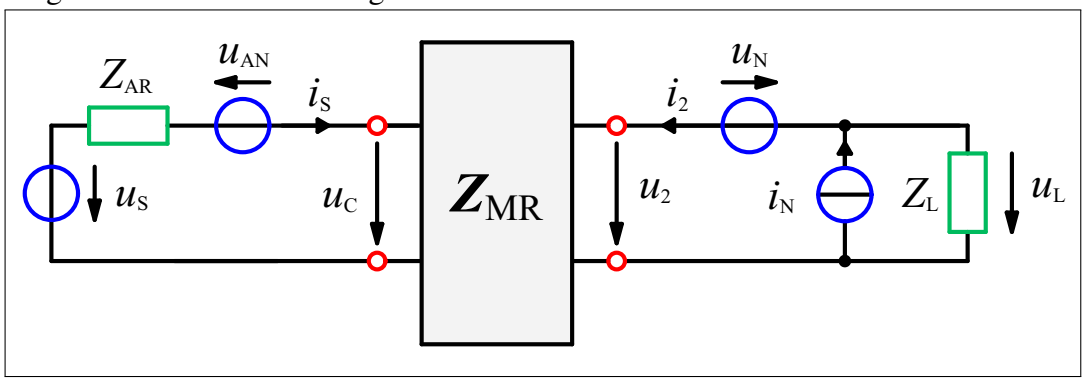

Source: The author, adapted from (IVRLAČ, 2017).

The $\boldsymbol{Z}_{MR}$ matching twoport transforms the antenna impedance Z_{AR} into a new one which is presented to the input of the noisy LNA. This output impedance of $\boldsymbol{Z}_{MR}$, referred to as Z'_{AR}, is the impedance which can be optimized to produce the smallest noise figure of the LNA. This computation demands the SNR, calculated using the powers of the noiseless signal, of the extrinsic noise–both transformed by $\boldsymbol{Z}_{MR}$–and of the intrinsic noise.

Helmholtz-Thévenin theorem is applied again, producing the model in Fig. 8 possessing these transformed variables. It is necessary to compute the relations between the transformed sources u'_S and u'_{AN} and their original counterparts. Since the matching twoport is a linear circuit, these two relations are the same, because the sources are connected in series.

Figure 8 – Helmholtz-Thévenin equivalent of the model in Fig. 7.

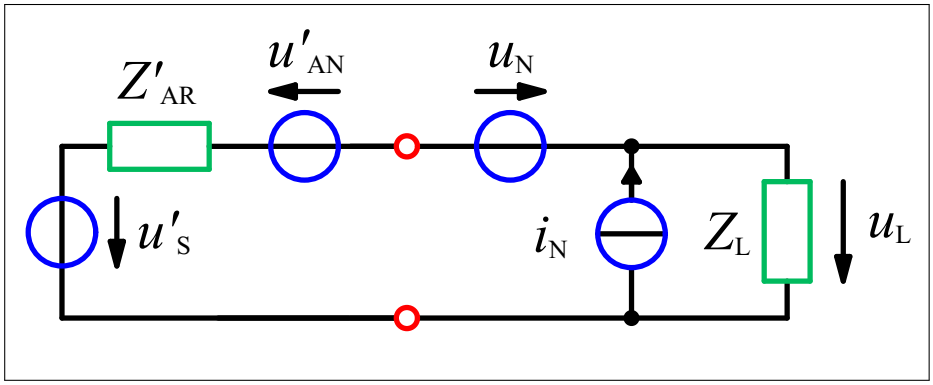

Source: The author, adapted from (IVRLAČ, 2017).

For this end, the twoport matrix equation of $\boldsymbol{Z}_{MR}$, (2.18), is applied in the single receive antenna model in Fig. 7 to read as

$$\begin{bmatrix} u_2 \\ u_C \end{bmatrix} = j \begin{bmatrix} a & b \\ b & c \end{bmatrix} \begin{bmatrix} i_2 \\ i_S \end{bmatrix}, \tag{2.80}$$

with $\{a, b, c\} \in \mathbb{R}\,\Omega$, because $\boldsymbol{Z}_{\mathrm{MR}}$ is a reciprocal and lossless network. To compute u'_{S}, the superposition theorem is used to deactivate the u_{AN} source. Then, it is noticed that the Helmholtz-Thévenin equivalent source u'_{S} is equal to the open-circuit voltage at the output of $\boldsymbol{Z}_{\mathrm{MR}}$ in Fig. 7. Due to the open-circuit computation, $i_2 = 0\,\mathrm{A}$, and the matrix equation above

$$
\begin{aligned}
&u_2 = u'_{\mathrm{S}} = jbi_{\mathrm{S}},\\
&u_{\mathrm{C}} = u_{\mathrm{S}} - Z_{\mathrm{AR}} i_{\mathrm{S}} = jci_{\mathrm{S}},\ i_{\mathrm{S}} = \frac{u_{\mathrm{S}}}{Z_{\mathrm{AR}} + jc},\\
&\implies u'_{\mathrm{S}} = \frac{jb}{Z_{\mathrm{AR}} + jc} u_{\mathrm{S}}.
\end{aligned}
\tag{2.81}
$$

Taking back the argument that, in Fig. 7, u_{S} and u_{AN} are connected in series and $\boldsymbol{Z}_{\mathrm{MR}}$ is a linear twoport, resulting in the same way it transforms the voltage sources,

$$
u'_{\mathrm{AN}} = \frac{jb}{Z_{\mathrm{AR}} + jc} u_{\mathrm{AN}}. \tag{2.82}
$$

To compute the equivalent series impedance Z'_{AR}, all voltage and current sources in Fig. 7 are respectively substituted by short- and open-circuits and the current i_2 is forced in the port to compute the output impedance of $\boldsymbol{Z}_{\mathrm{MR}}$ with (2.80)

$$
\begin{aligned}
&u_{\mathrm{C}} = -Z_{\mathrm{AR}} i_{\mathrm{S}} = jbi_2 + jci_{\mathrm{S}},\ i_{\mathrm{S}} = \frac{-jb}{Z_{\mathrm{AR}} + jc} i_2,\\
&u_2 = jai_2 + jbi_{\mathrm{S}} = \left(ja + \frac{b^2}{Z_{\mathrm{AR}} + jc} \right) i_2,\\
&\implies Z'_{\mathrm{AR}} = (\boldsymbol{Z}_{\mathrm{MR}})_{\mathrm{out}} = \frac{u_2}{i_2} = ja + \frac{b^2}{Z_{\mathrm{AR}} + jc}.
\end{aligned}
\tag{2.83}
$$

For the computation of the SNR, the noiseless signal and the extrinsic signal powers of the equivalent model in Fig. 8 are needed,

$$
\begin{aligned}
&\mathbb{E}\left[|u'_{\mathrm{S}}|^2 \right] = \mathbb{E}\left[|u_{\mathrm{S}}|^2 \right] \left(\frac{b^2}{\mathrm{Re}(Z_{\mathrm{AR}})^2 + (\mathrm{Im}(Z_{\mathrm{AR}}) + jc)^2} \right),\\
&\mathbb{E}\left[|u'_{\mathrm{AN}}|^2 \right] = \mathbb{E}\left[|u_{\mathrm{AN}}|^2 \right] \left(\frac{b^2}{\mathrm{Re}(Z_{\mathrm{AR}})^2 + (\mathrm{Im}(Z_{\mathrm{AR}}) + jc)^2} \right).
\end{aligned}
\tag{2.84}
$$

As it turns out, this multiplying fraction can be substituted by another fraction which bears values independent of the $\boldsymbol{Z}_{\mathrm{MR}}$ elements,

$$\begin{aligned}
\mathrm{Re}\left(Z'_{\mathrm{AR}}\right) &= \mathrm{Re}\left(ja + \frac{b^2 Z^*_{\mathrm{AR}}}{\mathrm{Re}(Z_{\mathrm{AR}})^2 + (\mathrm{Im}(Z_{\mathrm{AR}}) + jc)^2}\right), \\
\mathrm{Re}\left(Z'_{\mathrm{AR}}\right) &= \mathrm{Re}(Z_{\mathrm{AR}})\frac{b^2}{\mathrm{Re}(Z_{\mathrm{AR}})^2 + (\mathrm{Im}(Z_{\mathrm{AR}}) + jc)^2}, \\
\frac{\mathrm{Re}\left(Z'_{\mathrm{AR}}\right)}{\mathrm{Re}(Z_{\mathrm{AR}})} &= \frac{b^2}{\mathrm{Re}(Z_{\mathrm{AR}})^2 + (\mathrm{Im}(Z_{\mathrm{AR}}) + jc)^2},
\end{aligned} \tag{2.85}$$

leading to the relations between the powers of the transformed voltage sources and their original counterparts as functions only of the receive antenna self-impedance and of its transformed impedance presented by the Rx-DMN

$$\begin{aligned}
\mathbb{E}\left[|u'_{\mathrm{S}}|^2\right] &= \mathbb{E}\left[|u_{\mathrm{S}}|^2\right]\frac{\mathrm{Re}\left(Z'_{\mathrm{AR}}\right)}{\mathrm{Re}(Z_{\mathrm{AR}})}, \\
\mathbb{E}\left[|u'_{\mathrm{AN}}|^2\right] &= \mathbb{E}\left[|u_{\mathrm{AN}}|^2\right]\frac{\mathrm{Re}\left(Z'_{\mathrm{AR}}\right)}{\mathrm{Re}(Z_{\mathrm{AR}})}.
\end{aligned} \tag{2.86}$$

Finally, the SNR can be calculated using the simplified model in Fig. 8. At the input of the noiseless LNA, being u_{LS} the noiseless received signal while the received noise is u_{LN},

$$\begin{aligned}
u_{\mathrm{L}} &= u_{\mathrm{LS}} + u_{\mathrm{LN}}, \\
\mathrm{SNR} &= \frac{\mathbb{E}\left[|(u_{\mathrm{L}} \mid u_{\mathrm{LN}} = 0)|^2\right]}{\mathbb{E}\left[|(u_{\mathrm{L}} \mid u_{\mathrm{LS}} = 0)|^2\right]} = \frac{\mathbb{E}\left[|u_{\mathrm{LS}}|^2\right]}{\mathbb{E}\left[|u_{\mathrm{LN}}|^2\right]}.
\end{aligned} \tag{2.87}$$

According to the circuit analysis in Fig. 8, the voltage divider of the impedances Z'_{AR} and Z_{L} yields

$$\begin{aligned}
u_{\mathrm{LS}} &= u'_{\mathrm{S}}\frac{Z_{\mathrm{L}}}{Z_{\mathrm{L}} + Z'_{\mathrm{AR}}}, \\
u_{\mathrm{LN}} &= (u'_{\mathrm{AN}} - u_{\mathrm{N}} + Z'_{\mathrm{AR}} i_{\mathrm{N}})\frac{Z_{\mathrm{L}}}{Z_{\mathrm{L}} + Z'_{\mathrm{AR}}}, \\
\mathrm{SNR} &= \frac{\mathbb{E}\left[|u'_{\mathrm{S}}|^2 |Z_{\mathrm{L}}/(Z_{\mathrm{L}} + Z'_{\mathrm{AR}})|^2\right]}{\mathbb{E}\left[|u'_{\mathrm{AN}} - u_{\mathrm{N}} + Z'_{\mathrm{AR}} i_{\mathrm{N}}|^2 |Z_{\mathrm{L}}/(Z_{\mathrm{L}} + Z'_{\mathrm{AR}})|^2\right]} = \frac{\mathbb{E}\left[|u'_{\mathrm{S}}|^2\right]}{\mathbb{E}\left[|u'_{\mathrm{AN}} - u_{\mathrm{N}} + Z'_{\mathrm{AR}} i_{\mathrm{N}}|^2\right]}.
\end{aligned} \tag{2.88}$$

Alternatively, the Z_{L} load voltage modelling the input impedance of the LNA could be substituted by a noiseless multiport and an open-circuit, as was done in (IVRLAČ, 2017), whose output voltage would simply be an amplification of its input voltage by an established

factor, being equal to $u_{\mathrm{LNA_{output}}} = \xi u_{\mathrm{L}} = \xi(u_{\mathrm{LS}} + u_{\mathrm{LN}})$. However, this would not make any difference in the computation of the SNR, because no noise would be added

$$\mathrm{SNR} = \frac{\mathbb{E}\left[|(u_{\mathrm{LNA_{output}}} \mid \xi u_{\mathrm{LN}} = 0)|^2\right]}{\mathbb{E}\left[|(u_{\mathrm{LNA_{output}}} \mid \xi u_{\mathrm{LS}} = 0)|^2\right]} = \frac{|\xi|^2\mathbb{E}\left[|u_{\mathrm{LS}}|^2\right]}{|\xi|^2\mathbb{E}\left[|u_{\mathrm{LN}}|^2\right]} = \frac{\mathbb{E}\left[|u'_{\mathrm{S}}|^2\right]}{\mathbb{E}\left[|u'_{\mathrm{AN}} - u_{\mathrm{N}} + Z'_{\mathrm{AR}} i_{\mathrm{N}}|^2\right]}. \tag{2.89}$$

The statistical properties described in (2.12), (2.13), (2.14) and (2.15), although written in vector and matrix form for multi-antenna systems, are applicable for single-antenna receivers as well to have

$$\begin{aligned}\mathbb{E}\left[|u'_{\mathrm{AN}} - u_{\mathrm{N}} + Z'_{\mathrm{AR}} i_{\mathrm{N}}|^2\right] &= \mathbb{E}\left[|u'_{\mathrm{AN}}|^2\right] - 2\mathbb{E}\left[\mathrm{Re}(u'_{\mathrm{AN}} u^*_{\mathrm{N}})\right] + 2\mathbb{E}\left[\mathrm{Re}(u'_{\mathrm{AN}} Z'^*_{\mathrm{AR}} i^*_{\mathrm{N}})\right] + \\ &\quad + \mathbb{E}\left[|u_{\mathrm{N}}|^2\right] + |Z'_{\mathrm{AR}}|^2\mathbb{E}\left[|i_{\mathrm{N}}|^2\right] - 2\mathbb{E}\left[\mathrm{Re}(Z'_{\mathrm{AR}} i_{\mathrm{N}} u^*_{\mathrm{N}})\right] \\ \mathbb{E}\left[|u'_{\mathrm{AN}} - u_{\mathrm{N}} + Z'_{\mathrm{AR}} i_{\mathrm{N}}|^2\right] &= 4kT\Delta_f \,\mathrm{Re}(Z'_{\mathrm{AR}}) + \sigma_u^2 + |Z'_{\mathrm{AR}}|^2\sigma_i^2 - 2\sigma_u\sigma_i \,\mathrm{Re}(Z'_{\mathrm{AR}}\rho^*).\end{aligned} \tag{2.90}$$

Now it is possible to further develop the SNR equation in (2.88) (or (2.89)) using (2.86) and (2.90)

$$\begin{aligned}\mathrm{SNR} &= \frac{\mathbb{E}\left[|u_{\mathrm{S}}|^2\right]\mathrm{Re}(Z'_{\mathrm{AR}})/\mathrm{Re}(Z_{\mathrm{AR}})}{4kT\Delta_f \,\mathrm{Re}(Z'_{\mathrm{AR}}) + \sigma_u^2 + |Z'_{\mathrm{AR}}|^2\sigma_i^2 - 2\sigma_u\sigma_i \,\mathrm{Re}(Z'_{\mathrm{AR}}\rho^*)}, \\ \mathrm{SNR} &= \frac{\mathbb{E}\left[|u_{\mathrm{S}}|^2\right]\mathrm{Re}(Z'_{\mathrm{AR}})/\mathrm{Re}(Z_{\mathrm{AR}})}{4kT\Delta_f \,\mathrm{Re}(Z'_{\mathrm{AR}})\left[1 + \frac{\sigma_u^2 + |Z'_{\mathrm{AR}}|^2\sigma_i^2 - 2\sigma_u\sigma_i \,\mathrm{Re}(Z'_{\mathrm{AR}}\rho^*)}{4kT\Delta_f \,\mathrm{Re}(Z'_{\mathrm{AR}})}\right]}, \\ \mathrm{SNR} &= \frac{\mathbb{E}\left[|u_{\mathrm{S}}|^2\right]/4kT\Delta_f \,\mathrm{Re}(Z_{\mathrm{AR}})}{1 + \frac{\sigma_u^2 + |Z'_{\mathrm{AR}}|^2\sigma_i^2 - 2\sigma_u\sigma_i \,\mathrm{Re}(Z'_{\mathrm{AR}}\rho^*)}{4kT\Delta_f \,\mathrm{Re}(Z'_{\mathrm{AR}})}}.\end{aligned} \tag{2.91}$$

This last form of the SNR leads to the determination of the noise figure NF, from the definition in (FRIIS, 1944) and the formulation in (IVRLAČ; NOSSEK, 2010)

$$\begin{aligned}\mathrm{SNR} &= \frac{\mathrm{SNR_{available}}}{\mathrm{NF}}, \\ \mathrm{SNR_{available}} &= \frac{\mathbb{E}\left[|u_{\mathrm{S}}|^2\right]}{4kT\Delta_f \,\mathrm{Re}(Z_{\mathrm{AR}})}, \\ \mathrm{NF} &= 1 + \frac{\sigma_u^2 + |Z'_{\mathrm{AR}}|^2\sigma_i^2 - 2\sigma_u\sigma_i \,\mathrm{Re}(Z'_{\mathrm{AR}}\rho^*)}{4kT\Delta_f \,\mathrm{Re}(Z'_{\mathrm{AR}})}.\end{aligned} \tag{2.92}$$

The $\mathrm{SNR_{available}}$ is the SNR on the antenna element loaded by the noiseless LNA. As it can be seen in its formula, it relates the receive signal power with the background radiation

noise power. $\mathrm{SNR}_{\mathrm{available}}$ is the maximum SNR available from the output of the antennas before the noisy signal is passed through the LNA. If the latter is noiseless, then $\mathrm{SNR}_{\mathrm{available}}$ is also the SNR achieved at its output.

Since the low-noise amplifier (LNA) possesses noise, this available SNR is decreased by the factor of the noise figure NF. This is, then, a measure of how much SNR is lost due to the noise introduced by the circuitry in the LNA. This is also the measure that the strategy of noise matching aims to reduces to the maximum by selecting the proper impedance the matching twoport Z_{MR} will transform the antenna impedance into.

To do so, the real and the imaginary parts of Z'_{AR} need to be determined. The formula of the noise figure in (2.92) can be simplified to isolate the Z'_{AR} in one fraction

$$\begin{aligned}
\mathrm{NF} &= 1 + \frac{\sigma_i^2}{4kT\Delta_f}\left\{\frac{R_N^2 + |Z'_{\mathrm{AR}}|^2 - 2R_N\,\mathrm{Re}(Z'_{\mathrm{AR}}\rho^*)}{\mathrm{Re}(Z'_{\mathrm{AR}})}\right\},\\
\mathrm{NF} &= 1 + \frac{\sigma_i^2}{4kT\Delta_f}\left\{\frac{R_N^2 + \mathrm{Re}(Z'_{\mathrm{AR}})^2 + \mathrm{Im}(Z'_{\mathrm{AR}})^2}{\mathrm{Re}(Z'_{\mathrm{AR}})} + \right.\\
&\qquad\left. - \frac{2R_N[\mathrm{Re}(Z'_{\mathrm{AR}})\,\mathrm{Re}(\rho) + \mathrm{Im}(Z'_{\mathrm{AR}})\,\mathrm{Im}(\rho)]}{\mathrm{Re}(Z'_{\mathrm{AR}})}\right\}.
\end{aligned} \tag{2.93}$$

Taking the partial derivatives of NF in terms of the real and imaginary parts of the transformed antenna impedance Z'_{AR}

$$\frac{\partial \mathrm{NF}}{\partial\,\mathrm{Re}(Z'_{\mathrm{AR}})} = \frac{\sigma_i^2}{4kT\Delta_f}\left[\frac{\mathrm{Re}(Z'_{\mathrm{AR}})^2 - \mathrm{Im}(Z'_{\mathrm{AR}})^2 + 2R_N\,\mathrm{Im}(Z'_{\mathrm{AR}})\,\mathrm{Im}(\rho) - R_N^2}{\mathrm{Re}(Z'_{\mathrm{AR}})^2}\right], \tag{2.94}$$

$$\frac{\partial \mathrm{NF}}{\partial\,\mathrm{Im}(Z'_{\mathrm{AR}})} = \frac{\sigma_i^2}{4kT\Delta_f}\left[\frac{\mathrm{Im}(Z'_{\mathrm{AR}}) - \mathrm{Im}(\rho)R_N}{\mathrm{Re}(Z'_{\mathrm{AR}})}\right], \tag{2.95}$$

the optimal value of Z'_{AR} can be found by comparing these derivatives to zero

$$\frac{\partial \mathrm{NF}}{\partial\,\mathrm{Im}(Z'_{\mathrm{AR}})} = 0 \implies \mathrm{Im}(Z'_{\mathrm{AR}}) = \mathrm{Im}(\rho)R_N, \tag{2.96}$$

$$\left.\begin{aligned}\frac{\partial \mathrm{NF}}{\partial\,\mathrm{Re}(Z'_{\mathrm{AR}})} &= 0\\ \mathrm{Im}(Z'_{\mathrm{AR}}) &= \mathrm{Im}(\rho)R_N\end{aligned}\right\} \implies \mathrm{Re}(Z'_{\mathrm{AR}}) = \pm R_N\sqrt{1 - \mathrm{Im}(\rho)^2}. \tag{2.97}$$

Still, the real part of Z'_{AR} which minimizes the noise figure can't yet be determined. For this purpose, since this process is involving two derivatives of the noise figure with two different variables, the Hessian matrix must be used

$$\mathbf{H}(\mathrm{NF}) = \begin{bmatrix} \dfrac{\partial^2 \mathrm{NF}}{\partial^2 \operatorname{Re}(Z'_{\mathrm{AR}})} & \dfrac{\partial^2 \mathrm{NF}}{\partial \operatorname{Im}(Z'_{\mathrm{AR}}) \partial \operatorname{Re}(Z'_{\mathrm{AR}})} \\ \dfrac{\partial^2 \mathrm{NF}}{\partial \operatorname{Re}(Z'_{\mathrm{AR}}) \partial \operatorname{Im}(Z'_{\mathrm{AR}})} & \dfrac{\partial^2 \mathrm{NF}}{\partial^2 \operatorname{Im}(Z'_{\mathrm{AR}})} \end{bmatrix}. \tag{2.98}$$

For the values in (2.96) and (2.97) applied in the Hessian matrix it holds

$$\mathbf{H}(\mathrm{NF}) = \frac{\pm\sigma_i^2}{2kT\Delta_f R_N \sqrt{1 - \operatorname{Im}(\rho)^2}} \boldsymbol{I}_2. \tag{2.99}$$

In order to find the minimum of NF, $\mathbf{H}(\mathrm{NF})$ needs to be positive semi-definite in that point, i.e. to hold the positive sign in (2.99). This is held when (2.97) is positive, arriving at the optimal value of the real part of Z'_{AR}. Finally, for $Z'_{\mathrm{AR}} = Z_{\mathrm{opt}}$

$$Z_{\mathrm{opt}} = R_N \left(\sqrt{1 - \operatorname{Im}(\rho)^2} + j \operatorname{Im}(\rho) \right). \tag{2.100}$$

Two interesting features of Z_{opt} mentioned in (IVRLAČ, 2017) are that it does not depend on the real part of the intrinsic noise current and voltage sources correlation coefficient and that its absolute value is equal to the intrinsic noise resistance R_N for any value of ρ.

Resuming the noise matching strategy in (2.78), with the identity of Z_{opt} in (2.100) for a single-antenna receiver derived, it can be applied to extend the noise matching result to a multi-antenna system. With (2.29), the Rx-DMN can be designed to guarantee decoupling of the receive antenna ports and matching of their impedances to the receive low-noise amplifiers

$$\begin{aligned} &\boldsymbol{Z}_{\mathrm{R}} = Z_{\mathrm{opt}} \boldsymbol{I}_N, \\ &\boldsymbol{Z}_{\mathrm{MR}_{1,1}} - \boldsymbol{Z}_{\mathrm{MR}_{1,2}} (\boldsymbol{Z}_{\mathrm{AR}} + \boldsymbol{Z}_{\mathrm{MR}_{2,2}})^{-1} \boldsymbol{Z}_{\mathrm{MR}_{2,1}} = Z_{\mathrm{opt}} \boldsymbol{I}_N. \end{aligned} \tag{2.101}$$

The design of the Rx-DMN, like that of the Tx-DMN, is not fixed to one specific design. There is some degree of freedom in designing it. Since the equations of $\boldsymbol{Z}_{\mathrm{T}}$ (2.24) and $\boldsymbol{Z}_{\mathrm{R}}$ (2.29) have similar forms regarding their block matrices structures, and both aim to achieve

scaled identities for their specific purposes, the design adopted here is analog to that of the $\boldsymbol{Z}_{\mathrm{MT}}$ (2.70) and is the same of (IVRLAČ; NOSSEK, 2010)

$$\boldsymbol{Z}_{\mathrm{MR}} = \begin{bmatrix} \boldsymbol{Z}_{\mathrm{MR}_{1,1}} & \boldsymbol{Z}_{\mathrm{MR}_{1,2}} \\ \boldsymbol{Z}_{\mathrm{MR}_{2,1}} & \boldsymbol{Z}_{\mathrm{MR}_{2,2}} \end{bmatrix} = \begin{bmatrix} j\mathrm{Im}\left(Z_{\mathrm{opt}}\right)\boldsymbol{I}_M & j\sqrt{\mathrm{Re}(Z_{\mathrm{opt}})}\mathrm{Re}(\boldsymbol{Z}_{\mathrm{AR}})^{1/2} \\ j\sqrt{\mathrm{Re}(Z_{\mathrm{opt}})}\mathrm{Re}(\boldsymbol{Z}_{\mathrm{AR}})^{1/2} & -j\mathrm{Im}(\boldsymbol{Z}_{\mathrm{AR}}) \end{bmatrix}. \tag{2.102}$$

With the complete architecture of the Rx-DMN, it is possible to write the noise covariance matrix $\boldsymbol{R}_{\boldsymbol{\eta}}$, from (2.53), for the DMNs operating optimally, i.e. providing decoupled and noise matched antenna ports for the system

$$\boldsymbol{R}_{\boldsymbol{\eta}} = \frac{|Z_{\mathrm{L}}|^2}{R_{\mathrm{L}}|Z_{\mathrm{L}} + Z_{\mathrm{opt}}|^2}\left[4kT\Delta_f \mathrm{Re}\left(Z_{\mathrm{opt}}\right) + \sigma_u^2 + \sigma_i^2|Z_{\mathrm{opt}}|^2 - 2\sigma_u\sigma_i\,\mathrm{Re}(\rho Z_{\mathrm{opt}}^*)\right]\boldsymbol{I}_M. \tag{2.103}$$

2.2.3.3 The Topology of the Networks

The features of the decoupling and matching networks described so far have led to the design of two impedance matrices in (2.70) and (2.102). Not only is the design of these impedances not limited to the designs adopted as they don't have all of the information necessary to fully characterize a DMN. One of these informations needed is the topology of the networks from the circuit theoretic perspective, i.e. the layout of the circuits.

Observing that one impedance matrix does not correspond, necessarily, to only one topology, one circuit layout must be chosen to provide the desired effects of decoupling and matching the ports. Given a multiport impedance matrix, it is possible to adopt different strategies to determine suitable circuit layouts. The strategy adopted here uses the π-structure as the building block of the DMN's topology.

The π-structure, as depicted in Fig. 9 from the perspective of a twoport, consists of three admittances: two shunt admittances $\gamma_{1,1}$ and $\gamma_{2,2}$ connected to the input and to the output ports, respectively, and one series admittances $\gamma_{1,2}$ connected, from each side, to the upper nodes of the shunt admittances. These latter share the same reference node with the two ports.

Impedance matrices do not characterize easily π-structures. For them, admittance matrices are more natural to be determined due to the disposition of the shunt and series

Figure 9 – π-topology in a two-port network.

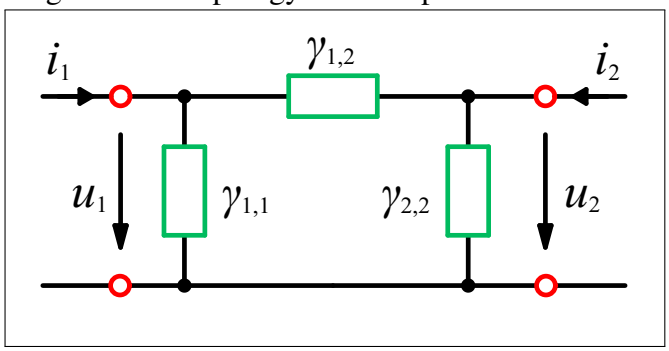

Source: The author.

Figure 10 – π-topology in a three-port network.

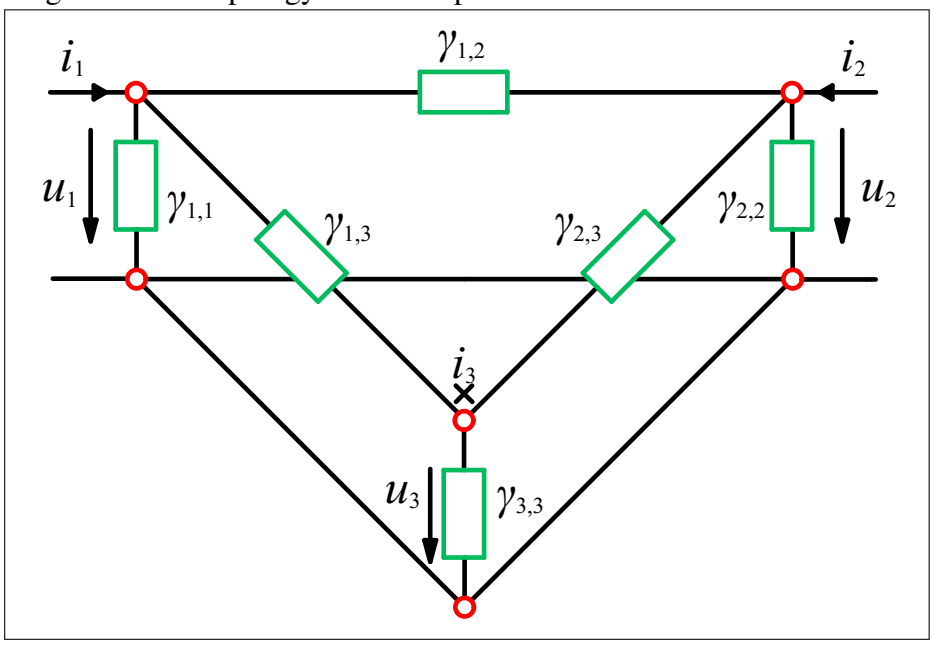

Source: The author.

admittances. Considering the π-structures in the three-port in Fig. 10, its admittance matrix

$$\begin{bmatrix} i_1 \\ i_2 \\ i_3 \end{bmatrix} = \begin{bmatrix} y_{1,1} & y_{1,2} & y_{1,3} \\ y_{2,1} & y_{2,2} & y_{2,3} \\ y_{3,1} & y_{3,2} & y_{3,3} \end{bmatrix} \begin{bmatrix} u_1 \\ u_2 \\ u_3 \end{bmatrix} \tag{2.104}$$

can be determined element-wise. It is important to notice that, while γ refers to the admittance of a lumped element in the network, y represents an admittance in the admittance matrix

representation of the same network. At first, the diagonal elements are computed as follows

$$\begin{aligned} y_{1,1} &= \left.\frac{i_1}{u_1}\right|_{u_2=u_3=0\,\mathrm{V}}, \\ y_{2,2} &= \left.\frac{i_2}{u_2}\right|_{u_1=u_3=0\,\mathrm{V}}, \\ y_{3,3} &= \left.\frac{i_3}{u_3}\right|_{u_1=u_2=0\,\mathrm{V}}. \end{aligned} \tag{2.105}$$

Considering one arbitrary port, when the other two port voltages are equal to zero, then its port voltage is being applied in parallel over the shunt and series elements connected to it. Thus, the current of this port is equal to the sum of the currents that flow through each of these elements. These currents are equal to the port voltage times the admittances of the elements through which they flow, resulting in

$$\begin{aligned} i_1 &= \gamma_{1,1}u_1 + \gamma_{1,2}u_1 + \gamma_{1,3}u_1 \implies y_{1,1} = \gamma_{1,1} + \gamma_{1,2} + \gamma_{1,3}, \\ i_2 &= \gamma_{2,2}u_2 + \gamma_{1,2}u_2 + \gamma_{2,3}u_2 \implies y_{2,2} = \gamma_{2,2} + \gamma_{1,2} + \gamma_{2,3}, \\ i_3 &= \gamma_{3,3}u_3 + \gamma_{1,3}u_3 + \gamma_{2,3}u_3 \implies y_{3,3} = \gamma_{3,3} + \gamma_{1,3} + \gamma_{2,3}. \end{aligned} \tag{2.106}$$

For the non-diagonal elements, ports 1 and 2 and the admittance $y_{1,2}$ are considered as examples. This admittance is calculated making the voltages of ports 1 and 3 equal to zero. The port voltage u_2 over the admittance $\gamma_{1,2}$ produces a current which flows in the opposite direction of the current i_2, but has the same intensity. Since u_1 and u_3 are equal to 0 V, the series admittance $\gamma_{1,3}$ is short-circuited and, thus, all of the current i_2 flows through $\gamma_{1,2}$.

$$y_{i,j} = \left.\frac{i_i}{u_j}\right|_{u_i=u_k=0\,\mathrm{V}} = \frac{-\gamma_{i,j}u_j}{u_j} = -\gamma_{i,j},\ i \neq j \neq k. \tag{2.107}$$

Finally, for the three-port π-structure in Fig. 10, the admittance matrix is

$$\begin{bmatrix} i_1 \\ i_2 \\ i_3 \end{bmatrix} = \begin{bmatrix} \gamma_{1,1} + \gamma_{1,2} + \gamma_{1,3} & -\gamma_{1,2} & -\gamma_{1,3} \\ -\gamma_{1,2} & \gamma_{2,2} + \gamma_{1,2} + \gamma_{2,3} & -\gamma_{2,3} \\ -\gamma_{1,3} & -\gamma_{2,3} & \gamma_{3,3} + \gamma_{1,3} + \gamma_{2,3} \end{bmatrix} \begin{bmatrix} u_1 \\ u_2 \\ u_3 \end{bmatrix}. \tag{2.108}$$

This procedure can be extended to the determination of the admittance matrix of arbitrarily large circuits with any number of ports connected between themselves with π-structures.

According to Fig. 3, the transmit decoupling and matching network is composed of $2N$ ports, N on one side connected to each of the transmit antennas and N on the other side connected to the N High-Power Amplifiers. On the receive side, each of the M receive antennas has its signals transmitted to a Low-Noise Amplifier, with the receive DMN sitting between these groups of elements, thus, possessing $2M$ ports.

Following the same logic of the three-port in a π-topology, for a $2N$-port

$$\begin{bmatrix} y_{1,1} & y_{1,2} & \cdots & y_{1,2N} \\ y_{2,1} & y_{2,2} & \cdots & y_{2,2N} \\ \vdots & \vdots & \vdots & \vdots \\ y_{2N,1} & y_{2N,2} & \cdots & y_{2N,2N} \end{bmatrix} = \begin{bmatrix} \gamma_{1,1}+\gamma_{1,2}+\ldots+\gamma_{1,2N} & -\gamma_{1,2} & \cdots & -\gamma_{1,2N} \\ -\gamma_{2,1} & \gamma_{2,1}+\gamma_{2,2}+\ldots+\gamma_{2,2N} & \cdots & -\gamma_{2,2N} \\ \vdots & \vdots & \vdots & \vdots \\ -\gamma_{2N,1} & -\gamma_{2N,2} & \cdots & \gamma_{2N,1}+\gamma_{2N,2}+\ldots+\gamma_{2N,2N} \end{bmatrix} \tag{2.109}$$

where $\gamma_{i,j} = \gamma_{j,i}$, $\forall i, j$, is the shunt admittance of port i if $i = j$ or the series admittance between the ports i and j if $i \neq j$.

Departing from the point of view of the decoupling and matching architectures of the DMNs, their designed impedance matrices can be inverted to obtain admittance matrices, which can be used to determine the values of the DMNs' lumped circuit elements connected in the π-topology. For this matter,

$$\mathbf{\Gamma} = \begin{bmatrix} y_{1,1}+y_{1,2}+\ldots+y_{1,2N} & -y_{1,2} & \cdots & -y_{1,2N} \\ -y_{2,1} & y_{2,1}+y_{2,2}+\ldots+y_{2,2N} & \cdots & -y_{2,2N} \\ \vdots & \vdots & \vdots & \vdots \\ -y_{2N,1} & -y_{2N,2} & \cdots & y_{2N,1}+y_{2N,2}+\ldots+y_{2N,2N} \end{bmatrix} \tag{2.110}$$

the matrix $\mathbf{\Gamma}$ containing the lumped elements' admittances is computed first, where $(\mathbf{\Gamma})_{i,j} = \gamma_{i,j}$.

Before continuing, it is worth to highlight that, in the $\mathbf{\Gamma}$ matrix, the admittance $\gamma_{i,j}$, $i \neq j$ is the admittance of the reactive element between ports i and j. Thus, not only

$$\gamma_{i,j} = -y_{i,j} = -y_{j,i} = \gamma_{j,i},\ i \neq j, \tag{2.111}$$

holds for the series lumped elements' admittances due to the reciprocity of the network, as $\gamma_{i,j}$ and $\gamma_{j,i}$ actually refer to the same circuit element inserted in the network, and for all i and j.

This is possible because the reciprocal nature of the decoupling and matching networks only demand three degrees of freedom to fully determine the impedances (or admittances) between any two given ports. The π-structures, modelled each for a pair of ports, provide this degree of freedom with their three elements whose values may be freely chosen to match the desired impedances for every combination of two ports in the multiport network.

Finally, if the imaginary part of a given admittance, $\mathrm{Im}(\gamma)$, is positive, then it is of a capacitor, else it is the admittance of an inductor. The capacitances and inductances are determined for a fixed value of frequency, which is the center frequency of the system

$$\begin{aligned} \mathrm{Im}(\gamma) > 0 &\implies C = -j\frac{\gamma}{\omega_\mathrm{c}} = \frac{\mathrm{Im}(\gamma)}{\omega_\mathrm{c}}\,\mathrm{F}, \\ \mathrm{Im}(\gamma) < 0 &\implies L = -j\frac{1}{\omega_\mathrm{c}\gamma} = -\frac{1}{\omega_\mathrm{c}\mathrm{Im}(\gamma)}\,\mathrm{H}. \end{aligned} \tag{2.112}$$

Following this procedure, the inversion of the impedance matrix of the Tx-DMN in (2.70) produces an admittance matrix with $2N \times 2N$ admittances. Likewise, for the Rx-DMN, a matrix with $2M \times 2M$ admittances is produced. Given the argument above that the non-diagonal elements $\gamma_{i,j}$ and $\gamma_{j,i}$ are the same, out of the $4N^2$ and $4M^2$ positions in the impedance matrices, the Tx- and Rx-DMN have

$$\begin{aligned} 2N + \frac{(2N)^2 - 2N}{2} &= 2N^2 + N, \\ 2M + \frac{(2M)^2 - 2M}{2} &= 2M^2 + M, \end{aligned} \tag{2.113}$$

lumped reactive elements, respectively, composing them.

The determination of the decoupling and matching networks topology and of the elements composing them are of big importance not only for the actual realization of the circuits,

but also for a complete physical analysis with the inclusion of parasitics into the theoretic background. Up to now and in the next section, the antenna elements and the DMNs are considered lossless and to be operating only at a single frequency.

Later in this chapter, in Section 2.4, the theoretical description of the systems will be generalized to include losses and frequency dependency to increase the physical consistency of the MCT modelling.

Finally, the presentation of the basic theoretical aspects of the system with DMNs is concluded. The next step is to delve into the system without DMNs.

2.3 System without Decoupling and Matching Networks

The system without DMNs, as the name suggests, does not make use of such networks to provide to the high-power amplifiers and to the low-noise amplifiers decoupled and matched antenna port impedances. This leads to disadvantages, because it never attains optimal performance in terms of achievable rates from energy efficiency on the transmit side and best possible SNR on the receive side.

Still, it has advantages over the system with DMNs, coming basically from the absence of the limitations inherent to the decoupling and matching networks, due to Ohmic losses, to frequency dependency and to the number of elements.

First, the DMNs in Section 2.2 were modelled with lossless reactive elements. Real reactive components, however, have small parasitic resistances. Although they might even be considered negligible individually, in networks of large numbers of elements, the losses caused by these resistances stack up and become important causes for loss of rates.

Secondly, the frequency sensitive parameters of the uniform circular arrays of $\lambda/2$-dipoles–most of the dimensional parameters such as the dipoles' arms length and the antenna spacing–and the values of the DMNs' reactances, chosen such as to produce the desired impedance matrices at a single frequency, are modelled based on the systems' center frequency.

Thirdly, the number of elements in the networks using the π-topology may grow very fast with the increase of the number of antennas, as the expressions in (2.113) show. Even in the best scenario, as mentioned in Chapter 1 Introduction, the number of elements grows more than quadratically in $N^2 + N$, according to (NIE *et al.*, 2014), for $2N$ ports.

Figure 11 – MCT model of the system without DMNs.

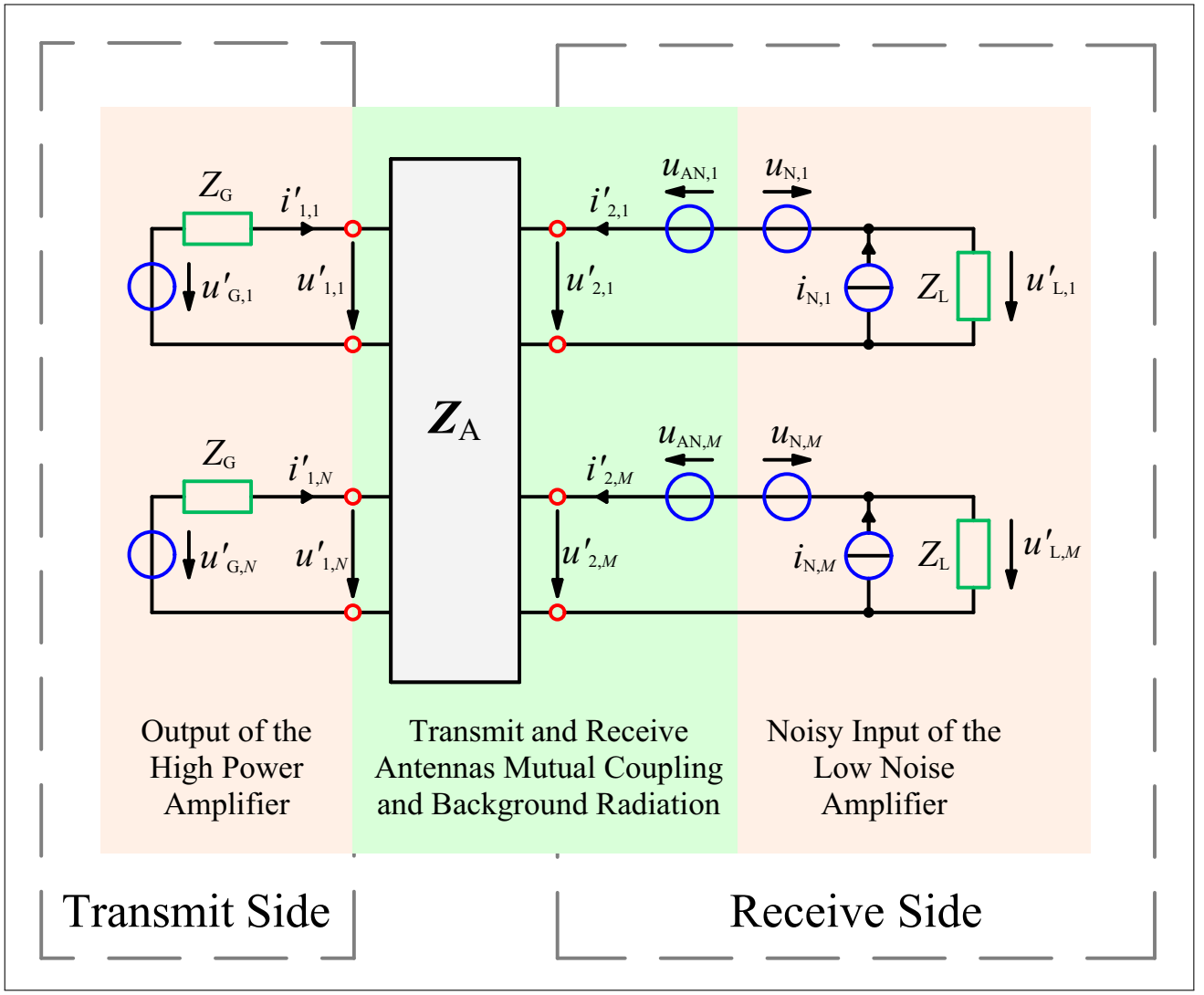

Source: The author, adapted from (LAAS *et al.*, 2017).

Thus, for systems operating at frequencies too distant from the center frequency and at the presence of losses in the DMNs, this may lead to non-negligible loss of performance. Not to mention the very high number of elements for a high number of antennas. For this kind of scenario, the system without DMNs may be a better solution. Nonetheless, the analysis that follows consider lossless antennas and the equations are formulated at the center frequency.

Moreover, the concept of the system without DMNs is not only an alternative to the system with DMNs, as it is meant to be regarded as the physically consistent evaluation of the achievable rates of systems in which no decoupling and matching strategy is implemented.

The system in Fig. 11 is entirely modelled using circuit elements also present in the model of the system with DMNs in Fig 3. As such, they present the same mathematical and statistical properties of their counterparts in the model with DMNs.

Some of the elements are represented with primes for the sake of differentiating them from the variables related to the system with DMNs. This will be clearer later. Impedances are kept without primes because they can be (and are) chosen to be same as those in the system with DMNs, including the arrays' impedance matrices, which are from the same arrays as well.

As this system does not employ DMNs, the strategy is to connect each of the high-power amplifiers and of the low-noise amplifiers directly to one of the antennas in the transmit and in the receive antenna arrays, respectively. The HPAs are, again, modelled using voltage sources $\boldsymbol{u}'_{\mathrm{G}}$ generating the signals to be transmitted and series impedances Z_{G} as the generators' inner impedances.

Connected to the outputs of the HPAs is the transmit UCA of $\lambda/2$-dipoles, whose impedance matrix is $\boldsymbol{Z}_{\mathrm{AT}}$. Schematically, in Fig. 11, the HPAs are connected to the multiport $\boldsymbol{Z}_{\mathrm{A}}$, which is connected on the other side with the input of the noisy LNAs. The matrix equation of the $\boldsymbol{Z}_{\mathrm{A}}$ multiport is

$$\begin{bmatrix} \boldsymbol{u}'_1 \\ \boldsymbol{u}'_2 \end{bmatrix} = \begin{bmatrix} \boldsymbol{Z}_{\mathrm{AT}} & \boldsymbol{Z}_{\mathrm{ATR}} \\ \boldsymbol{Z}_{\mathrm{ART}} & \boldsymbol{Z}_{\mathrm{AR}} \end{bmatrix} \begin{bmatrix} \boldsymbol{i}'_1 \\ \boldsymbol{i}'_2 \end{bmatrix}, \tag{2.114}$$

where $\boldsymbol{Z}_{\mathrm{AR}}$ is the receive antenna array impedance matrix. Being the Tx- and Rx-UCAs reciprocal systems, $\boldsymbol{Z}_{\mathrm{AT}} = \boldsymbol{Z}_{\mathrm{AT}}^{\mathrm{T}}$ and $\boldsymbol{Z}_{\mathrm{AR}} = \boldsymbol{Z}_{\mathrm{AR}}^{\mathrm{T}}$. For $\boldsymbol{Z}_{\mathrm{A}}$ is the transmit and receive array mutual coupling matrix, it is also a reciprocal system, thus: $\boldsymbol{Z}_{\mathrm{A}} = \boldsymbol{Z}_{\mathrm{A}}^{\mathrm{T}}$, implying $\boldsymbol{Z}_{\mathrm{ART}} = \boldsymbol{Z}_{\mathrm{ATR}}^{\mathrm{T}}$.

The Unilateral Approximation (explained in the introduction of Section 2.2) can,

again, be applied on this system, giving that the influence of the receive port-currents $\boldsymbol{i}'_2$ is negligible on the transmit port-voltages $\boldsymbol{u}'_1$, implying $\boldsymbol{Z}_{\mathrm{ATR}} = \boldsymbol{0}_{N,M}\,\Omega$.

On the receive side, in addition to the receive antenna array, the voltage source $\boldsymbol{u}_{\mathrm{AN}}$ stands for the antennas' background radiation noise and the voltage and current sources $\boldsymbol{u}_{\mathrm{N}}$ and $\boldsymbol{i}_{\mathrm{N}}$ represent the low-noise amplifiers' intrinsic noise. Their statistical properties are the same as those presented in (2.12), (2.13), (2.14) and (2.15). Besides the sources modelling the noisy parts of the LNAs, their noiseless parts are modelled with simply the impedances $\boldsymbol{Z}_{\mathrm{L}}$.

Similar to the theoretical development done in Section 2.2, the circuit theoretic equations are obtained with the encapsulation of the electromagnetic effects and then are unified with the information theoretic equations via the mapping which uses the transmit power and the noise covariance matrix as connecting characteristic items.

2.3.1 Circuit Theoretic Model of the System without DMNs

A function of the load voltage $\boldsymbol{u}'_{\mathrm{L}}$ in terms of the voltage and current sources in the system must be found. It represents the relation of the receive signal with the transmit and noise signals from the circuit theoretic perspective. Since the system in Fig. 11 is linear, by the principle of superposition, the complete description of the load voltage in terms of the system's sources is equal to the sum of the individual contributions of each source.

$$\begin{aligned} &\boldsymbol{u}'_{\mathrm{L}} = g(\boldsymbol{u}'_{\mathrm{G}}, \boldsymbol{u}_{\mathrm{AN}}, \boldsymbol{u}_{\mathrm{N}}, \boldsymbol{i}_{\mathrm{N}}), \\ &g(\boldsymbol{u}'_{\mathrm{G}}, \boldsymbol{u}_{\mathrm{AN}}, \boldsymbol{u}_{\mathrm{N}}, \boldsymbol{i}_{\mathrm{N}}) = g_1(\boldsymbol{u}'_{\mathrm{G}}) + g_2(\boldsymbol{u}_{\mathrm{AN}}) + g_3(\boldsymbol{u}_{\mathrm{N}}) + g_4(\boldsymbol{i}_{\mathrm{N}}). \end{aligned} \tag{2.115}$$

To obtain the set of functions $\{g_1, g_2, g_3, g_4\}$, the multiport $\boldsymbol{Z}_{\mathrm{A}}$ and its matrix equation (2.114) serve as the main parts to connect the transmit side to the receive side and to relate the receive side noise sources with the load voltage. The development of (2.114) with the Unilateral Approximation results in

$$\begin{aligned} \boldsymbol{u}'_1 &= \boldsymbol{Z}_{\mathrm{AT}}\boldsymbol{i}'_1 + \boldsymbol{Z}_{\mathrm{ATR}}\boldsymbol{i}'_2 = \boldsymbol{Z}_{\mathrm{AT}}\boldsymbol{i}'_1, \\ \boldsymbol{u}'_2 &= \boldsymbol{Z}_{\mathrm{ART}}\boldsymbol{i}'_1 + \boldsymbol{Z}_{\mathrm{AR}}\boldsymbol{i}'_2, \end{aligned} \tag{2.116}$$

allowing to obtain the relations between the desired variables making the pertinent circuit analysis in every step of the superposition procedure.

2.3.1.1 *Superposition Step 1:* $\boldsymbol{u}_{\mathrm{AN}} = \boldsymbol{u}_{\mathrm{N}} = \mathbf{0}_{M,1}\mathrm{V}$ *and* $\boldsymbol{i}_{\mathrm{N}} = \mathbf{0}_{M,1}\mathrm{A}$

Only the voltage generators $\boldsymbol{u}'_{\mathrm{G}}$ are operating in this step. The other voltage sources are deactivated, becoming now as short-circuits, whereas the deactivation of the current sources $\boldsymbol{i}_{\mathrm{N}}$ results in open-circuits. In this scenario, (2.116) and the circuit analysis give

$$\boldsymbol{u}'_{\mathrm{G}} = Z_{\mathrm{G}}\boldsymbol{i}'_1 + \boldsymbol{u}'_1 = (Z_{\mathrm{G}}\boldsymbol{I}_N + \boldsymbol{Z}_{\mathrm{AT}})\boldsymbol{i}'_1 \implies \boldsymbol{i}'_1 = (Z_{\mathrm{G}}\boldsymbol{I}_N + \boldsymbol{Z}_{\mathrm{AT}})^{-1}\boldsymbol{u}'_{\mathrm{G}} \tag{2.117}$$

$$\boldsymbol{u}'_2 = \boldsymbol{Z}_{\mathrm{ART}}(Z_{\mathrm{G}}\boldsymbol{I}_N + \boldsymbol{Z}_{\mathrm{AT}})^{-1}\boldsymbol{u}'_{\mathrm{G}} + \boldsymbol{Z}_{\mathrm{AR}}\boldsymbol{i}'_2. \tag{2.118}$$

On the loads Z_{L}, the currents $\boldsymbol{i}'_2$ flow through them producing $-\boldsymbol{u}'_{\mathrm{L}}$, which are the same of $-\boldsymbol{u}'_2$, since $\boldsymbol{u}'_2 = \boldsymbol{u}'_{\mathrm{L}}$, resulting in

$$\boldsymbol{u}'_2 = \boldsymbol{u}'_{\mathrm{L}} = \boldsymbol{Z}_{\mathrm{ART}}(Z_{\mathrm{G}}\boldsymbol{I}_N + \boldsymbol{Z}_{\mathrm{AT}})^{-1}\boldsymbol{u}'_{\mathrm{G}} - \frac{1}{Z_{\mathrm{L}}}\boldsymbol{Z}_{\mathrm{AR}}\boldsymbol{u}'_{\mathrm{L}}, \tag{2.119}$$

$$\boldsymbol{u}'_{\mathrm{L}} + \frac{1}{Z_{\mathrm{L}}}\boldsymbol{Z}_{\mathrm{AR}}\boldsymbol{u}'_{\mathrm{L}} = \boldsymbol{Z}_{\mathrm{ART}}(Z_{\mathrm{G}}\boldsymbol{I}_N + \boldsymbol{Z}_{\mathrm{AT}})^{-1}\boldsymbol{u}'_{\mathrm{G}}, \tag{2.120}$$

$$\implies \boldsymbol{u}'_{\mathrm{L}} = Z_{\mathrm{L}}(Z_{\mathrm{L}}\boldsymbol{I}_N + \boldsymbol{Z}_{\mathrm{AR}})^{-1}\boldsymbol{Z}_{\mathrm{ART}}(Z_{\mathrm{G}}\boldsymbol{I}_N + \boldsymbol{Z}_{\mathrm{AT}})^{-1}\boldsymbol{u}'_{\mathrm{G}}. \tag{2.121}$$

From (2.115), g_1 is obtained

$$\begin{aligned}\boldsymbol{u}'_{\mathrm{L}} &= g_1(\boldsymbol{u}'_{\mathrm{G}}) = \boldsymbol{D}'\boldsymbol{u}'_{\mathrm{G}},\\ \boldsymbol{D}' &= Z_{\mathrm{L}}(Z_{\mathrm{L}}\boldsymbol{I}_N + \boldsymbol{Z}_{\mathrm{AR}})^{-1}\boldsymbol{Z}_{\mathrm{ART}}(Z_{\mathrm{G}}\boldsymbol{I}_N + \boldsymbol{Z}_{\mathrm{AT}})^{-1}.\end{aligned} \tag{2.122}$$

2.3.1.2 *Superposition Step 2:* $\boldsymbol{u}'_{\mathrm{G}} = \mathbf{0}_{N,1}\mathrm{V}$, $\boldsymbol{u}_{\mathrm{N}} = \mathbf{0}_{M,1}\mathrm{V}$ *and* $\boldsymbol{i}_{\mathrm{N}} = \mathbf{0}_{M,1}\mathrm{A}$

When the $\boldsymbol{u}'_{\mathrm{G}}$ generators become short-circuits, $\boldsymbol{i}'_1$ also disappears, because there is no other source generating it and since $\boldsymbol{u}'_1$ is independent of $\boldsymbol{i}'_2$, there is no way to produce voltage drops across the terminals of the transmit ports such as to induce currents over the impedances Z_{G}. This will also be the case for the subsequent superposition steps.

From (2.116), $\boldsymbol{u}'_2 = \boldsymbol{Z}_{\mathrm{AR}}\boldsymbol{i}'_2$. Now, the voltage loop analysis in the receive side gives

$$\begin{aligned}&\boldsymbol{u}'_{\mathrm{L}} = \boldsymbol{u}'_2 + \boldsymbol{u}_{\mathrm{AN}} = \boldsymbol{Z}_{\mathrm{AR}}\boldsymbol{i}'_2 + \boldsymbol{u}_{\mathrm{AN}},\ \boldsymbol{i}'_2 = -\frac{1}{Z_{\mathrm{L}}}\boldsymbol{u}'_{\mathrm{L}},\\ &\boldsymbol{u}'_{\mathrm{L}} = -\boldsymbol{Z}_{\mathrm{AR}}\frac{1}{Z_{\mathrm{L}}}\boldsymbol{u}'_{\mathrm{L}} + \boldsymbol{u}_{\mathrm{AN}} \implies \frac{1}{Z_{\mathrm{L}}}(Z_{\mathrm{L}}\boldsymbol{I}_N + \boldsymbol{Z}_{\mathrm{AR}})\boldsymbol{u}'_{\mathrm{L}} = \boldsymbol{u}_{\mathrm{AN}},\end{aligned} \tag{2.123}$$

which results in the function g_2 from (2.115)

$$\boldsymbol{u}'_{\mathrm{L}} = g_2(\boldsymbol{u}_{\mathrm{AN}}) = Z_{\mathrm{L}}(Z_{\mathrm{L}}\boldsymbol{I}_N + \boldsymbol{Z}_{\mathrm{AR}})^{-1}\boldsymbol{u}_{\mathrm{AN}}. \tag{2.124}$$

2.3.1.3 Superposition Step 3: $\boldsymbol{u}'_{\mathrm{G}} = \boldsymbol{0}_{N,1}\mathrm{V}$, $\boldsymbol{u}_{\mathrm{AN}} = \boldsymbol{0}_{M,1}\mathrm{V}$ *and* $\boldsymbol{i}_{\mathrm{N}} = \boldsymbol{0}_{M,1}\mathrm{A}$

This step can follow the same procedure in the last step, with the difference that $\boldsymbol{u}_{\mathrm{N}}$ are the only sources active now. Since they are connected, in Fig. 11, in series with $\boldsymbol{u}_{\mathrm{AN}}$ but with their electromotive forces in the opposite direction, the same relation with the inverted signal relates the load voltages with $\boldsymbol{u}_{\mathrm{N}}$.

$$\boldsymbol{u}'_{\mathrm{L}} = g_3(\boldsymbol{u}_{\mathrm{N}}) = -Z_{\mathrm{L}}(Z_{\mathrm{L}}\boldsymbol{I}_N + \boldsymbol{Z}_{\mathrm{AR}})^{-1}\boldsymbol{u}_{\mathrm{N}}. \tag{2.125}$$

2.3.1.4 Superposition Step 4: $\boldsymbol{u}'_{\mathrm{G}} = \boldsymbol{0}_{N,1}\mathrm{V}$ *and* $\boldsymbol{u}_{\mathrm{AN}} = \boldsymbol{u}_{\mathrm{N}} = \boldsymbol{0}_{M,1}\mathrm{V}$

With $\boldsymbol{i}'_1 = \boldsymbol{0}_N\mathrm{A}$ still holding, it implies $\boldsymbol{u}'_2 = \boldsymbol{u}'_{\mathrm{L}} = \boldsymbol{Z}_{\mathrm{AR}}\boldsymbol{i}'_2$. In addition to it, the circuit analysis of the currents on the nodes above the $\boldsymbol{i}_{\mathrm{N}}$ sources gives the following

$$\begin{aligned}
&\boldsymbol{i}_{\mathrm{N}} = \boldsymbol{i}'_2 + \frac{1}{Z_{\mathrm{L}}}\boldsymbol{u}'_{\mathrm{L}}, \\
&\boldsymbol{Z}_{\mathrm{AR}}\boldsymbol{i}_{\mathrm{N}} = \boldsymbol{Z}_{\mathrm{AR}}\boldsymbol{i}'_2 + \boldsymbol{Z}_{\mathrm{AR}}\frac{1}{Z_{\mathrm{L}}}\boldsymbol{u}'_{\mathrm{L}} = \boldsymbol{u}'_{\mathrm{L}} + \boldsymbol{Z}_{\mathrm{AR}}\frac{1}{Z_{\mathrm{L}}}\boldsymbol{u}'_{\mathrm{L}}.
\end{aligned} \tag{2.126}$$

This leads basically to the two preceding steps' results, but with $\boldsymbol{Z}_{\mathrm{AR}}\boldsymbol{i}_{\mathrm{N}}$ as a voltage source. Finally,

$$\boldsymbol{u}'_{\mathrm{L}} = g_4(\boldsymbol{i}_{\mathrm{N}}) = Z_{\mathrm{L}}(Z_{\mathrm{L}}\boldsymbol{I}_N + \boldsymbol{Z}_{\mathrm{AR}})^{-1}\boldsymbol{Z}_{\mathrm{AR}}\boldsymbol{i}_{\mathrm{N}}. \tag{2.127}$$

2.3.1.5 *Superposition Final Step:* $g = g_1 + g_2 + g_3 + g_4$

It is possible to obtain, at last, the complete description of $\boldsymbol{u}'_{\mathrm{L}}$ as a function of the set of sources $\{\boldsymbol{u}'_{\mathrm{G}}, \boldsymbol{u}_{\mathrm{AN}}, \boldsymbol{u}_{\mathrm{N}}, \boldsymbol{i}_{\mathrm{N}}\}$ with the function g from (2.115)

$$
\begin{aligned}
&g_1(\boldsymbol{u}'_{\mathrm{G}}) = \boldsymbol{D}'\boldsymbol{u}'_{\mathrm{G}} = Z_{\mathrm{L}}(Z_{\mathrm{L}}\boldsymbol{I}_N + \boldsymbol{Z}_{\mathrm{AR}})^{-1}\boldsymbol{Z}_{\mathrm{ART}}(Z_{\mathrm{G}}\boldsymbol{I}_N + \boldsymbol{Z}_{\mathrm{AT}})^{-1}\boldsymbol{u}'_{\mathrm{G}},\\
&g_2(\boldsymbol{u}_{\mathrm{AN}}) = Z_{\mathrm{L}}(Z_{\mathrm{L}}\boldsymbol{I}_N + \boldsymbol{Z}_{\mathrm{AR}})^{-1}\boldsymbol{u}_{\mathrm{AN}},\\
&g_3(\boldsymbol{u}_{\mathrm{N}}) = -Z_{\mathrm{L}}(Z_{\mathrm{L}}\boldsymbol{I}_N + \boldsymbol{Z}_{\mathrm{AR}})^{-1}\boldsymbol{u}_{\mathrm{N}},\\
&g_4(\boldsymbol{i}_{\mathrm{N}}) = Z_{\mathrm{L}}(Z_{\mathrm{L}}\boldsymbol{I}_N + \boldsymbol{Z}_{\mathrm{AR}})^{-1}\boldsymbol{Z}_{\mathrm{AR}}\boldsymbol{i}_{\mathrm{N}},\\
&g(\boldsymbol{u}'_{\mathrm{G}}, \boldsymbol{u}_{\mathrm{AN}}, \boldsymbol{u}_{\mathrm{N}}, \boldsymbol{i}_{\mathrm{N}}) = g_1(\boldsymbol{u}'_{\mathrm{G}}) + g_2(\boldsymbol{u}_{\mathrm{AN}}) + g_3(\boldsymbol{u}_{\mathrm{N}}) + f_4(\boldsymbol{i}_{\mathrm{N}}),
\end{aligned}
\tag{2.128}
$$

$$
\boldsymbol{u}'_{\mathrm{L}} = \boldsymbol{D}'\boldsymbol{u}'_{\mathrm{G}} + Z_{\mathrm{L}}(Z_{\mathrm{L}}\boldsymbol{I}_N + \boldsymbol{Z}_{\mathrm{AR}})^{-1}(\boldsymbol{u}_{\mathrm{AN}} - \boldsymbol{u}_{\mathrm{N}} + \boldsymbol{Z}_{\mathrm{AR}}\boldsymbol{i}_{\mathrm{N}}). \tag{2.129}
$$

Similarly as it was done with (2.43) to give (2.44), (2.129) is reformulated to give

$$
\boldsymbol{u}'_{\mathrm{L}} = \boldsymbol{D}'\boldsymbol{u}'_{\mathrm{G}} + \sqrt{R_{\mathrm{L}}}\boldsymbol{\eta}', \tag{2.130}
$$

allowing for the noise covariance matrix, defined as $\boldsymbol{R}'_{\boldsymbol{\eta}} = \mathbb{E}\left[\boldsymbol{\eta}'\boldsymbol{\eta}'^{\mathrm{H}}\right]$, to be in Watts.

2.3.2 Information Theoretic Model for the System without DMNs

After obtaining (2.129), the mapping from Circuit Theory to Information Theory must keep the physical consistency of the latter. In order to do so, the mapping is made, again, via the Transmit Power and on the Noise Covariance Matrix from the perspective of the circuit theoretic model in Fig. 11. For this matter, (2.45) is used one more time, with the same variables and bearing the same meaning.

Nevertheless, a prime is added to help distinguishing the new variables of the system without DMNs from the variables of the system with DMNs,

$$
\boldsymbol{y}' = \boldsymbol{H}'\boldsymbol{x}' + \boldsymbol{\nu}'. \tag{2.131}
$$

Not using decoupling and matching networks brings advantages, such as not being susceptible to the limitations imposed by the network itself. However, the biggest disadvantage

is the fact that the system without DMNs does never attain optimal behavior and operation. It means that power matching, noise matching and the antennas' ports decoupling don't happen.

As explained in the Introduction, the real importance of the DMNs designed for and operating in a communication system are not the networks themselves, but the capacity of bringing physical consistency to classical information and signal theoretical modelling through its decoupling and matching features.

2.3.2.1 Circuit Theoretic Transmit Power

The transmit power computation, as done before in (2.46) uses the N antennas port-voltages and currents $\boldsymbol{u}'_1$ and $\boldsymbol{i}'_1$ of the Tx-UCA

$$P_{\mathrm{T}} = \mathbb{E}\left\{\sum_{n=1}^{N} \mathrm{Re}\left[{i'_{1,n}}^{*} u'_{1,n}\right]\right\} = \mathbb{E}\left\{\mathrm{Re}\left[{\boldsymbol{i}'_1}^{\mathrm{H}} \boldsymbol{u}'_1\right]\right\} = \frac{1}{2}\mathbb{E}\left[{\boldsymbol{i}'_1}^{\mathrm{H}} \boldsymbol{u}'_1 + {\boldsymbol{u}'_1}^{\mathrm{H}} \boldsymbol{i}'_1\right]. \tag{2.132}$$

Now $\boldsymbol{u}'_1 = \boldsymbol{Z}_{\mathrm{AT}} \boldsymbol{i}'_1$, from (2.116), and $\boldsymbol{i}'_1$ in terms of $\boldsymbol{u}'_{\mathrm{G}}$, from (2.117), are plugged in to further develop the transmit power equation

$$\begin{aligned} P_{\mathrm{T}} &= \frac{1}{2}\mathbb{E}\left[{\boldsymbol{i}'_1}^{\mathrm{H}} (\boldsymbol{Z}_{\mathrm{AT}} + \boldsymbol{Z}_{\mathrm{AT}}^{\mathrm{H}}) \boldsymbol{i}'_1\right] = \mathbb{E}\left[{\boldsymbol{i}'_1}^{\mathrm{H}} \mathrm{Re}(\boldsymbol{Z}_{\mathrm{AT}}) \boldsymbol{i}'_1\right], \\ P_{\mathrm{T}} &= \mathbb{E}\left[{\boldsymbol{u}'_{\mathrm{G}}}^{\mathrm{H}} (Z_{\mathrm{G}} \boldsymbol{I}_N + \boldsymbol{Z}_{\mathrm{AT}})^{-\mathrm{H}} \mathrm{Re}(\boldsymbol{Z}_{\mathrm{AT}}) (Z_{\mathrm{G}} \boldsymbol{I}_N + \boldsymbol{Z}_{\mathrm{AT}})^{-1} \boldsymbol{u}'_{\mathrm{G}}\right]. \end{aligned} \tag{2.133}$$

The power coupling matrix $\boldsymbol{B}$ can be defined also for the system without DMNs

$$\boldsymbol{B}' = 4R_{\mathrm{G}}[(Z_{\mathrm{G}} \boldsymbol{I}_N + \boldsymbol{Z}_{\mathrm{AT}})^{-\mathrm{H}} \mathrm{Re}(\boldsymbol{Z}_{\mathrm{AT}}) (Z_{\mathrm{G}} \boldsymbol{I}_N + \boldsymbol{Z}_{\mathrm{AT}})^{-1}], \tag{2.134}$$

As it can be seen, $\boldsymbol{B}'$ is not an identity nor even a scaled identity matrix, in contrast to the power coupling matrix in (2.74), where a decoupling and power matching network is designed to guarantee this result, as in 2.2.3.1. The consequence of this on the transmit power

$$P_{\mathrm{T}} = \frac{1}{4R_{\mathrm{G}}}\mathbb{E}\left[{\boldsymbol{u}'_{\mathrm{G}}}^{\mathrm{H}} \boldsymbol{B}' \boldsymbol{u}'_{\mathrm{G}}\right], \tag{2.135}$$

is that the transmit power is not equal to the available power, which is, for the system without DMNs, computed using the definition given in 2.2.3.1

$$P_{\mathrm{A}} = \frac{1}{2}\mathbb{E}\left[\left(\frac{1}{2R_{\mathrm{G}}}\boldsymbol{u}_{\mathrm{G}}\right)^{\mathrm{H}}\left(\frac{1}{2}\boldsymbol{u}_{\mathrm{G}}\right) + \left(\frac{1}{2}\boldsymbol{u}_{\mathrm{G}}\right)^{\mathrm{H}}\left(\frac{1}{2R_{\mathrm{G}}}\boldsymbol{u}_{\mathrm{G}}\right)\right] = \frac{1}{4R_{\mathrm{G}}}\mathbb{E}\left[\|\boldsymbol{u}_{\mathrm{G}}\|_2^2\right], \tag{2.136}$$

because this is the power delivered at the output of the HPAs when their output ports impedances are power matched with their series impedances. Since $\boldsymbol{B}'$ is not the identity matrix,

$$P_{\mathrm{A}} = \frac{1}{4R_{\mathrm{G}}}\mathbb{E}\left[\|\boldsymbol{u}_{\mathrm{G}}\|_2^2\right] \neq \frac{1}{4R_{\mathrm{G}}}\mathbb{E}\left[\boldsymbol{u}_{\mathrm{G}}'^{\mathrm{H}}\boldsymbol{B}'\boldsymbol{u}_{\mathrm{G}}'\right] = P_{\mathrm{T}}, \tag{2.137}$$

being this the mathematical result of what was expected: to have the available power of the HPAs transferred to feed the transmit antennas and them to be radiated, an optimal decoupling and matching strategy had to be used.

2.3.2.2 Circuit Theoretic Noise Covariance

For the computation of the noise covariance matrix, the statistical properties of the noises in (2.12), (2.13), (2.14) and (2.15) are applied to solve the computations of the self- and cross-correlations of the different noises. Although in the scope of the system with DMNs, the computations exemplified in (2.54) and done in (2.52) are valid for the system without DMNs, respecting the use of the pertinent variables due to the models' differences.

For the noise as defined in (2.130)

$$\boldsymbol{\eta}' = \frac{1}{\sqrt{R_{\mathrm{L}}}}Z_{\mathrm{L}}(Z_{\mathrm{L}}\boldsymbol{I}_M + \boldsymbol{Z}_{\mathrm{AR}})^{-1}(\boldsymbol{u}_{\mathrm{AN}} - \boldsymbol{u}_{\mathrm{N}} + \boldsymbol{Z}_{\mathrm{AR}}\boldsymbol{i}_{\mathrm{N}}), \tag{2.138}$$

the noise covariance matrix becomes

$$\begin{aligned}\boldsymbol{R}_{\boldsymbol{\eta}}' = \frac{|Z_{\mathrm{L}}|^2}{R_L}(Z_{\mathrm{L}}\boldsymbol{I}_M + \boldsymbol{Z}_{\mathrm{AR}})^{-1}\Big[&4kT\Delta_f\,\mathrm{Re}(\boldsymbol{Z}_{\mathrm{AR}}) + \sigma_u^2\boldsymbol{I}_M + \\ &+ \sigma_i^2\boldsymbol{Z}_{\mathrm{AR}}\boldsymbol{Z}_{\mathrm{AR}}^{\mathrm{H}} - 2\sigma_u\sigma_i\,\mathrm{Re}(\rho\boldsymbol{Z}_{\mathrm{AR}}^{\mathrm{H}})\Big](Z_{\mathrm{L}}\boldsymbol{I}_M + \boldsymbol{Z}_{\mathrm{AR}})^{-\mathrm{H}}.\end{aligned} \tag{2.139}$$

Although the noise statistics being the same in both systems has led to the form of $\boldsymbol{R}_{\boldsymbol{\eta}}'$ to be very similar to the form of $\boldsymbol{R}_{\boldsymbol{\eta}}$, in (2.53), the noise covariance matrix here developed is actually not equal to an identity nor to a scaled identity and is not even diagonal.

Basically, this is a reflection of the system without DMNs not having any decoupling of the receive antennas ports, since $\boldsymbol{Z}_{\mathrm{AR}}$ is a full matrix, whereas in (2.53) $\boldsymbol{Z}_{\mathrm{R}}$ can be designed to be equal to a scaled identity and make $\boldsymbol{F}_{\mathrm{R}}\,\mathrm{Re}(\boldsymbol{Z}_{\mathrm{AR}})\boldsymbol{F}_{\mathrm{R}}^{\mathrm{H}}$ also equal to a scaled identity. Thus, $\boldsymbol{R}_{\boldsymbol{\eta}}$ itself becomes equal to a scaled identity.

2.3.2.3 The Channel Matrix

These mathematical results demonstrate that, to consider the antennas decoupled in a system which the transmitters see mutually-coupled antenna elements (e.g. the system without DMNs), leads to physically inconsistent results when working with information theoretic models. In addition, the lack of proper port-impedance matching reduces the energy efficiency and the SNR of the system.

The last effects are unavoidable, but to make use of a physically consistent information theoretic model, the mappings of the variables $\boldsymbol{u}'_{\mathrm{G}}$ and $\boldsymbol{u}'_{\mathrm{L}}$ (from (2.129)) to the variables $\boldsymbol{x}'$ and $\boldsymbol{y}'$ (from (2.131)), respectively, are performed. The transmit variables mapping is done via the transmit power

$$
\begin{aligned}
&P_{\mathrm{T}} = \mathbb{E}\left[\|\boldsymbol{x}'\|_2^2\right] = \frac{1}{4R_{\mathrm{G}}}\mathbb{E}\left[{\boldsymbol{u}'_{\mathrm{G}}}^{\mathrm{H}}\boldsymbol{B}'\boldsymbol{u}'_{\mathrm{G}}\right] = \mathbb{E}\left[\frac{1}{4R_{\mathrm{G}}}{\boldsymbol{u}'_{\mathrm{G}}}^{\mathrm{H}}\boldsymbol{B}'\boldsymbol{u}'_{\mathrm{G}}\right] = \mathbb{E}\left[\frac{1}{4R_{\mathrm{G}}}{\boldsymbol{u}'_{\mathrm{G}}}^{\mathrm{H}}{\boldsymbol{B}'}^{1/2}{\boldsymbol{B}'}^{\mathrm{H}/2}\boldsymbol{u}'_{\mathrm{G}}\right],\\
&\boldsymbol{x}' = \frac{1}{2\sqrt{R_{\mathrm{G}}}}{\boldsymbol{B}'}^{\mathrm{H}/2}\boldsymbol{u}'_{\mathrm{G}}.
\end{aligned}
\tag{2.140}
$$

The $\boldsymbol{B}'$ matrix is positive semi-definite, because $P_{\mathrm{T}} \geq 0\,\mathrm{W}$, $\forall \boldsymbol{u}'_{\mathrm{G}} \in \mathbb{R}^N\mathrm{V}$. Thus, it can be decomposed according to (LAAS *et al.*, 2017), similarly to what is done in (2.57),

$$
\begin{aligned}
&\boldsymbol{B}' = {\boldsymbol{B}'}^{1/2}{\boldsymbol{B}'}^{\mathrm{H}/2},\\
&{\boldsymbol{B}'}^{1/2} = 2\sqrt{R_{\mathrm{G}}}(Z_{\mathrm{G}}\boldsymbol{I}_N + \boldsymbol{Z}_{\mathrm{AT}})^{-\mathrm{H}}\,\mathrm{Re}(\boldsymbol{Z}_{\mathrm{AT}})^{\mathrm{H}/2},\\
&{\boldsymbol{B}'}^{\mathrm{H}/2} = 2\sqrt{R_{\mathrm{G}}}\,\mathrm{Re}(\boldsymbol{Z}_{\mathrm{AT}})^{1/2}(Z_{\mathrm{G}}\boldsymbol{I}_N + \boldsymbol{Z}_{\mathrm{AT}})^{-1}.
\end{aligned}
\tag{2.141}
$$

For the receive variables, the intermediate of the mapping is the noise covariance matrix, which is plugged in by taking the statistical correlation of $\boldsymbol{y}'$ when $\boldsymbol{x}' = \boldsymbol{0}_N$ and (2.131) and (2.130) hold. The relation between $\boldsymbol{y}'$ and $\boldsymbol{u}'_{\mathrm{L}}$ should be a linear mapping, such as it is for $\boldsymbol{y}$ and $\boldsymbol{u}_{\mathrm{L}}$ in the system with DMNs in (2.59)

$$
\boldsymbol{y}' = \boldsymbol{A}'\boldsymbol{u}'_{\mathrm{L}} = \boldsymbol{A}'(\boldsymbol{D}'\boldsymbol{u}'_{\mathrm{G}} + \sqrt{R_{\mathrm{L}}}\boldsymbol{\eta}') \implies \boldsymbol{A}'\boldsymbol{D}'\boldsymbol{u}'_{\mathrm{G}} + \sqrt{R_{\mathrm{L}}}\boldsymbol{A}'\boldsymbol{\eta}' = \boldsymbol{H}'\boldsymbol{x}' + \boldsymbol{\nu}',
\tag{2.142}
$$

Being $\boldsymbol{B}'$ also Hermitian, the decomposition above results in $\boldsymbol{B}'^{\mathrm{H}/2}$ being Hermitian positive definite matrix, which, in its turn, makes $\boldsymbol{x}' = \boldsymbol{0}_N \iff \boldsymbol{u}'_{\mathrm{G}} = \boldsymbol{0}_N \mathrm{V}$,

$$\begin{aligned}
&\mathbb{E}\left[\boldsymbol{\nu}'\boldsymbol{\nu}'^{\mathrm{H}}\right] = \mathbb{E}\left[\boldsymbol{y}'\boldsymbol{y}'^{\mathrm{H}} \mid \boldsymbol{x}' = \boldsymbol{0}_N\right] \iff \mathbb{E}\left[\boldsymbol{y}'\boldsymbol{y}'^{\mathrm{H}}\right]\Big|_{\boldsymbol{u}'_{\mathrm{G}}=\boldsymbol{0}\,\mathrm{V}}, \\
&\mathbb{E}\left[\boldsymbol{\nu}'\boldsymbol{\nu}'^{\mathrm{H}}\right] = R_{\mathrm{L}}\boldsymbol{A}'\mathbb{E}\left[\boldsymbol{\eta}'\boldsymbol{\eta}'^{\mathrm{H}}\right]\boldsymbol{A}'^{\mathrm{H}}.
\end{aligned} \tag{2.143}$$

The noise sources have the same statistical properties of those in the system with DMNs, and, hence, it is also assumed that they produce Gaussian noise. Over any linear transformation $\boldsymbol{A}'$, the Gaussian noise variable $\boldsymbol{\eta}'$ becomes another Gaussian noise variable $\boldsymbol{\nu}'$, for which its noise covariance matrix is a scaled identity

$$\begin{aligned}
&\mathbb{E}\left[\boldsymbol{\nu}'\boldsymbol{\nu}'^{\mathrm{H}}\right] = \sigma_\nu^2 \boldsymbol{I}_M, \\
&\boldsymbol{A}'\boldsymbol{R}_{\boldsymbol{\eta}}'^{\,1/2} = \frac{\sigma_\nu}{\sqrt{R_{\mathrm{L}}}}\boldsymbol{I}_M \implies \boldsymbol{A}' = \frac{\sigma_\nu}{\sqrt{R_{\mathrm{L}}}}\boldsymbol{R}_{\boldsymbol{\eta}}'^{\,-1/2},
\end{aligned} \tag{2.144}$$

allowing for the physically consistent definition of $\boldsymbol{y}'$ and $\boldsymbol{\nu}'$ in terms of, respectively, $\boldsymbol{u}'_{\mathrm{L}}$ and $\boldsymbol{\eta}'$

$$\boldsymbol{\nu}' = \sigma_\nu \boldsymbol{R}_{\boldsymbol{\eta}}'^{\,-1/2}\boldsymbol{\eta}', \tag{2.145}$$

$$\boldsymbol{y}' = \sqrt{\frac{\sigma_\nu^2}{R_{\mathrm{L}}}}\boldsymbol{R}_{\boldsymbol{\eta}}'^{\,-1/2}\boldsymbol{u}'_{\mathrm{L}}, \tag{2.146}$$

where, from the physical consistency of the noise powers sum, it holds again

$$\mathbb{E}\left[\boldsymbol{\nu}'^{\mathrm{H}}\boldsymbol{\nu}'\right] = \mathbb{E}\left[\boldsymbol{\eta}'^{\mathrm{H}}\boldsymbol{\eta}'\right] \implies \sigma_\nu^2 = \frac{\mathrm{Tr}(\boldsymbol{R}_{\boldsymbol{\eta}})}{M}. \tag{2.147}$$

To obtain $\boldsymbol{R}_{\boldsymbol{\eta}}'^{\,-1/2}$, the noise covariance matrix $\boldsymbol{R}'_{\boldsymbol{\eta}}$ is decomposed in $\boldsymbol{R}_{\boldsymbol{\eta}}'^{\,1/2}\boldsymbol{R}_{\boldsymbol{\eta}}'^{\,\mathrm{H}/2}$, also according to (LAAS *et al.*, 2017),

$$\begin{aligned}
&\boldsymbol{R}'_{\boldsymbol{\eta}} = \frac{|Z_{\mathrm{L}}|^2}{R_L}(Z_{\mathrm{L}}\boldsymbol{I}_M + \boldsymbol{Z}_{\mathrm{AR}})^{-1}\boldsymbol{N}'^{1/2}\boldsymbol{N}'^{\mathrm{H}/2}(Z_{\mathrm{L}}\boldsymbol{I}_M + \boldsymbol{Z}_{\mathrm{AR}})^{-\mathrm{H}} \\
&\boldsymbol{N}' = 4kT\Delta_f \mathrm{Re}(\boldsymbol{Z}_{\mathrm{AR}}) + \sigma_u^2\boldsymbol{I}_M + \sigma_i^2\boldsymbol{Z}_{\mathrm{AR}}\boldsymbol{Z}_{\mathrm{AR}}^{\mathrm{H}} - 2\sigma_u\sigma_i\mathrm{Re}\left(\rho\boldsymbol{Z}_{\mathrm{AR}}^{\mathrm{H}}\right), \\
&\boldsymbol{R}_{\boldsymbol{\eta}}'^{\,1/2} = \frac{Z_{\mathrm{L}}}{R_L}(Z_{\mathrm{L}}\boldsymbol{I}_M + \boldsymbol{Z}_{\mathrm{AR}})^{-1}\boldsymbol{N}'^{1/2}.
\end{aligned} \tag{2.148}$$

By the information theoretic equation (2.131), the physically consistent channel matrix equation can be determined using the definitions of $\boldsymbol{y}'$ (2.146), $\boldsymbol{x}'$ (2.140) and $\boldsymbol{\nu}'$ ((2.145)

$$\sqrt{\frac{\sigma_\nu^2}{R_\mathrm{L}}}\boldsymbol{R}_\eta'^{\,-1/2}\boldsymbol{u}_\mathrm{L}' = \boldsymbol{H}'\frac{1}{2\sqrt{R_\mathrm{G}}}\boldsymbol{B}'^{\mathrm{H}/2}\boldsymbol{u}_\mathrm{G}' + \sigma_\nu\boldsymbol{R}_\eta'^{\,-1/2}\boldsymbol{\eta}',$$
$$\sqrt{\frac{\sigma_\nu^2}{R_\mathrm{L}}}\boldsymbol{R}_\eta'^{\,-1/2}\boldsymbol{D}'\boldsymbol{u}_\mathrm{G}' + \sqrt{\frac{\sigma_\nu^2}{R_\mathrm{L}}}\boldsymbol{R}_\eta'^{\,-1/2}\sqrt{R_\mathrm{L}}\boldsymbol{\eta}' = \boldsymbol{H}'\frac{1}{2\sqrt{R_\mathrm{G}}}\boldsymbol{B}'^{\mathrm{H}/2}\boldsymbol{u}_\mathrm{G}' + \sigma_\nu\boldsymbol{R}_\eta'^{\,-1/2}\boldsymbol{\eta}',$$
$$\sqrt{\frac{\sigma_\nu^2}{R_\mathrm{L}}}\boldsymbol{R}_\eta'^{\,-1/2}\boldsymbol{D}'\boldsymbol{u}_\mathrm{G}' = \frac{1}{2\sqrt{R_\mathrm{G}}}\boldsymbol{H}'\boldsymbol{B}'^{\mathrm{H}/2}\boldsymbol{u}_\mathrm{G}' \implies \sqrt{\frac{\sigma_\nu^2}{R_\mathrm{L}}}\boldsymbol{R}_\eta'^{\,-1/2}\boldsymbol{D}' = \frac{1}{2\sqrt{R_\mathrm{G}}}\boldsymbol{H}'\boldsymbol{B}'^{\mathrm{H}/2},$$
$$\boldsymbol{H}' = 2\sigma_\nu\sqrt{\frac{R_\mathrm{G}}{R_\mathrm{L}}}\boldsymbol{R}_\eta'^{\,-1/2}\boldsymbol{D}'\boldsymbol{B}'^{-\mathrm{H}/2}. \tag{2.149}$$

It is noticeable that both channel equations, with (2.66) and without (2.149) DMNs, have the same quantities, in the same order and under the same operations. The difference is the structure of these quantities and, consequently, the structures of the channel matrices (or vectors for systems with single-antenna in one side of the link).

Equation (2.66), with perfect decoupling, power and noise matchings, results in the product of the circuit theoretic model's channel matrix $\boldsymbol{Z}_\mathrm{ART}$ with scaled identities ($\boldsymbol{R}_\eta^{\,-1/2}$ and $\boldsymbol{B}^{-\mathrm{H}/2}$) by both sides and with a scalar ($2\sigma_\nu\sqrt{R_\mathrm{G}/R_\mathrm{L}}$). Thus, the statistical distribution of the $\boldsymbol{Z}_\mathrm{ART}$ elements remain unchanged.

Conversely, given that all of the matrix quantities in (2.149) are full matrices, $\boldsymbol{H}'$ elements might not present the same distribution as $\boldsymbol{Z}_\mathrm{ART}$ elements do, because only Gaussian distributions remain Gaussian under any linear transformations.

2.4 Parasitics and Generalization

Although in possession of the physically consistent channel modelling of both systems, there is space for improving the consistency with the introduction of parasitics: losses and frequency dependency, in the systems' elements. This allows for having fairer comparisons between the use or the non-use of decoupling and matching strategies on the systems and have a better comprehension of the extension of the advantages and disadvantages of both systems.

In non-ideal scenarios, thermal losses are present in the antenna elements as the phenomenon known as skin effect and in the DMNs' lumped reactive elements as parasitic Ohmic losses, both causing dissipation of power that would, otherwise, be available for the detection process. To model the former, resistors are connected in series with the antennas in

their respective ports. Modelling the latter is also done by connecting parasitic resistors in series to each of the reactive elements.

Including these parasitic resistances to the ideal models allows for the computation of the voltage generators $\boldsymbol{u}_{\mathrm{G}}$ (or $\boldsymbol{u}'_{\mathrm{G}}$ for the systems without DMNs) as functions of variables and quantities carrying these additional resistances in the system. Thus, more power needs to be drawn from the generators to produce the same transmit power which would be produced had the system been lossless.

How this is taken into account to evidence the impact of the losses is better explained in Chapter 3, when computing the channel capacities in terms of the available power.

After the inclusion of the losses in the two models, the frequency dependency of some of the elements is also included. This is a necessary step to make in order to be able to analyse the achievable rates in frequency points rather distant from the center frequency, which is needed for the case for wideband communications.

The proper description of the parasitics and their inclusion in the systems' models allows for the generalization of the systems' equations to consider non-ideal (i.e. real) scenarios. In the generalized equations it is possible to notice the intricate balance of the quantities and variables in the equations when the HPAs and LNAs ports are decoupled and matched and when they are not, whether due to the lack of DMNs, due to parasitics or due to both.

2.4.1 The Skin Effect

The alternating current density in a conductor is largest at the most superficial layers and decreases exponentially as the more in depth the layers are in the conductor, constituting the so-called skin effect. To proceed on incorporating the losses in an array of half-wavelength dipoles, this phenomenon, which is responsible for the dissipated power in the antennas, must be modelled.

For this end, classical theory of electrodynamics can be used to compute first the electric resistance per unit of length of an infinitely long cylindrical wire made of a homogeneous material. Considering a cylindrical wire of finite length with a very small width, compared to its length, the aforementioned resistance can be used to compute an adequately approximated value of the dissipated power in this finitely long wire.

We can also consider the wire to be a half-wave antenna with feeding point in the center of its length and that, instead of power being dissipated throughout the length of the wire,

the whole dissipated power is on the feeding point of the antenna. These approximations allow for the modelling of the dissipated power as coming from a series resistance connected to the lossless antenna port.

Figure 12 – Series dissipation resistances in the $\lambda/2$-dipoles ports in the system with DMNs.

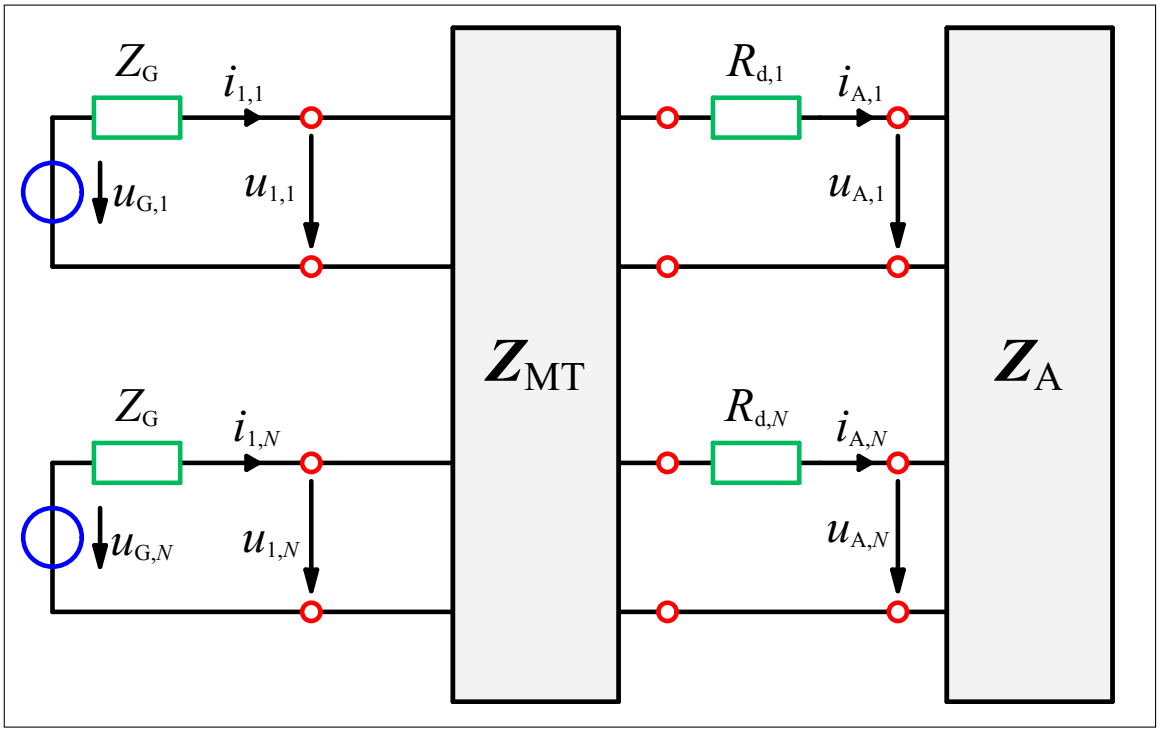

Source: The author.

In Fig. 12, a dissipation resistance is connected to each of the $\lambda/2$-dipoles, whose value is calculated, according to the equation

$$R_{\mathrm{d}} = \frac{\sqrt{2}c}{4\pi f_{\mathrm{c}}(w/2)^2\chi^2}\mathrm{Re}\left(\frac{(w/2)\sqrt{-j2\pi f_{\mathrm{c}}\chi/(\varepsilon_0 c^2)}}{2}\frac{\mathtt{J}_0(\sqrt{-j2\pi f_{\mathrm{c}}\chi/(\varepsilon_0 c^2)})}{\mathtt{J}_1(\sqrt{-j2\pi f_{\mathrm{c}}\chi/(\varepsilon_0 c^2)})}\right), \tag{2.150}$$

at the center frequency f_{c}, with c as the vacuum speed of light, χ as the conductivity, w as the $\lambda/2$-dipole's width and ε_0 as the vacuum conductivity. Besides these parameters, there are also the Bessel functions of first kind of zeroth $\mathtt{J}_0$ and first $\mathtt{J}_1$ order.

Although (2.150) uses the center frequency, instead of it other frequencies may be plugged in. However, for the range of frequencies intended for this thesis, R_{d} does not change considerably, which allows to use its value at f_{c} at all frequencies

$$R_{\mathrm{d}}(f) \approx R_{\mathrm{d}}(f_{\mathrm{c}}) = R_{\mathrm{d}},\ \forall f. \tag{2.151}$$

This was similarly done in (VASCONCELOS *et al.*, 2020), but for a ratio of the dipole's self-impedance, which actually results in R_d, simply put.

Since every antenna in the array is the same, then $R_{\mathrm{d},i} = R_\mathrm{d}$, $\forall i$. Thus, computing, e.g. the Tx-UCA of $\lambda/2$-dipoles impedance matrix with the thermal losses is done by adding to the $\boldsymbol{Z}_\mathrm{AT}$ impedance matrix a R_d scaled identity

$$\boldsymbol{Z}_\mathrm{AT} \leftarrow \boldsymbol{Z}_\mathrm{AT} + R_\mathrm{d}\boldsymbol{I}_N = \begin{bmatrix} (\boldsymbol{Z}_\mathrm{AT})_{1,1} + R_\mathrm{d} & (\boldsymbol{Z}_\mathrm{AT})_{1,2} & \cdots & (\boldsymbol{Z}_\mathrm{AT})_{1,N} \\ (\boldsymbol{Z}_\mathrm{AT})_{2,1} & (\boldsymbol{Z}_\mathrm{AT})_{2,2} + R_\mathrm{d} & \cdots & (\boldsymbol{Z}_\mathrm{AT})_{2,N} \\ \vdots & \vdots & \vdots & \vdots \\ (\boldsymbol{Z}_\mathrm{AT})_{N,1} & (\boldsymbol{Z}_\mathrm{AT})_{N,2} & \cdots & (\boldsymbol{Z}_\mathrm{AT})_{N,N} + R_\mathrm{d} \end{bmatrix}, \tag{2.152}$$

and the same is done for the receive array with $\boldsymbol{Z}_\mathrm{AR} \leftarrow \boldsymbol{Z}_\mathrm{AR} + R_\mathrm{d}\boldsymbol{I}_N$. In the lossy model, the skin effect affects only the antenna elements in the transmit and receive sides.

2.4.2 Thermal Losses in the Decoupling and Matching Networks

The theoretical values of the lumped elements' impedances determined by the DMNs' matrices (2.70) and (2.102) for a π-topology in (2.110), correspond to purely imaginary values, meaning ideal reactances. However, real world reactive components, inductors and capacitors, have parasitic Ohmic losses.

As shortly mentioned before, the modelling of these losses consists in adding to each reactance in the network a series parasitic resistance. For a two-port in the π-topology, the Ohmic losses' circuit modelling in a simpler scenario of a single-antenna is illustrated in Fig. 13.

What is left, after the design of this model is to compute the value of the resistances. For this end, in order to have a single parameter reasonably determining the value of all of the resistances in terms of their respective reactances, the quality Q-factor is adopted. For a specific value of the Q-factor, the value of the parasitic resistance R_p can be calculated as

$$R_\mathrm{p} = \begin{cases} (2\pi f_\mathrm{c} C Q)^{-1}, \text{ if in series with a capacitor or} \\ 2\pi f_\mathrm{c} L/Q, \text{ if in series with an inductor.} \end{cases} \tag{2.153}$$

Although the computation of the parasitic resistance R_p of each lumped reactance might be simple, the addition of the Ohmic losses in the lossless $\boldsymbol{Z}_\mathrm{MT}$ and $\boldsymbol{Z}_\mathrm{MR}$ is not straight-

Figure 13 – Single-antenna lossy matching network in π-topology

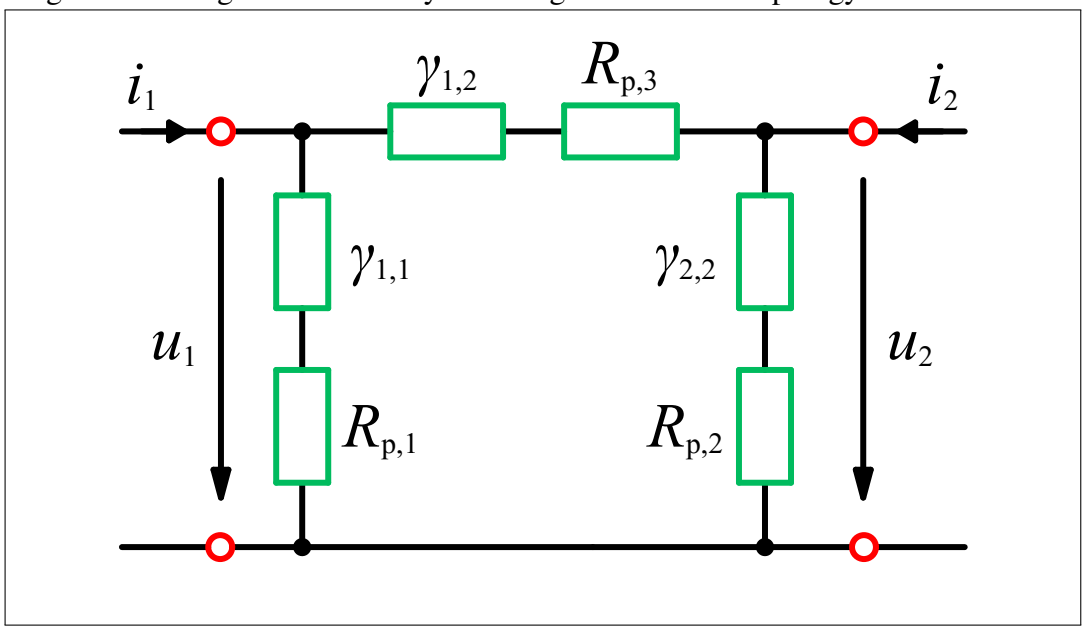

Source: The author.

forward, possessing intermediate steps. As mentioned before, one impedance matrix does not correspond to only one topology, necessarily.

Even though it might be possible to find a simple rule to add losses in the impedance matrix of a single antenna matching network (i.e. a two-port π-structure), for large numbers of elements, the network becomes too intricate. Thus, the best way to insert the losses in the impedance matrices is to, first, determine the values of the reactances via the admittance matrix.

After this step, the values of the parasitic resistances are calculated with the Q-factor for each of the reactive elements. Following this, the new admittance matrix of the lossy circuit is calculated, which, by inversion, gives the lossy impedance matrix. This procedure is summarized in the Algorithm 1, with the frequency dependency inclusion in the computation of the DMNs' impedance matrices with parasitics.

2.4.3 Frequency Dependent Variables

As it was seen in section 2.1, the equations for the self- and mutual-impedances, respectively (2.4) and (2.7), had the variable frequency (of the impinging or radiating waves) encapsulated in the wavenumber $k = 2\pi f/c$. For the UCAs operating at any frequency, the impedance matrices can be generalized by setting the wavenumber as a variable to compute the

self- and mutual-impedances at the desired frequency

$$\boldsymbol{Z}_{\text{array}}(f) = \begin{bmatrix} Z_{1,1}(f) & Z_{1,2}(f) & \cdots & Z_{1,N}(f) \\ Z_{2,1}(f) & Z_{2,2}(f) & \cdots & Z_{2,N}(f) \\ \vdots & \vdots & \ddots & \vdots \\ Z_{N,1}(f) & Z_{N,2}(f) & \cdots & Z_{N,N}(f) \end{bmatrix} \tag{2.154}$$

As to the DMNs, for the same reasons exposed before, to compute their impedance matrices at other frequencies demands the determination of the networks' topology and, consequently, their reactance values determined at the center frequency. With the latter, their admittances can be calculated at any frequency and, with the former, can also the whole impedance matrix, according to the Algorithm 1.

2.4.4 Systems' General Descriptions

The modelling of dissipative elements and frequency dependency, as explained before, in the uniform circular arrays of $\lambda/2$-dipoles is straight-forward. For the more involved process of modelling these parasitics in the decoupling and matching networks, Algorithm 1 summarizes the whole process described in the previous subsections.

It takes the array of lumped capacitances and inductances $\boldsymbol{\Pi}$, the Q-factor and the new frequency f to compute the parasitic resistances R_{p} of each lumped element and the lossy impedance matrix of the DMN at the desired frequency ($\boldsymbol{Z}_{\text{MT}}(f)$ or $\boldsymbol{Z}_{\text{MR}}(f)$). In the algorithm, there is also the pertinent procedures to obtain the network's admittance matrix $\boldsymbol{Y}$ from the network's lumped admittance array $\boldsymbol{\Gamma}$, as in 2.2.3.3.

For a matter of keeping the mathematical notations concise, the presence of losses in the variables is not displayed by any symbol, but can be implicitly noticed by the context. In general, nevertheless, variables with (f) are also generalized with losses.

Different matrix quantities and variables susceptible to these parasitics are found in the various equations of the systems with and without DMNs. First, the generalized circuit

Algorithm 1: Generation of the DMN's impedance matrix with parasitics

Input: Array containing the reactive elements' admittances $\mathbf{\Gamma}$, frequency f and the quality factor Q;

Output: Generalized admittance matrix of the DMN $\boldsymbol{Y}(f)$, $(\boldsymbol{Y}(f))_{i,j} = y_{i,j}\ \forall i, j = 1, ..., 2N$ at frequency f and elements with Q-factor;

$\gamma_{i,j}(f_\mathrm{c}) = (\mathbf{\Gamma})_{i,j}(f_\mathrm{c}),\ \forall i, j = 1, ..., 2N$;

if $-j\gamma_{i,j}(f_\mathrm{c}) > 0$: $\gamma_{i,j}(f_\mathrm{c}) = j2\pi f_\mathrm{c} C_{i,j}$, $C_{i,j} > 0\,\mathrm{F}$, $f_\mathrm{c} > 0\,\mathrm{Hz}$;

$$Q = \frac{1}{2\pi f_\mathrm{c} C_{i,j} R_\mathrm{p}}, \qquad R_\mathrm{p} = \frac{1}{2\pi f_\mathrm{c} C_{i,j} Q} = \frac{-1}{j\gamma_{i,j}(f_\mathrm{c})Q};$$

$$\gamma_{i,j}(f) = \frac{1}{R_\mathrm{p} + \frac{1}{j2\pi f_\mathrm{c} C_{i,j}}} = \frac{1}{\frac{1}{f/f_\mathrm{c}\ \gamma_{i,j}(f_\mathrm{c})} - \frac{1}{j\gamma_{i,j}(f_\mathrm{c})Q}} = \\ = \frac{\gamma_{i,j}(f_\mathrm{c})}{f/f_\mathrm{c} + j/Q};$$

else-if $-j\gamma_{i,j}(f_\mathrm{c}) < 0$: $\gamma_{i,j}(f_\mathrm{c}) = \dfrac{1}{j2\pi f_\mathrm{c} L_{i,j}}$, $L_{i,j} > 0\,\mathrm{H}$, $f_\mathrm{c} > 0\,\mathrm{Hz}$;

$$Q = \frac{2\pi f_\mathrm{c} L_{i,j}}{R_\mathrm{p}}, \qquad R_\mathrm{p} = \frac{2\pi f_\mathrm{c} L_{i,j}}{Q} = \frac{-1}{j\gamma_{i,j}(f_\mathrm{c})Q};$$

$$\gamma_{i,j}(f) = \frac{1}{R_\mathrm{p} + j2\pi f L_{i,j}} = \frac{1}{R_\mathrm{p} + \frac{f}{f_\mathrm{c}} j2\pi f_\mathrm{c} L_{i,j}} = \\ = \frac{\gamma_{i,j}(f_\mathrm{c})}{f/f_\mathrm{c} - j/Q};$$

end if

$y_{i,j} = -\gamma_{i,j}(f),\ i \neq j$;

$y_{i,i} = \gamma_{i,i} + \sum_{j=1_{j\neq i}}^{2N} \gamma_{i,j}$;

theoretic equations of the system with DMNs are written down.

$$\begin{aligned}
\boldsymbol{Z}_\mathrm{T}(f) &= \boldsymbol{Z}_{\mathrm{MT}_{1,1}}(f) - \boldsymbol{Z}_{\mathrm{MT}_{1,2}}(f)(\boldsymbol{Z}_\mathrm{AT}(f) + \boldsymbol{Z}_{\mathrm{MT}_{2,2}}(f))^{-1}\boldsymbol{Z}_{\mathrm{MT}_{2,1}}(f), \\
\boldsymbol{Z}_\mathrm{RT}(f) &= \boldsymbol{F}_\mathrm{R}(f)\boldsymbol{Z}_\mathrm{ART}(f)(\boldsymbol{Z}_\mathrm{AT}(f) + \boldsymbol{Z}_{\mathrm{MT}_{2,2}}(f))^{-1}\boldsymbol{Z}_{\mathrm{MT}_{2,1}}(f), \\
\boldsymbol{Z}_\mathrm{R}(f) &= \boldsymbol{Z}_{\mathrm{MR}_{1,1}}(f) - \boldsymbol{F}_\mathrm{R}(f)\boldsymbol{Z}_{\mathrm{MR}_{2,1}}(f), \\
\boldsymbol{F}_\mathrm{R}(f) &= \boldsymbol{Z}_{\mathrm{MR}_{1,2}}(f)(\boldsymbol{Z}_\mathrm{AR}(f) + \boldsymbol{Z}_{\mathrm{MR}_{2,2}}(f))^{-1},
\end{aligned} \tag{2.155}$$

Second, the generalized circuit theoretic multiport model equation relating the input

voltage to the output voltage can also be determined with the previous multiport equations.

$$\begin{aligned}
\boldsymbol{Q}(f) &= Z_{\mathrm{L}}(Z_{\mathrm{L}}\boldsymbol{I}_M + \boldsymbol{Z}_{\mathrm{R}}(f))^{-1}, \\
\boldsymbol{\eta}(f) &= \frac{1}{\sqrt{R_{\mathrm{L}}}}\boldsymbol{Q}(f)(\boldsymbol{F}_{\mathrm{R}}(f)\boldsymbol{u}_{\mathrm{AN}} - \boldsymbol{u}_{\mathrm{N}} + \boldsymbol{Z}_{\mathrm{R}}(f)\boldsymbol{i}_{\mathrm{N}}), \\
\boldsymbol{D}(f) &= Z_{\mathrm{L}}(Z_{\mathrm{L}}\boldsymbol{I}_M + \boldsymbol{Z}_{\mathrm{R}}(f))^{-1}\boldsymbol{Z}_{\mathrm{RT}}(f)(Z_{\mathrm{G}}\boldsymbol{I}_N + \boldsymbol{Z}_{\mathrm{T}}(f))^{-1},
\end{aligned} \tag{2.156}$$

from which the output voltage equation is obtained

$$\boldsymbol{u}_{\mathrm{L}} = \boldsymbol{D}(f)\boldsymbol{u}_{\mathrm{G}} + \sqrt{R_{\mathrm{L}}}\boldsymbol{\eta}(f). \tag{2.157}$$

The physical model of the propagation channel in the transimpedance $\boldsymbol{Z}_{\mathrm{ART}}$ can be defined to be frequency dependent, but this is not considered in this thesis, because the adopted frequency independent model is used to keep consistency with other publications. It is defined in details in Chapter 4. As to the information theoretic equations of the system with DMNs, the power coupling matrix and the noise covariance matrix are written as follows

$$\begin{aligned}
\boldsymbol{B}(f) &= \boldsymbol{B}(f)^{1/2}\boldsymbol{B}(f)^{\mathrm{H}/2}, \\
\boldsymbol{B}(f)^{1/2} &= 2\sqrt{R_{\mathrm{G}}}\Big[(Z_{\mathrm{G}}\boldsymbol{I}_N + \boldsymbol{Z}_{\mathrm{T}}(f))^{-\mathrm{H}}\boldsymbol{Z}_{\mathrm{MT}_{2,1}}(f)^{\mathrm{H}} \\
&\qquad (\boldsymbol{Z}_{\mathrm{AT}}(f) + \boldsymbol{Z}_{\mathrm{MT}_{2,2}}(f))^{-\mathrm{H}}\Big]\,\mathrm{Re}(\boldsymbol{Z}_{\mathrm{AT}}(f))^{\mathrm{H}/2},
\end{aligned} \tag{2.158}$$

$$\begin{aligned}
\boldsymbol{R}_{\boldsymbol{\eta}}(f) &= \frac{|Z_{\mathrm{L}}|^2}{R_L}(Z_{\mathrm{L}}\boldsymbol{I}_M + \boldsymbol{Z}_{\mathrm{R}}(f))^{-1}\boldsymbol{N}(f)(Z_{\mathrm{L}}\boldsymbol{I}_M + \boldsymbol{Z}_{\mathrm{R}}(f))^{-\mathrm{H}} \\
\boldsymbol{N}(f) &= 4kT\Delta_f\boldsymbol{F}_{\mathrm{R}}(f)\,\mathrm{Re}(\boldsymbol{Z}_{\mathrm{AR}}(f))\boldsymbol{F}_{\mathrm{R}}(f)^{\mathrm{H}} + \sigma_u^2\boldsymbol{I}_M + \\
&\qquad + \sigma_i^2\boldsymbol{Z}_{\mathrm{R}}(f)\boldsymbol{Z}_{\mathrm{R}}(f)^{\mathrm{H}} - 2\sigma_u\sigma_i\,\mathrm{Re}(\rho\boldsymbol{Z}_{\mathrm{R}}(f)^{\mathrm{H}}), \\
\boldsymbol{R}_{\boldsymbol{\eta}}(f)^{1/2} &= \frac{Z_{\mathrm{L}}}{R_L}(Z_{\mathrm{L}}\boldsymbol{I}_M + \boldsymbol{Z}_{\mathrm{R}}(f))^{-1}\boldsymbol{N}(f)^{1/2}.
\end{aligned} \tag{2.159}$$

While the $\boldsymbol{B}$ matrix was equal to an identity, the noise covariance matrix $\boldsymbol{R}_{\boldsymbol{\eta}}$ was equal to a scaled identity when considering the ideal scenario of lossless elements operating at the center frequency. Inserting the parasitics breaks the balances of the variables with the

structure of the DMNs, losing, thus, the optimal decoupling and matching features. With these quantities, the information theoretic variables can be determined

$$\boldsymbol{y}(f) = \boldsymbol{H}(f)\boldsymbol{x}(f) + \boldsymbol{\nu}(f), \text{ with } \begin{cases} \boldsymbol{x}(f) = \dfrac{1}{2\sqrt{R_{\mathrm{G}}}}\boldsymbol{B}(f)^{\mathrm{H}/2}\boldsymbol{u}_{\mathrm{G}}, \\ \boldsymbol{\nu}(f) = \sigma_{\boldsymbol{\nu}}\boldsymbol{R}_{\boldsymbol{\eta}}(f)^{-1/2}\boldsymbol{\eta}, \\ \boldsymbol{y}(f) = \sqrt{\dfrac{\sigma_{\boldsymbol{\nu}}^2}{R_{\mathrm{L}}}}\boldsymbol{R}_{\boldsymbol{\eta}}(f)^{-1/2}\boldsymbol{u}_{\mathrm{L}}, \\ \boldsymbol{H}(f) = 2\sigma_{\boldsymbol{\nu}}\sqrt{\dfrac{R_{\mathrm{G}}}{R_{\mathrm{L}}}}\boldsymbol{R}_{\boldsymbol{\eta}}(f)^{-1/2}\boldsymbol{D}(f)\boldsymbol{B}(f)^{-\mathrm{H}/2}. \end{cases} \tag{2.160}$$

The same is done for the circuit theoretic equations of the system without DMNs

$$\begin{aligned} \boldsymbol{D}'(f) &= Z_{\mathrm{L}}(Z_{\mathrm{L}}\boldsymbol{I}_M + \boldsymbol{Z}_{\mathrm{AR}}(f))^{-1}\boldsymbol{Z}_{\mathrm{ART}}(f)(Z_{\mathrm{G}}\boldsymbol{I}_N + \boldsymbol{Z}_{\mathrm{AT}}(f))^{-1}, \\ \boldsymbol{\eta}'(f) &= \frac{Z_{\mathrm{L}}}{\sqrt{R_{\mathrm{L}}}}(Z_{\mathrm{L}}\boldsymbol{I}_N + \boldsymbol{Z}_{\mathrm{AR}}(f))^{-1}(\boldsymbol{u}_{\mathrm{AN}} - \boldsymbol{u}_{\mathrm{N}} + \boldsymbol{Z}_{\mathrm{AR}}(f)\boldsymbol{i}_{\mathrm{N}}) \\ \boldsymbol{u}'_{\mathrm{L}} &= \boldsymbol{D}'(f)\boldsymbol{u}'_{\mathrm{G}} + \sqrt{R_{\mathrm{L}}}\boldsymbol{\eta}'(f), \end{aligned} \tag{2.161}$$

and the power coupling and noise covariance matrices

$$\begin{aligned} \boldsymbol{B}'(f) &= \boldsymbol{B}'(f)^{1/2}\boldsymbol{B}'(f)^{\mathrm{H}/2}, \\ \boldsymbol{B}'(f)^{1/2} &= 2\sqrt{R_{\mathrm{G}}}(Z_{\mathrm{G}}\boldsymbol{I}_N + \boldsymbol{Z}_{\mathrm{AT}}(f))^{-\mathrm{H}}\,\mathrm{Re}(\boldsymbol{Z}_{\mathrm{AT}}(f))^{\mathrm{H}/2}, \end{aligned} \tag{2.162}$$

$$\begin{aligned} \boldsymbol{R}'_{\boldsymbol{\eta}} &= \frac{|Z_{\mathrm{L}}|^2}{R_L}(Z_{\mathrm{L}}\boldsymbol{I}_M + \boldsymbol{Z}_{\mathrm{AR}}(f))^{-1}\boldsymbol{N}'(f)(Z_{\mathrm{L}}\boldsymbol{I}_M + \boldsymbol{Z}_{\mathrm{AR}}(f))^{-\mathrm{H}} \\ \boldsymbol{N}'(f) &= 4kT\Delta_f\mathrm{Re}(\boldsymbol{Z}_{\mathrm{AR}}(f)) + \sigma_u^2\boldsymbol{I}_M + \\ &\qquad + \sigma_i^2\boldsymbol{Z}_{\mathrm{AR}}(f)\boldsymbol{Z}_{\mathrm{AR}}(f)^{\mathrm{H}} - 2\sigma_u\sigma_i\mathrm{Re}\left(\rho\boldsymbol{Z}_{\mathrm{AR}}(f)^{\mathrm{H}}\right), \\ \boldsymbol{R}_{\boldsymbol{\eta}}{}'(f)^{1/2} &= \frac{Z_{\mathrm{L}}}{R_L}(Z_{\mathrm{L}}\boldsymbol{I}_M + \boldsymbol{Z}_{\mathrm{AR}}(f))^{-1}\boldsymbol{N}'(f)^{1/2}, \end{aligned} \tag{2.163}$$

to, finally, hold the set of generalized information theoretic equations

$$\boldsymbol{y}'(f) = \boldsymbol{H}'(f)\boldsymbol{x}'(f) + \boldsymbol{\nu}'(f), \text{ with } \begin{cases} \boldsymbol{x}'(f) = \dfrac{1}{2\sqrt{R_{\mathrm{G}}}}\boldsymbol{B}'(f)^{\mathrm{H}/2}\boldsymbol{u}_{\mathrm{G}}, \\ \boldsymbol{\nu}'(f) = \sigma_{\nu}\boldsymbol{R}_{\boldsymbol{\eta}}{}'(f)^{-1/2}\boldsymbol{\eta}, \\ \boldsymbol{y}'(f) = \sqrt{\dfrac{\sigma_{\nu}^2}{R_{\mathrm{L}}}}\boldsymbol{R}_{\boldsymbol{\eta}}{}'(f)^{-1/2}\boldsymbol{u}_{\mathrm{L}}, \\ \boldsymbol{H}'(f) = 2\sigma_{\nu}\sqrt{\dfrac{R_{\mathrm{G}}}{R_{\mathrm{L}}}}\boldsymbol{R}_{\boldsymbol{\eta}}{}'(f)^{-1/2}\boldsymbol{D}'(f)\boldsymbol{B}'(f)^{-\mathrm{H}/2}. \end{cases} \tag{2.164}$$

With the generalized equations in hands, the achievable rates can be computed for ideal and non-ideal systems in different multi-antenna scenarios. This is done in Chapter 3, in which the problematic of the available and transmit powers on the capacity computations arises and enables the visualization of the parasitics' influence on power losses.

3 MULTI-ANTENNA SYSTEMS' RATES AND CAPACITY

The different multi-antenna systems explored in this thesis consider a single cell, i.e. one BS establishing the communication link with mobile terminals around it. The number of these users characterize the scenario as single-user (SU) or multi-user (MU).

From each of these two scenarios stem 3 configurations, classified based on the number of antennas on the mobile(s), characterizing multiple-input-single-output (MISO), single-input-multiple-output (SIMO) and multiple-input-multiple-output (MIMO) systems. The base station is always equipped with an antenna array of the same number of elements in every scenario. These antennas are used for both transmitting and receiving on the BS and on the mobiles.

In this chapter, capacity equations are presented for some of the scenarios aforementioned with their particularities, similarly to how it was previously done in the work of (LAAS *et al.*, 2018). As it was done in the publication just mentioned, in Chapter 4 the propagation channel will be drawn from a statistical distribution and will be plugged into the expressions of the information theoretic channels to, in the end, compute the rates and capacity values.

These values, obtained in each realization of the propagation channel, will be averaged out of the number of times the channel was generated, yielding the ergodic rates and capacity

$$C_{\text{erg}} = \mathbb{E}_{\boldsymbol{Z}_{\text{ART}}}\left[C\right]. \tag{3.1}$$

At the end of the chapter, the problem of computing the capacity using the available power is investigated, allowing for the comprehension of how to perform the capacity evaluations to obtain the results presented in Chapter 4.

3.1 Single-user Scenarios

For a single-user, the three input-output scenarios aforementioned are investigated. The mobile may be equipped in two possible ways: with a single $\lambda/2$-dipole or with a uniform circular array of $\lambda/2$-dipoles with fewer elements than in the BS's UCA but with the same antenna spacing. The dipoles in both cases have the same physical characteristics as those in the BS.

Having only one single-antenna mobile operating provides two of these configurations based on the direction of the data transmission and reception: in the downlink, we have a MISO system and in the uplink a SIMO. In the SU scenario with a $\lambda/2$-dipole UCA at the mobile,

both the downlink and the uplink form MIMO systems. Nevertheless, both directions are still investigated because they differ in the number of antennas in the transmit and in the receive side.

3.1.1 Single-antenna Mobile Downlink: MISO

With only one antenna, on the receive side there is not an array impedance matrix, but the dipole's self impedance $Z_{\mathrm{AR}} \in \mathbb{C}\,\Omega$. The BS's antennas transmit a signal vector which has its elements linearly combined in the propagation channel and the single-antenna receives this combination as a scalar. Already, it is possible to verify, with the help of (2.11) and (2.114) for $\boldsymbol{u}_{\mathrm{B}}$ and $\boldsymbol{u}'_2$ scalars, that the physical channel $\boldsymbol{Z}^{\mathrm{T}}_{\mathrm{ART}}$ is a row vector in $\mathbb{C}^{1\times N}\Omega$.

Additionally, the Rx-DMN is only a 2-port network. Thus, its elements are scalars instead of block matrices. One advantage of the MISO system is the fact that the receiver does not require decoupling to obtain higher values of SNR. It needs only the noise matching strategy to reduce the noise figure to the smallest value possible.

By observation of the variables' and quantities' dimensions corresponding to a MISO system in (2.156) and in (2.161), it can be noticed that $\boldsymbol{D}(f)$, $\boldsymbol{D'}(f)$ are vectors in $\mathbb{C}^{1\times N}$

$$
\begin{aligned}
z^{\mathrm{T}}_{\mathrm{RT}}(f) &= \frac{Z_{\mathrm{MR}_{1,2}}(f)}{(Z_{\mathrm{AR}}(f)+Z_{\mathrm{MR}_{2,2}}(f))} z^{\mathrm{T}}_{\mathrm{ART}}(f)(\boldsymbol{Z}_{\mathrm{AT}}(f)+\boldsymbol{Z}_{\mathrm{MT}_{2,2}}(f))^{-1}\boldsymbol{Z}_{\mathrm{MT}_{2,1}}(f),\\
Z_{\mathrm{R}}(f) &= Z_{\mathrm{MR}_{1,1}}(f) - \frac{Z_{\mathrm{MR}_{1,2}}(f)Z_{\mathrm{MR}_{2,1}}(f)}{(Z_{\mathrm{AR}}(f)+Z_{\mathrm{MR}_{2,2}}(f))},\\
\boldsymbol{d}^{\mathrm{T}}(f) &= \frac{Z_{\mathrm{L}}(f)}{(Z_{\mathrm{L}}(f)+Z_{\mathrm{R}}(f))} z^{\mathrm{T}}_{\mathrm{RT}}(f)(Z_{\mathrm{G}}(f)\boldsymbol{I}_N+\boldsymbol{Z}_{\mathrm{T}}(f))^{-1}, \qquad (3.2)\\
\boldsymbol{d'}^{\mathrm{T}}(f) &= \frac{Z_{\mathrm{L}}(f)}{(Z_{\mathrm{L}}(f)+Z_{\mathrm{AR}}(f))} z^{\mathrm{T}}_{\mathrm{ART}}(f)(Z_{\mathrm{G}}(f)\boldsymbol{I}_N+\boldsymbol{Z}_{\mathrm{AT}}(f))^{-1}. \qquad (3.3)
\end{aligned}
$$

As the receiver possesses only one port, the noise covariance is a scalar and, thus, following (2.160) and (2.164), $\boldsymbol{H}(f)$ and $\boldsymbol{H'}(f)$ are also vectors. They have the same dimensions of their respective $\boldsymbol{d}$ vectors composing them, i.e. they are in $\mathbb{C}^{1\times N}$

$$
\begin{aligned}
\boldsymbol{h}^{\mathrm{T}}(f) &= 2\sqrt{\frac{\sigma_v^2}{R_\eta(f)}}\sqrt{\frac{R_{\mathrm{G}}}{R_{\mathrm{L}}}}\boldsymbol{d}^{\mathrm{T}}(f)\boldsymbol{B}(f)^{-\mathrm{H}/2}, \qquad (3.4)\\
\boldsymbol{h'}^{\mathrm{T}}(f) &= 2\sqrt{\frac{\sigma_v^2}{R_\eta{}'(f)}}\sqrt{\frac{R_{\mathrm{G}}}{R_{\mathrm{L}}}}\boldsymbol{d'}^{\mathrm{T}}(f)\boldsymbol{B'}(f)^{-\mathrm{H}/2}. \qquad (3.5)
\end{aligned}
$$

The single antenna can receive only one scalar symbol at a time, thus, $\boldsymbol{x}$ is the product of the transmit symbol with a beamforming vector. The latter can be chosen to maximize the

output rate of the system.

In (LAAS *et al.*, 2018), the authors applied the linear precoder $\boldsymbol{f} = \dfrac{\boldsymbol{h}^{\mathrm{H}}}{\|\boldsymbol{h}\|_2}$ to the signal $\boldsymbol{x} = \boldsymbol{f}s$, in order to achieve capacity, where $s \sim \mathcal{N}_C(0\sqrt{\mathrm{W}}, P_{\mathrm{T}})$ is the random symbol generated for a given transmit power P_{T}. Then, the equation of the capacity holds, as it is in the work of Laas *et al.*,

$$C_{\mathrm{SUMISO}} = \log_2\left(1 + \frac{P_{\mathrm{T}}}{\sigma_{\boldsymbol{\nu}}^2}\|\boldsymbol{h}\|_2^2\right), \tag{3.6}$$

where $\boldsymbol{h}$ can be the information theoretic channel vector of either system, with or without DMNs.

3.1.2 Single-antenna Mobile Uplink: SIMO

As mentioned before, the same BS's and mobile's antennas are used to transmit and to receive. However, in order for the communication to work in both directions of the link, the BS and the mobile must have two sets of RF-chains and amplifiers to switch from one to the other when transmitting and when receiving. In the system with DMNs, transmit and receive DMNs are connected to the appropriate sets of RF-chains and amplifiers of the BS and of the mobile.

In this manner, the mobile in the downlink receives the signal impinging on the $\lambda/2$-dipole and forwards it towards the LNA and, then, sends it through the receive RF-chain. In the uplink, the mobile generates the transmit signal, passes it through the transmit RF-chain, amplifies it with the HPA, to be further radiated by the same dipole. This transition with switches occurs according to a time division duplex operation scheme.

For a communication system operating in a frequency division duplex scheme, the two sets of RF-chain and the two DMNs are also necessary, in addition to 3-ports branching filters to allow for transmission and reception to happen simultaneously and other strategies to avoid interference of the stronger transmitting signals over the weaker receiving signals, such as guard bands between the pair of carrier frequencies and strong RF-filters.

The single-antenna mobile in the uplink configures a SIMO system. As such, it brings the advantage of decoupling transmit ports being unnecessary. Still, in order to grant maximum power transfer from the output of the HPA to the dipole, power matching is needed.

Just like in the downlink, the single port in the uplink simplifies some expressions, specifically those related to the transmit side, since there is only an antenna self impedance

instead of a mutual impedance matrix and the physical channel, again, becomes a vector, as it can be seen in (2.11) and (2.114) for $\boldsymbol{u}_{\mathrm{A}}$ and $\boldsymbol{u}'_1$ scalars.

$$Z_{\mathrm{T}}(f) = Z_{\mathrm{MT}_{1,1}}(f) - \frac{Z_{\mathrm{MT}_{1,2}}(f) Z_{\mathrm{MT}_{2,1}}(f)}{(Z_{\mathrm{AT}}(f) + Z_{\mathrm{MT}_{2,2}}(f))},$$

$$\boldsymbol{Z}_{\mathrm{RT}}(f) = \boldsymbol{Z}_{\mathrm{MR}_{1,2}}(f)(\boldsymbol{Z}_{\mathrm{AR}}(f) + \boldsymbol{Z}_{\mathrm{MR}_{2,2}}(f))^{-1} \boldsymbol{z}_{\mathrm{ART}}(f) \frac{Z_{\mathrm{MT}_{2,1}}(f)}{(Z_{\mathrm{AT}}(f) + Z_{\mathrm{MT}_{2,2}}(f))},$$

$$\boldsymbol{d}(f) = \frac{Z_{\mathrm{L}}(f)}{(Z_{\mathrm{G}}(f) + Z_{\mathrm{T}}(f))} (Z_{\mathrm{L}}(f)\boldsymbol{I}_M + \boldsymbol{Z}_{\mathrm{R}}(f))^{-1} \boldsymbol{z}_{\mathrm{RT}}(f), \tag{3.7}$$

$$\boldsymbol{d}'(f) = \frac{Z_{\mathrm{L}}(f)}{(Z_{\mathrm{G}}(f) + Z_{\mathrm{AT}}(f))} (Z_{\mathrm{L}}(f)\boldsymbol{I}_M + \boldsymbol{Z}_{\mathrm{AR}}(f))^{-1} \boldsymbol{z}_{\mathrm{ART}}(f). \tag{3.8}$$

Now, with $\boldsymbol{z}_{\mathrm{ART}}$, $\boldsymbol{z}_{\mathrm{RT}} \in \mathbb{C}^{N\times 1}\Omega$, so are also $\boldsymbol{d}(f)$, $\boldsymbol{d}'(f) \in \mathbb{C}^{N\times 1}$. Together with the power coupling matrix, which is simply a scalar for this case, the following holds

$$\boldsymbol{h}(f) = 2\sigma_{\boldsymbol{\nu}} \sqrt{\frac{R_{\mathrm{G}}}{B(f)^* R_{\mathrm{L}}}} \boldsymbol{R}_{\eta}{}^{-1/2}(f) \boldsymbol{d}(f)^{-\mathrm{H}/2}, \tag{3.9}$$

$$\boldsymbol{h}'(f) = 2\sigma_{\boldsymbol{\nu}} \sqrt{\frac{R_{\mathrm{G}}}{B'(f)^* R_{\mathrm{L}}}} \boldsymbol{R}_{\eta}{}'^{-1/2}(f) \boldsymbol{d}'(f)^{-\mathrm{H}/2}, \tag{3.10}$$

$$\tag{3.11}$$

resulting in the information theoretic channels as column vectors in $\mathbb{C}^{N\times 1}$.

The single-antenna can transmit but one symbol at a time and, since there is only one antenna, it cannot generate any beamforming vector to precode the channel. The transmit signal is, then, $x = s$, $s \sim \mathcal{N}_C(0\sqrt{\mathrm{W}}, P_{\mathrm{T}})$. With the radiation of the signal, the base station's UCA of half-wavelength dipoles receive the impinging signal and passes it through a receive filter.

As it was done in (LAAS *et al.*, 2018) for the SIMO scenario, the capacity is achieved for a matched received filter $\boldsymbol{g} = \dfrac{\boldsymbol{h}}{\|\boldsymbol{h}\|_2}$, that maximizes the SNR, and results in

$$C_{\mathrm{SUSIMO}} = \log_2 \left(1 + \frac{P_{\mathrm{T}}}{\sigma_{\boldsymbol{\nu}}^2} \|\boldsymbol{h}\|_2^2\right). \tag{3.12}$$

3.1.3 Multi-antenna Mobile Link: MIMO

In this configuration, both directions of the communication link characterize MIMO systems. If the number of antennas in the BS's and mobile's arrays is the same, down and uplink represent essentially the same MIMO system, because the set of circuitry and antennas used on

one side of the link for one transmission-reception direction has a similar set of elements on the other side for the opposite direction.

However, for distinct numbers of antennas in the arrays, down and uplink have different characteristics. The theoretical formulation of the capacity might be the same for these two directions, but the performance might not be the same. This is basically due to the different coupling intensities for different numbers of antennas in the array.

The larger the number of antennas, the larger the achievable rates are, according to information theory. However, in the system without DMNs and in both systems with parasitics, the disbalance of the elements' interactions is larger, due to the lack of optimal decoupling and matching. Then, the question arises of which coupling, power or noise, is less sensitive to the increase of the antenna numbers and, thus, is worth to be stronger while still giving high rates.

In a SU-MIMO communication scenario, only one propagation channel is composed of subchannels. The transmit power can, in that way, be optimally distributed among the subchannels such as to yield the achievable rates of the system. According to (TELATAR, 1999) and as it was done in (LAAS *et al.*, 2017), capacity in this scenario is given by

$$C_{\mathrm{SUMIMO}}(P_{\mathrm{T}}) = \log_2 \left| \boldsymbol{I}_N + \boldsymbol{H}^{\mathrm{H}} \boldsymbol{H} \boldsymbol{R}_{\boldsymbol{x}} \right|, \tag{3.13}$$

where $\boldsymbol{R}_{\boldsymbol{x}} = \boldsymbol{V}\boldsymbol{\Psi}\boldsymbol{V}^{\mathrm{H}}$ and $\mathrm{Tr}(\boldsymbol{\Psi}) = P_{\mathrm{T}}$. The matrix $\boldsymbol{V}$ is obtained via the eigenvalue decomposition (EVD) $\boldsymbol{H}^{\mathrm{H}}\boldsymbol{H} = \boldsymbol{V}\boldsymbol{\Phi}\boldsymbol{V}^{\mathrm{H}}$ and $\boldsymbol{\Psi}$ is the diagonal matrix which has in its diagonal entries the transmit power distributed among the subchannels by the waterfilling method.

The two antenna arrays transmitting and receiving allow for the simultaneous transmission of more than one symbol at a time. The symbols are modelled as the random vectors $\boldsymbol{s} \sim \mathcal{N}_C(\boldsymbol{0}_N \sqrt{\mathrm{W}}, \boldsymbol{\Psi})$. To achieve capacity, the transmit symbols must be precoded with the matrix $\boldsymbol{V}$, from the EVD, to yield the transmit signal $\boldsymbol{x} = \boldsymbol{V}\boldsymbol{s}$.

3.2 Multiuser Scenarios

For this case of multiple non-collaborative users, two scenarios are explored: when the mobiles are equipped with only one antenna and when the mobiles are equipped with antenna arrays. Only the downlink is investigated, characterizing, then, MU-MISO and MU-MIMO systems. In both cases, the total number of antennas on the mobiles is smaller than or equal to the number of antennas on the base station.

The physically consistent modelling of the multiuser system is similar to what has been done until now regarding the downlink transmitter, the base station. The particularity now is related to the modelling of the channel and of the mobiles on the receive side. To deal with this, it is assumed that the users are sufficiently separated, such as to consider the coupling between antennas of different users negligible. For each user, a different instance of the physical propagation channel $\boldsymbol{Z}_{\mathrm{ART}}$ is generated.

Assuming so, the first possibility is to consider the mobile terminals as part of a single "large"receive system. Thus, the receive array impedance matrix $\boldsymbol{Z}_{\mathrm{AR}}$ becomes a diagonal matrix for multiuser, single-antenna mobiles or a block diagonal matrix for multi-antenna users. The blocks stand for the array impedance matrices of each mobile. From there, accordingly, other quantities such as the noise covariance become diagonal or block diagonal matrices.

All of the circuit and information theoretic equations are, thus, evaluated using $\boldsymbol{Z}_{\mathrm{AR}}$ structured in either of the diagonal fashions mentioned above. The propagation channels are stacked corresponding to the organization of $\boldsymbol{Z}_{\mathrm{AR}}$ in (2.11). The channels are, finally, computed using (2.160) or (2.164), resulting in a matrix with the individual channels stacked in the same manner as the propagation channels.

The second strategy, slightly different of the first idea, is to simply consider separate MCT models (as in Figs. 3 and 11) for the mobile terminals and to compute all of the circuit and information theoretic equations separately, including, finally, the users' channels. The two strategies have no difference regarding the efficiency and the possibility of including at the same time users with and without DMNs.

Still, the problems of the interference between the non-collaborative users and of how to distribute the transmit power among the channels and subchannels must be dealt with. For this end, the efficient weighted sum rate algorithm proposed in (GUTHY *et al.*, 2010) was implemented to compute the sum rates in the two downlink scenarios: MU-MISO and MU-MIMO.

The computation of capacity in multiuser scenarios require non-linear techniques, such as dirty-paper coding (Costa, 1983). In this technique, these scenarios become equivalent, in capacity computation terms, to interference free Gaussian channels, provided that the encoder in the transmitter has information on the interfering random signals. However, these techniques, including dirty paper, present high computational costs.

In this circumstance, the efficient weighted sum rate algorithm is adopted, because it

gives rates close to capacity values with less computational cost.

The algorithm makes use of linear signal processing, specifically by the introduction of zero forcing constraints, to nullify the interference between the streams of data transmitted in different channels. Initially, it selects the user to whom the transmission of the first data stream using the entire transmit power would give the best rate and computes a receive filter for it.

It, then, successively assigns data streams to the users which would increase the rate, according to their respective channels. For each data stream assigned, the optimal receive filter of the stream's recipient channel, or subchannel, is kept for the next iterations. Following this, the algorithm computes the channel gains and finally, in the sequence, the transmit power distribution among the data streams is computed based on a waterfilling solution over the channel gains.

After running the algorithm, the rates can be calculated according to (GUTHY *et al.*, 2009), for the sum rate without weights

$$R(P_{\mathrm{T}}) = \sum_{j=1}^{d}(1+\psi_j\zeta_j^2), \qquad \mathbf{\Psi} = \mathrm{diag}(\psi_1,\psi_2,...,\psi_d),\ \mathrm{Tr}(\mathbf{\Psi}) = P_{\mathrm{T}}. \tag{3.14}$$

where ψ_j is the share of the transmit power allocated to the jth data stream, whose channel (or subchannel) gain is ζ_j. The algorithm also computes the effective precoders of the assigned data streams. The transmit signal $\boldsymbol{x}$ are the precoded symbols $\boldsymbol{s} \sim \mathcal{N}_C(\mathbf{0}_N\sqrt{\mathrm{W}}, \mathbf{\Gamma})$.

The weighted sum rate algorithm is an efficient and smart computational technique that can also be used to compute the achievable rates in the single-user scenarios mentioned previously. In any case, the MCT modelling is always necessary, because it gives the physically consistent information theoretical channel equations used in the algorithm.

Before the simulations can be presented, it is necessary to discuss the problem of the difference between available and transmit power.

3.3 Rates and Capacity and Available Power

When comparing the systems with and without DMNs in the different scenarios to investigate the effects of optimal, suboptimal and no decoupling, the systems' rates and capacity are the figures of merit. The capacity equations, however, in the scenarios presented are all computed with the transmit power, but they will be plot on the scale of the available power.

Transmit power is, according to (2.46) or (2.132), computed using the antennas port voltages and currents, even with the inclusion of the resistances in modelling the skin effect as in Fig. 12.

For any determined value of the transmit power, these port variables, on their own, essentially bring no information about the coupling and mismatch effects on the transmitters. This information can only be found in the relation between the transmit power and the power that could be drawn from the HPAs, a power efficiency ratio.

3.3.1 Available and Transmit Power Ratio

Including the power efficiency in the capacity equation consists in finding the ratio between the available and the transmit powers and using it to compute the rates and capacity of the systems with the same value of available power divided by their respective ratios instead of the transmit power. Doing so, the rates and capacity will bear the information of how much of the available power is being transmitted due to the intensity of coupling and mismatch.

The key to calculate this ratio is to, within the conditions the system is submitted to, find the generators' voltages necessary to produce the antennas' currents which would be produced if the transmitter had been under perfect decoupling and power matching. These antennas' currents are expressed, in their turn, in terms of the generators' voltages of the system under these perfect conditions

$$
\begin{aligned}
&\boldsymbol{u}_{\mathrm{G}}(f) = h_1(\boldsymbol{i}_{\mathrm{A}}(f)),\ \boldsymbol{i}_{\mathrm{A}}(f) = \boldsymbol{i}_{\mathrm{A}},\\
&\boldsymbol{u}'_{\mathrm{G}}(f) = h_2(\boldsymbol{i}'_1(f)),\ \boldsymbol{i}'_1(f) = \boldsymbol{i}_{\mathrm{A}},\\
&\boldsymbol{i}_{\mathrm{A}} = h(\boldsymbol{u}_{\mathrm{G}}) \implies \begin{cases} \boldsymbol{u}_{\mathrm{G}}(f) = h_1(h(\boldsymbol{u}_{\mathrm{G}})) = \boldsymbol{M}(f)^{\mathrm{H}/2}\boldsymbol{u}_{\mathrm{G}} \\ \boldsymbol{u}'_{\mathrm{G}}(f) = h_2(h(\boldsymbol{u}_{\mathrm{G}})) = \boldsymbol{M}'(f)^{\mathrm{H}/2}\boldsymbol{u}_{\mathrm{G}}. \end{cases}
\end{aligned}
\tag{3.15}
$$

To obtain $h(\cdot)$, (2.22) and (2.30) are referred to, $\boldsymbol{Z}_{\mathrm{T}}$ is expanded with (2.24) and the quantities in the optimal Tx-DMN matrix are substituted for their identities according to the DMN's design in (2.70),

$$\boldsymbol{i}_\mathrm{A} = (\boldsymbol{Z}_\mathrm{AT} + \boldsymbol{Z}_{\mathrm{MT}_{2,2}})^{-1}\boldsymbol{Z}_{\mathrm{MT}_{2,1}}\left[Z_\mathrm{G}\boldsymbol{I}_N + \boldsymbol{Z}_{\mathrm{MT}_{1,1}} - \boldsymbol{Z}_{\mathrm{MT}_{1,2}}(\boldsymbol{Z}_\mathrm{AT} + \boldsymbol{Z}_{\mathrm{MT}_{2,2}})^{-1}\boldsymbol{Z}_{\mathrm{MT}_{2,1}}\right]^{-1}\boldsymbol{u}_\mathrm{G},$$
$$\boldsymbol{i}_\mathrm{A} = \mathrm{Re}(\boldsymbol{Z}_\mathrm{AT})^{-1}(-j\sqrt{R_\mathrm{G}}\mathrm{Re}(\boldsymbol{Z}_\mathrm{AT})^{1/2})\frac{1}{2R_\mathrm{G}}\boldsymbol{u}_\mathrm{G},$$
$$\boldsymbol{i}_\mathrm{A} = h(\boldsymbol{u}_\mathrm{G}) = -j\frac{1}{2\sqrt{R_\mathrm{G}}}\mathrm{Re}(\boldsymbol{Z}_\mathrm{AT})^{-1/2}\boldsymbol{u}_\mathrm{G}. \tag{3.16}$$

Now, to obtain $\boldsymbol{M}^{\mathrm{H}/2}$ and $\boldsymbol{M'}^{\mathrm{H}/2}$, circuit analysis of the models in Figs. 3 and 11 with the generalized variables are made. Finally, plugging $h(\boldsymbol{u}_\mathrm{G})$ in $h_1(\cdot)$ and $h_2(\cdot)$ yields

$$\boldsymbol{u}_\mathrm{G}(f) = \boldsymbol{M}(f)^{\mathrm{H}/2}\boldsymbol{u}_\mathrm{G},$$
$$\boldsymbol{M}(f)^{\mathrm{H}/2} = \Bigg[(Z_\mathrm{G}(f)\boldsymbol{I}_N + \boldsymbol{Z}_{\mathrm{MT}_{1,1}}(f))\boldsymbol{Z}_{\mathrm{MT}_{2,1}}(f)^{-1}$$
$$(\boldsymbol{Z}_\mathrm{AT}(f) + \boldsymbol{Z}_{\mathrm{MT}_{2,2}}(f)) - \boldsymbol{Z}_{\mathrm{MT}_{1,2}}(f)\Bigg]\left(-j\frac{1}{2\sqrt{R_\mathrm{G}}}\mathrm{Re}(\boldsymbol{Z}_\mathrm{AT})^{-1/2}\right), \tag{3.17}$$

for the generalized system with DMNs, and for the generalized system without DMNs

$$\boldsymbol{u}'_\mathrm{G}(f) = \boldsymbol{M'}(f)^{\mathrm{H}/2}\boldsymbol{u}_\mathrm{G} = (Z_\mathrm{G}(f)\boldsymbol{I}_N + \boldsymbol{Z}_\mathrm{AT}(f))\left(-j\frac{1}{2\sqrt{R_\mathrm{G}}}\mathrm{Re}(\boldsymbol{Z}_\mathrm{AT})^{-1/2}\right)\boldsymbol{u}_\mathrm{G}. \tag{3.18}$$

It is worth to mention that the quantity $\mathrm{Re}(\boldsymbol{Z}_\mathrm{AT})$ in both equations above does not include losses and is not generalized as a function of frequency, because this is the reference for the ideal situation at the center frequency f_c.

The ratios, finally, are calculated dividing the analysed systems' available powers by their transmit powers. Given that the generators' voltages of the analysed systems produce the transmit power that would have been produced under perfect decoupling and power matching, this transmit power is equal to the available power (2.77) of the perfectly decoupled and power matched system.

For the generalized system with DMNs, the powers ratio $K(f)$ is

$$K(f) = \frac{P_\mathrm{avail}}{P_\mathrm{T}} = \frac{1/(4R_\mathrm{G})\mathbb{E}\left[\boldsymbol{u}_\mathrm{G}^\mathrm{H}(f)\boldsymbol{u}_\mathrm{G}(f)\right]}{1/(4R_\mathrm{G})\mathbb{E}\left[\boldsymbol{u}_\mathrm{G}^\mathrm{H}\boldsymbol{u}_\mathrm{G}\right]} = \frac{\mathbb{E}\left[\boldsymbol{u}_\mathrm{G}^\mathrm{H}\boldsymbol{M}(f)^{1/2}\boldsymbol{M}(f)^{\mathrm{H}/2}\boldsymbol{u}_\mathrm{G}\right]}{\mathbb{E}\left[\boldsymbol{u}_\mathrm{G}^\mathrm{H}\boldsymbol{u}_\mathrm{G}\right]},$$
$$K(f) = \frac{\mathbb{E}\left[\boldsymbol{u}_\mathrm{G}^\mathrm{H}\boldsymbol{M}(f)\boldsymbol{u}_\mathrm{G}\right]}{\mathbb{E}\left[\boldsymbol{u}_\mathrm{G}^\mathrm{H}\boldsymbol{u}_\mathrm{G}\right]}, \tag{3.19}$$

whereas for the generalized system without DMNs, the powers ratio $K'(f)$ is

$$K'(f) = \frac{P_{\text{avail}}}{P_{\text{T}}} = \frac{1/(4R_{\text{G}})\mathbb{E}\left[\boldsymbol{u}'_{\text{G}}{}^{\text{H}}(f)\boldsymbol{u}'_{\text{G}}(f)\right]}{1/(4R_{\text{G}})\mathbb{E}\left[\boldsymbol{u}_{\text{G}}{}^{\text{H}}\boldsymbol{u}_{\text{G}}\right]} = \frac{\mathbb{E}\left[\boldsymbol{u}_{\text{G}}{}^{\text{H}}\boldsymbol{M}'(f)^{1/2}\boldsymbol{M}'(f)^{\text{H}/2}\boldsymbol{u}_{\text{G}}\right]}{\mathbb{E}\left[\boldsymbol{u}_{\text{G}}{}^{\text{H}}\boldsymbol{u}_{\text{G}}\right]},$$
$$K'(f) = \frac{\mathbb{E}\left[\boldsymbol{u}_{\text{G}}{}^{\text{H}}\boldsymbol{M}'(f)\boldsymbol{u}_{\text{G}}\right]}{\mathbb{E}\left[\boldsymbol{u}_{\text{G}}{}^{\text{H}}\boldsymbol{u}_{\text{G}}\right]}. \tag{3.20}$$

A good intuition behind these fractions is: how large must the systems' available powers be in order to radiate the same power as the perfect system does, which radiates all of its available power?

Following what was explained in the beginning of this chapter, related to the statistical realizations of the propagation channel $\boldsymbol{Z}_{\text{ART}}$ and equation $C_{\text{erg}} = \mathbb{E}_{\boldsymbol{Z}_{\text{ART}}}[C]$, in each realization, the generators' voltages $\boldsymbol{u}_{\text{G}}$ and any other variable will have fixed values. Thus, the ratios in the equations above will become Rayleigh quotients of the expressions inside the expectation operators and will be plugged into the capacity equations dividing the available power

$$C_{\text{erg}} = \mathbb{E}_{\boldsymbol{Z}_{\text{ART}}}\left[C\left(\frac{P_{\text{avail}}}{K(f)\big|_{\boldsymbol{Z}_{\text{ART}}}}\right)\right],$$
$$C'_{\text{erg}} = \mathbb{E}_{\boldsymbol{Z}_{\text{ART}}}\left[C'\left(\frac{P_{\text{avail}}}{K'(f)\big|_{\boldsymbol{Z}_{\text{ART}}}}\right)\right]. \tag{3.21}$$

The powers ratios $K(f)$ and $K'(f)$ are computed in each realization of the propagation channel by computing the transmit signal $\boldsymbol{x}$ and then mapping it to the perfect system's generators' voltage $\boldsymbol{u}_{\text{G}}$ by (2.56). Thus, $\boldsymbol{u}_{\text{G}}$ also, in the end, depends on the channel realization

$$\boldsymbol{u}_{\text{G}} = 2\sqrt{R_{\text{G}}}\boldsymbol{B}^{-\text{H}/2}\boldsymbol{V}\boldsymbol{s}, \tag{3.22}$$

since the signal $\boldsymbol{x}$ is the product of a precoder $\boldsymbol{V}$ and randomly generated transmit symbols $\boldsymbol{s} \sim \mathcal{N}_C(\boldsymbol{0}_N\sqrt{\text{W}}, \Psi)$, $\text{Tr}(\Psi) = P_{\text{T}}$. These two, for their parts, are computed and generated according to the scenarios of the systems analysed, as explained in the previous section.

3.3.2 The Circular Dependency

Rates and capacity can be calculated by dividing the determined available power by the powers ratios to yield the corresponding transmit power that is plugged into the capacity

equations. However, in order to compute the ratios, the generators' voltages $\boldsymbol{u}_{\mathrm{G}}$ must be calculated, and they depend on the random generation of the symbols $\boldsymbol{s}$ and the precoders $\boldsymbol{V}$, which depend on the time-variant channel. The symbols are drawn from statistical distributions with variance equal to the transmit power.

In short, transmit power is required to calculate the transmit power that will be applied into the rates computations. In order to deal with this circular dependency, Algorithm 2 is designed to discover the possible transmit power by successive updates of the powers ratio.

The algorithm divides the predetermined available power successively by the updated versions of the powers ratio and, when the transmit power (result of the division) of an iteration does not change much from the transmit power of the previous iteration, then the algorithm has converged and an approximate value of the proper powers ratio is obtained, allowing to insert the approximately precise transmit power into the capacity equations.

Algorithm 2: Available and transmit power ratio determination

Input: Available power P_{avail}, channel matrix $\boldsymbol{H}$ and noise covariance matrix $\boldsymbol{R}_{\boldsymbol{\eta}}$;

Output: Transmit power P_{T}, precoding matrix $\boldsymbol{V}$ and power distribution matrix $\boldsymbol{\Psi}$;

Initialization: $K = 1, \quad P_{\mathrm{T}} = \dfrac{P_{\mathrm{avail}}}{K}$;

$\boldsymbol{V} = f_{\boldsymbol{V}}(\boldsymbol{H}, \boldsymbol{R}_{\boldsymbol{\eta}}, P_{\mathrm{avail}}), \quad \boldsymbol{\Psi} = f_{\boldsymbol{\Psi}}(\boldsymbol{H}, \boldsymbol{R}_{\boldsymbol{\eta}}, P_{\mathrm{avail}})$;

$\boldsymbol{s} \sim \mathcal{N}_C(\boldsymbol{0}_N\sqrt{\mathrm{W}},\ \boldsymbol{\Psi}), \quad \boldsymbol{x} = \boldsymbol{V}\boldsymbol{s}$;

$\boldsymbol{u}_{\mathrm{G}} = 2\sqrt{R_{\mathrm{G}}}\boldsymbol{B}^{-\mathrm{H}/2}\boldsymbol{x}, \quad K = \dfrac{\boldsymbol{u}_{\mathrm{G}}^{\mathrm{H}}\boldsymbol{M}\boldsymbol{u}_{\mathrm{G}}}{\boldsymbol{u}_{\mathrm{G}}^{\mathrm{H}}\boldsymbol{u}_{\mathrm{G}}}$;

error $= P_{\mathrm{T}} - P_{\mathrm{avail}}/K$;

while error $>$ mark : $P_{\mathrm{T}} = \dfrac{P_{\mathrm{avail}}}{K}$;

$\boldsymbol{V} = f_{\boldsymbol{V}}(\boldsymbol{H}, \boldsymbol{R}_{\boldsymbol{\eta}}, P_{\mathrm{T}}), \quad \boldsymbol{\Psi} = f_{\boldsymbol{\Psi}}(\boldsymbol{H}, \boldsymbol{R}_{\boldsymbol{\eta}}, P_{\mathrm{T}})$;

$\boldsymbol{s} \sim \mathcal{N}_C(\boldsymbol{0}_N\sqrt{\mathrm{W}},\ \boldsymbol{\Psi}), \quad \boldsymbol{x} = \boldsymbol{V}\boldsymbol{s}$;

$\boldsymbol{u}_{\mathrm{G}} = 2\sqrt{R_{\mathrm{G}}}\boldsymbol{B}^{-\mathrm{H}/2}\boldsymbol{x}, \quad K = \dfrac{\boldsymbol{u}_{\mathrm{G}}^{\mathrm{H}}\boldsymbol{M}\boldsymbol{u}_{\mathrm{G}}}{\boldsymbol{u}_{\mathrm{G}}^{\mathrm{H}}\boldsymbol{u}_{\mathrm{G}}}$;

error $= P_{\mathrm{T}} - P_{\mathrm{avail}}/K$;

end while

With all of the theoretical background and mathematical formulations in hands, we proceed to the simulation results of the scenarios exposed in two cases: narrow and wideband.

4 SIMULATIONS AND CASES

The performance of the systems with and without DMNs is based on their capacity in the different cases and scenarios which the systems are submitted to. Their performance is analysed in two cases: the narrowband and the wideband. In the narrowband, the system is considered to operate in a relative band of 1% of the center frequency. For this width, the case can be even further simplified to consider only the operation at exactly the center frequency.

In the narrowband case, the frequency bin is fixed and capacity in the different scenarios is computed for crescent values of the available power. The aim is to investigate how the decoupling and matching strategies increase the capacity when the power available at the output of the high-power amplifiers is subject to a coupled or to a decoupled and matched multiport.

In the wideband case, the available power of the HPAs is kept constant for both systems while the operation frequency is swept over the range of a wide frequency band. In this case, the objective is to analyse the performance of the systems in the different scenarios, considering the components' impedances to be prone to frequency changes, thus changing the balance of the intricate and sensible decoupling and matching design.

First, for all scenarios, capacity is computed at each frequency bin separately and, then, the individual values of capacity are summed over crescent windows of the frequency band in one scenario. This simulation configuration brings forth the width of the band, referred to as the critical bandwidth, in which the two systems have the same total ergodic rates and the width in which the difference between the total rates of the systems is the highest, the optimal bandwidth.

Finally, this same type of simulation is repeated for different values of the Q-factor, to generate curves of the critical and of the optimal bandwidths in terms of the Q-factor, resulting in the perception of how much the system with DMNs is degraded by the Ohmic losses inside the multiport networks.

The Monte Carlo method is implemented for every simulation case. By repeatedly drawing random realizations of the propagation channel $\boldsymbol{Z}_{\mathrm{ART}}$ from a statistical distribution–e.g., a classical distribution with determined parameters and the QuaDRiGa model (JAECKEL *et al.*, 2014), as done in (LAAS *et al.*, 2017)–and computing capacity in each realization, the final ergodic capacity on each simulation bin is evaluated according to (3.21).

The achievable and ergodic rates and capacity are computed in bits per channel-use (bpcu) for the simulations in terms of the available power and in terms of the frequency. For the achievable and ergodic rates and capacity in frequency bands, they are computed in Gb/s.

4.1 Systems' Parameters

Many parameters of the systems have not yet been determined, but have been kept as variables or abstract quantities for the sake of generality. Some characteristics, features and parts, though, have been clearly chosen, such as the antennas type, the geometry of the arrays and the DMNs' architectures.

Nonetheless, even these can be changed or traded for something else, as long as the motivations for their choices keep satisfied. For example, the $\lambda/2$-dipoles can be substituted for any other kind of antenna element, the choice being conditioned only to employing canonical minimum scattering antennas to be able to compute the arrays' impedance matrices as it was described in this thesis.

For the non-determined parameters, they can be freely chosen to satisfy custom requirements, such as the area occupied by the antenna array and the topology of the DMNs. In this thesis, almost all parameters, including the above mentioned, have been chosen according to the equivalent parameters in (VASCONCELOS *et al.*, 2020). The main differences are the number of antennas in the mobiles in multi-antenna scenarios and the bandwidth of the noise. The latter entails other parameter changes and is covered in details in section 4.2.

In the publication, the authors approached only single-user scenarios and in the SU-MIMO the number of antennas of the receiver was chosen equal to 9, whereas here a smaller number is adopted, 3. It was decided so in order to maintain a consistent proportionality between the results of the single and multiuser scenarios. The multiuser simulations consider 2 non-cooperative users.

The systems' center frequency is $f_c = 3\,\text{GHz}$. From this value, the spatial parameters of the antennas and of the arrays can be exactly determined. By definition, given $\lambda_c \approx 10\,\text{cm}$, the length of the half-wavelength dipoles' arms is approximately equal to 2.5 cm. The width of the dipoles is chosen to be equal to 1.5 mm and consist in a pair of copper wires, one wire for each of the arms.

The UCA's dimensions can be determined by, at least, two variables: the number of elements and the antenna spacing or the UCA's radius.

As mentioned previously in Section 2.1, the number of antenna elements on the base station is 9. On the users is 1 for single-antenna or 3 for multi-antenna mobiles. The arrays antennas spacing is chosen to be $s = 0.35\lambda_c \approx 3.5\,\text{cm}$, ensuring the value of the radius $r_{\text{array}} \approx 5\,\text{cm}$ for the BS's UCA and 2 cm for the multi-antenna terminals, calculated by (2.10).

With these parameters in hand, it is possible to determine antennas' self impedance with (2.4) (for the single-antennas scenarios), mutual impedance (2.7) and an array's impedance matrix through completion of (2.11), using the two impedance equations just referenced (for the multi-antennas scenarios). These allow further determinations of other quantities in equations, statistics and, consequently, the DMNs' structures.

The generators' and load impedances, respectively Z_{G} and Z_{L}, of the models in Figs. 3 and 11 are modelled as resistances equal to the real part of the half-wavelength dipoles' self impedance computed at f_{c}, hence Z_{G}, Z_{L} and their real parts, R_{G} and R_{L}, fulfill

$$\begin{aligned} &Z_{\mathrm{G}} = Z_{\mathrm{L}} = \mathrm{Re}(Z_{\mathrm{A}}(f_{\mathrm{c}})) = R_{\mathrm{A}}(f_{\mathrm{c}}), \\ &R_{\mathrm{G}} = R_{\mathrm{L}} = R_{\mathrm{A}}(f_{\mathrm{c}}). \end{aligned} \tag{4.1}$$

As to the background radiation noise of the antennas, described in (2.14), the noise bandwidth and the antennas' absolute temperature are determined, respectively, as $\Delta_f = 10\,\mathrm{MHz}$ and $T = 290\,\mathrm{K}$. Together with the Boltzmann constant k and the real part of the self impedances of the antennas or of the impedance matrices of the arrays, the statistics can be fully calculated.

For the LNAs' intrinsic noise statistics in the same ports in (2.13), the variance of the voltage noise sources, the variance of the current noise sources and the cross-correlation of the voltage and current sources are

$$\sigma_{\mathrm{u}}^2 = 2kTBR_{\mathrm{A}},\ \sigma_{\mathrm{i}}^2 = 2kTB\frac{1}{R_{\mathrm{A}}},\ \rho = 0. \tag{4.2}$$

The noise statistics between intrinsic noise sources in different ports in (2.12) and between intrinsic and extrinsic noise sources in (2.15) are not altered from their definitions.

Using these values, originally proposed in (IVRLAČ; NOSSEK, 2016), the noise figure becomes equal to 3 dB at the center frequency and the optimum impedance for noise matching becomes equal to the real part of the half-wavelength dipoles' self impedance $Z_{\mathrm{opt}} = R_{\mathrm{A}}$.

Consecutively, the impedance matrices of the transmit (2.70) and receive (2.102) DMNs, whose architectures use these impedance quantities and noise statistics, can finally be defined. Consequently, the physical realization of the DMNs is also possible with the determination of the constituting reactive elements according to (2.109) and (2.112).

Interestingly, in a time division duplex scheme, applying these determined values, the transmit and receive matrices become equal for either single or multi-antenna cases

$$\boldsymbol{Z}_{\mathrm{MT}} = \boldsymbol{Z}_{\mathrm{MR}} = \begin{bmatrix} \mathbf{0}_K & -j\sqrt{R_{\mathrm{A}}}\mathrm{Re}(\boldsymbol{Z})^{1/2} \\ -j\sqrt{R_{\mathrm{A}}}\mathrm{Re}(\boldsymbol{Z})^{1/2} & -j\mathrm{Im}(\boldsymbol{Z}) \end{bmatrix}, \tag{4.3}$$
$$\boldsymbol{Z} = \boldsymbol{Z}_{\mathrm{AT}} = \boldsymbol{Z}_{\mathrm{AR}} \text{ or } \boldsymbol{Z} = Z_{\mathrm{A}} \text{ and } K = N \text{ or } M,$$

meaning the same DMN can be used in both directions of the link: transmitting while aiming for power matching and receiving while aiming for noise matching. Naturally, given the different number of antennas, one DMN is designed for the base station and one for each mobile.

A very good outcome of this design is that the numbers of elements in (2.113) in the transmit and receive DMNs reduce to, respectively, $N^2 + N$ and $M^2 + M$, the theoretical lower bound of the number of elements in a DMN, according to (NIE *et al.*, 2014). This is due to the $\mathbf{0}_K$ block that correspond to the absence of elements in the according ports, after transforming the impedance matrix into the admittance matrix and following the process in 2.2.3.3.

Regarding the losses of the system, parasitic resistances are added to the multiport systems in order to model the power dissipative parts of the antenna elements and of the DMNs' reactances. To obtain the dissipation resistance of the antennas, (2.150) is referred to, using the width of the dipoles aforementioned, the center frequency and the conductivity of the dipoles, equal to that of a copper wire. This results in the dissipation resistance $R_{\mathrm{d}} = 0.107\,\Omega$.

The parasitic resistances of the DMNs' reactances are computed individually for each element in terms of the Q-factor, fixed for all elements. For most of the simulations, $Q = 150$. Through (2.153), the values of the parasitic resistances are computed, given the DMNs' elements and circuit layout determined by (4.3). For the simulations of the critical and optimal bandwidths in terms of decreasing Q-factors, the values are 150, 125, 100, 75 and 50.

The Monte Carlo simulations consist of 10000 realizations of the physical propagation channel $\boldsymbol{Z}_{\mathrm{ART}}$, which is modelled as an independent and identically distributed (i.i.d.) vector or matrix, whose elements are drawn from $\mathcal{N}_C(0, \sigma_Z^2)$, where $\sigma_Z^2 = \mathbb{E}[|(\boldsymbol{Z}_{\mathrm{ART}})_{m,n}|^2] = 0.019085^2\,\Omega^2\,\forall m, n$. This is equivalent to the mutual impedance between two $\lambda/2$-dipoles $1000\lambda_{\mathrm{c}}$ spaced. The statistical nature of this model automatically introduces fading.

However, 1000 iterations were used for the computation of capacity in terms of the frequency bands and 100 iterations for obtaining the critical and optimal bands. The reduced numbers are due to these simulations' very large computational demands.

4.2 Narrowband Case

In this case, the systems with and without DMNs transmit and receive signals in frequency bands so narrow that the systems' behaviors inside this width can be reliably considered to be constant around the center frequency. It means that the figure of merit, capacity, can be computed solely at the center frequency and still provide a good estimate of the performance of the systems at the other frequencies inside the narrowband.

It is assumed that systems operating in relative bandwidths smaller than or equal to 1% of the center frequency, i.e. 1% of 3 GHz = 30 MHz, have practically the same frequency response, in terms of capacity, at all frequencies inside the band. It can be seen further, in section 4.3, that this assumption is satisfactory for calculating the achievable rates only at the center frequency, since the rates change little at its vicinity.

The width of the band is chosen equal to 10 MHz, even narrower than the 1% bandwidth, and, thus, so is the bandwidth of the noise models. In (VASCONCELOS *et al.*, 2020), the noise bandwidth was chosen equal 740 kHz following the noise parameters given in (LEHMEYER *et al.*, 2017), including the room temperature of the system on 290 K.

The main objective of the narrowband case is to analyse the ergodic rates of the systems in situations in which they supply maximum capacity. At the center frequency, the systems with and without DMNs have the $\lambda/2$-dipoles and the DMNs operating exactly at the frequency they were designed to, providing maximal performance. Ultimately, the narrowband case analysis is the basis of the wideband case, as it will be verified in section 4.3.

Capacity is analysed, in this case, at the center frequency in terms of the total available power of the high-power amplifiers, which varies from -88.7 to -53.7 dBW, at a step of -2.5 dB. The results are rather straight-forward in which the increase of the total available power does not introduce any unexpected behavior to the operation of the systems. Thus, it rather provides comparisons of the systems' spectral efficiency in different scenarios.

In (VASCONCELOS *et al.*, 2020), the available power variation was between -100 and -65 dBW because there the noise model bandwidth was equal to 740 kHz. In order to keep the results (curves shapes and values) consistent with the publication, it was decided to scale the available power and, thus, the transmit power in $\frac{10\,\text{MHz}}{740\,\text{kHz}} \approx 11.3$ dB, in order to keep the same SNR. In this way, e.g. -65 dBW in 740 kHz and -53.7 dBW in 10 MHz yield the same capacity.

In each Monte Carlo iteration, the same statistical realization of the propagation channel is used to compute capacity on all available power points, in order to guarantee a fairer

analysis of the performance enhancement with the available power increase. In the end of the Monte Carlo method run, the achievable rates of the realizations are averaged out of the 10000 iterations to result in the ergodic capacity of the systems on every available power point.

The first system whose simulations' results are analysed is the single-user MISO. The scenario is equivalent of the downlink communication between the base station and a single-antenna terminal. The plots of the ergodic capacity in bpcu is in Fig. 14.

Figure 14 – SU-MISO ergodic capacity and available power

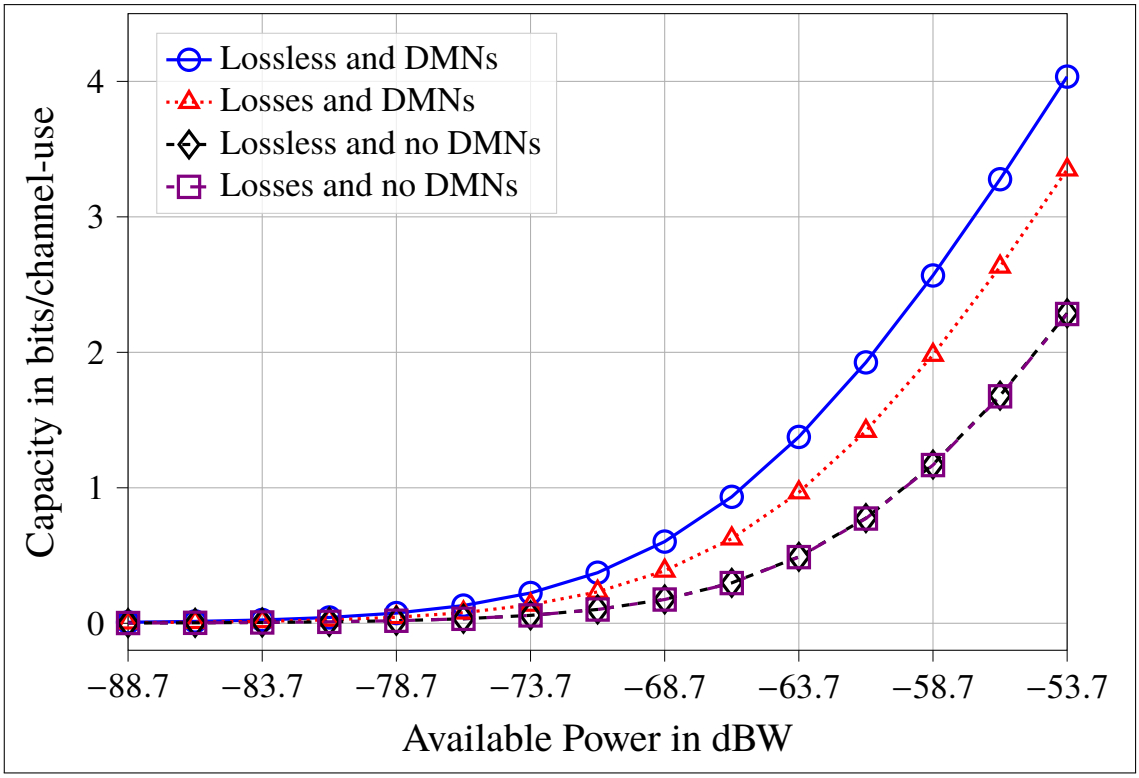

Source: The author.

As expected, Fig. 14 demonstrates that the system with DMNs has better performance than the system without DMNs, even in the presence of losses. In the narrowband case, the frequency dependency is not playing any role, and this is valid for all scenarios. Overall, capacity in both systems increased as the total available power increased as well.

One interesting thing to be noticed already is that the curves of the lossless system without DMNs -◇- and of the same system with losses -□- overlap. The only source of power dissipation in this system comes from the skin effect of the antennas. Thus, it is noticeable that the losses in the antennas by themselves practically do not reduce capacity.

For the adopted parameters of the half-wavelength dipoles, the self impedance is equal to $73.13\,\Omega$. Considering the value of the skin effect dissipation resistance $R_{\mathrm{d}} = 0.107\,\Omega$,

in (2.152) it represents only 0.146% of the dipoles' self impedance. This reinforces that the inclusion of the skin effect on the capacity computations should not have great impact.

If this observation is brought to the system with DMNs, it can be noticed that the majority of the losses in this system, creating the non-negligible separation between the lossless and lossy curves, are caused by the power dissipation in the DMNs. Indeed, this is a major source of power losses since the number of elements is rather large, e.g. the 18-ports transmit decoupling and matching network: 90.

Moving on to the scenario equivalent to the uplink of the same base station and single-antenna user setup, the simulations' results are plotted in Fig. 15.

Figure 15 – SU-SIMO ergodic capacity and available power

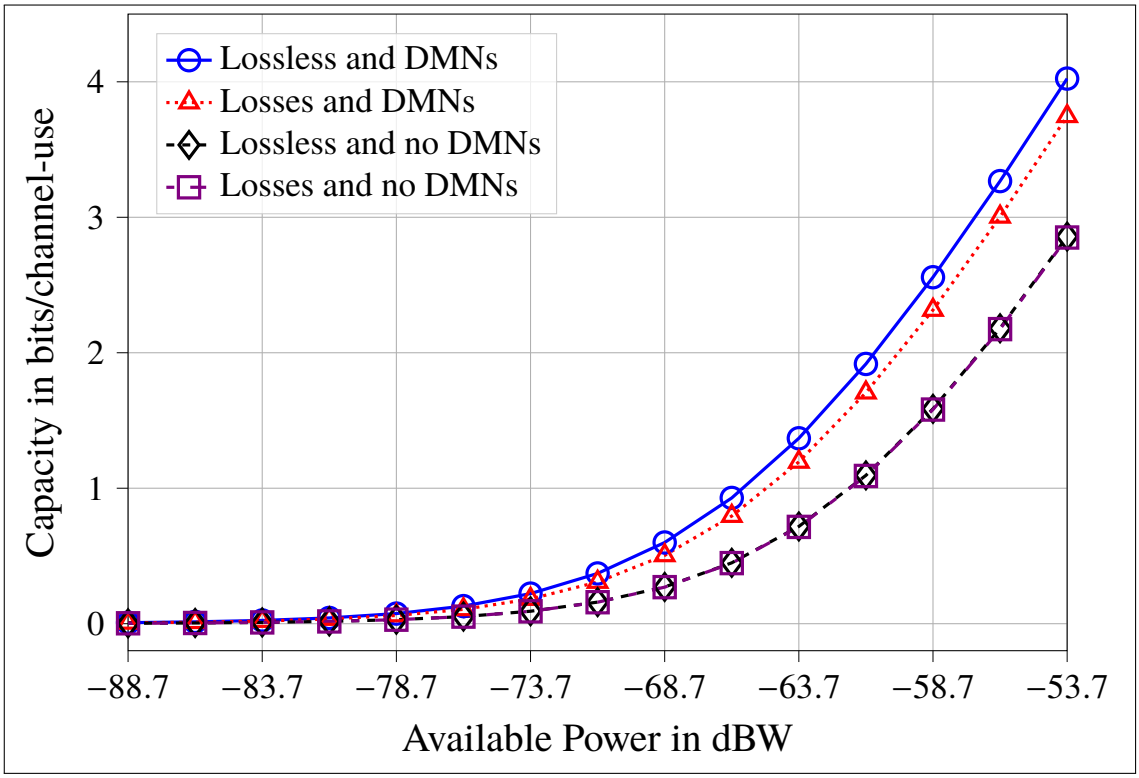

Source: The author.

The general behavior is basically repeated: system with DMNs providing better results than the system without. However, in Fig. 15, two key observations can be made about the decoupling and matching strategies. The first one is regarding the curve of the lossless system with DMNs: it presents the same values as the curve in the SU-MISO scenario, because both curves in this parasitics-free situation grant perfect decoupling and matching effects.

The second key observation is related to the situations with non-optimal (either suboptimal or completely absent) decoupling and matching effects. It happens suboptimally

in the lossy system with DMNs and these effects are completely absent in the system without DMNs. The non-optimal curves in Fig. 15 have higher capacity than their counterparts in the MISO scenario.

As mentioned in subsections 3.1.1 and 3.1.3 and in section 3.2, the transmit vectors $\boldsymbol{x}$ are the product of a randomly generated symbol s or vector of symbols $\boldsymbol{s}$ and a precoding vector or matrix which matches the randomly generated channel. This procedure, thus, produces a vector signal $\boldsymbol{x}$ subject to two random draws.

Finally, mapping (3.22) generates the HPAs' voltage vector $\boldsymbol{u}_{\mathrm{G}}$, a function of $\boldsymbol{x}$, that is used to compute the available and transmit power ratio, according to algorithm 2. The ratios are, consequently, also random. Finally, they are included in the ergodic capacity computations by (3.21) and, thus, the capacity values suffer fluctuations due to the random channel generation.

For the non-optimal systems in the SIMO scenario, the powers ratios are independent of the random channel generation and, thus, suffer no fluctuation regarding how large the transmit power is compared to the total available power. These same phenomenons are also present in the other scenarios to be investigated.

The next scenario is that which corresponds to the SU-MIMO. Here, the base station is equipped with 9 $\lambda/2$-dipoles, whereas the mobile terminals only with 3 $\lambda/2$-dipoles, both sets arranged in UCAs with same antenna spacing. Only the downlink here is investigated.

Similar curves to what was obtained already are expected, regarding the same behavior of capacity and the available power. The key observation is only to see how capacity grows if the single-antenna of the receiver is replaced by an array of 3 $\lambda/2$-dipoles.

This means that even the suboptimal use of decoupling and matching strategies by lossy DMNs and antennas provides better results and scaling when increasing from 1 to 3 antennas on the terminal. However, it could be expected that, the larger the number of antennas, the larger the losses in the system. Possibly, there is a sort of maximum value of capacity gain, after which the losses might take over the capacity gains of the increased number of antennas.

The following scenarios in Figs. 17 and 18 move on to multiple users, specifically 2, in the same cell, connected to the same base station. For them, the ergodic rates were computed.

Their ergodic rates computations required the weighted sum-rate maximization algorithm exposed in Section 3.2 and the results are also straight-forward in the sense of what would be expected: the same type of plot, a similar relation between the systems' curves and higher overall ergodic rates than the single-user counterparts because of more data being

Figure 16 – SU-MIMO ergodic capacity and available power

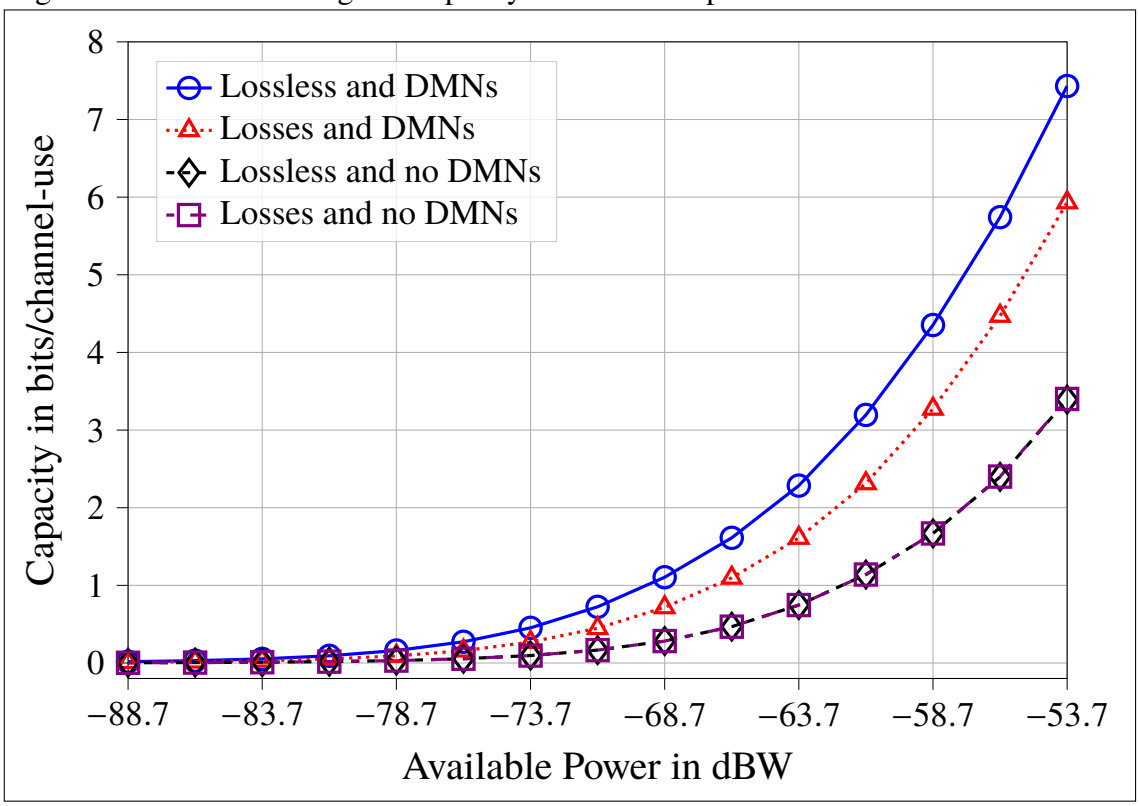

Source: The author.

transmitted, given enough available power, in data streams over the channels and subchannels.

Figure 17 – MU-MISO ergodic rates and available power

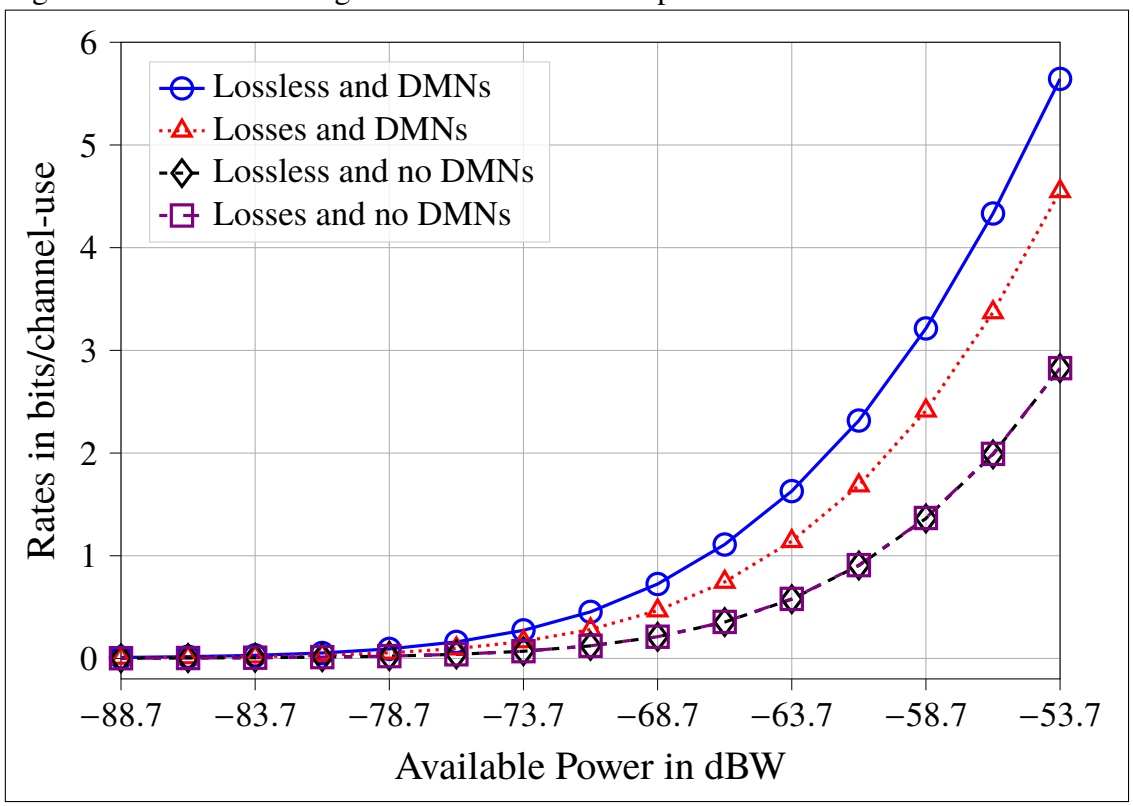

Source: The author.

Figure 18 – MU-MIMO ergodic rates and available power

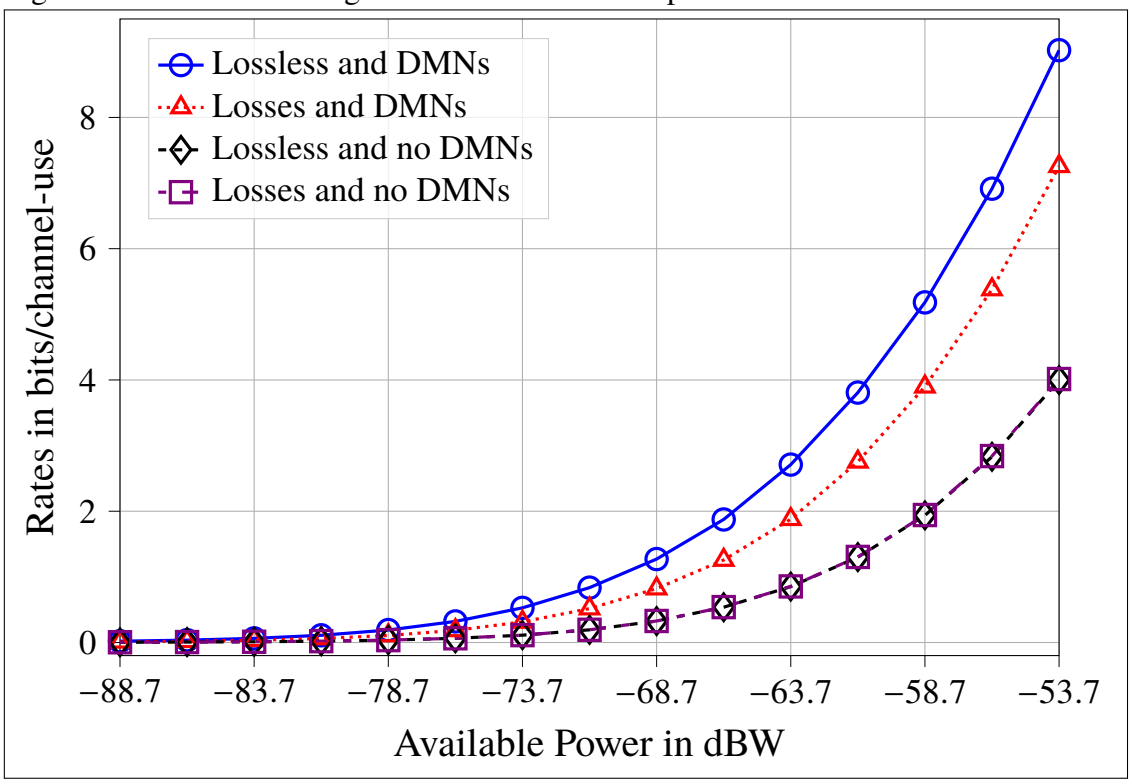

Source: The author.

4.3 Wideband Case

In practice, narrowband communications are not as commonly used as wideband, the latter being broadly employed in cellular mobile communications in a daily basis, for example. Thus, not only is it interesting to delve into the decoupling and matching strategies in more common situations, as it is necessary to investigate the behavior of systems with and without DMNs at frequencies close or distant to the center frequency in a wideband transmission.

For this end, the bandwidth of the signals in the wideband case is equal to 400 MHz around the center frequency, spanning from 2.8 to 3.2 GHz, and the total available power of the HPAs is kept fixed. The frequency band is discretized along its width in 41 bins, with 10 MHz spacing between them.

At each frequency bin, capacity is computed separately for a narrowband 10 MHz wide as in the narrowband case, but now with the frequency band centered around a carrier frequency equivalent to the respective bin value. The HPAs' available power is kept constant on -53.7 dBW for each of the 41 frequency bins (narrowbands), meaning a total available power of $-53.7\,\text{dBW} + 10\log(41)\,\text{dB} \approx -37.57\,\text{dBW}$ uniformly distributed throughout the wideband.

In the statistical Monte Carlo method, each propagation channel realization is used for all of the frequency bins, individually, to compute the achievable rates of the systems with and without DMNs at the respective bin. In the end, these achievable rates are averaged out of the number of realizations, yielding the ergodic capacity correspondent to each frequency bin.

The main objective of the wideband case is to analyse how the two systems, with and without DMNs, behave under the change of frequencies, from small to large changes. Their designs can be expected to deliver the best performance at the center frequency and be susceptible to increasing performance degradation the "farther"the operation frequency becomes from the center frequency.

However, as the results of the simulations display, the ergodic capacities of the two systems are not symmetrically decreasing curves centered on the highest valued capacity point at the center frequency. The first simulations are executed in the SU-MISO scenario and the lossless and lossy ergodic capacity curves are plotted in Fig. 19.

Figure 19 – SU-MISO ergodic capacity and frequency

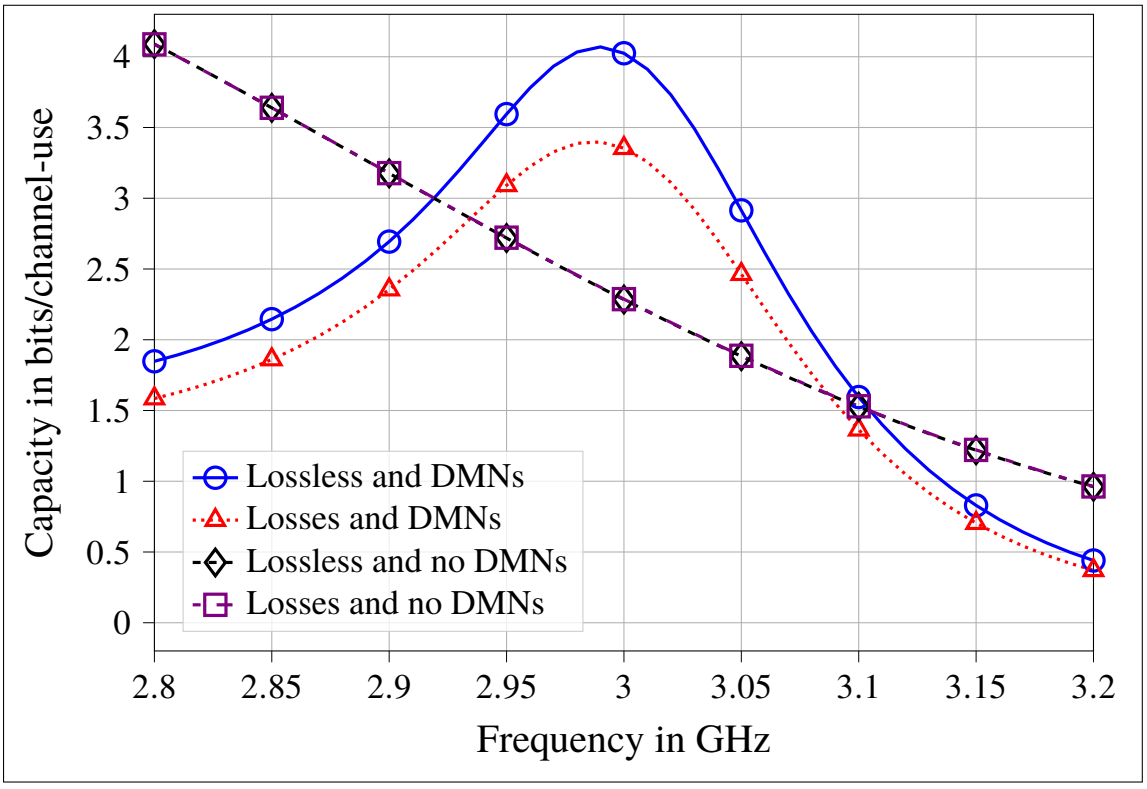

Source: The author.

Indeed, as it could be expected, the lossless and lossy curves of the system with DMNs have better capacity around the center frequency and worse capacity at bins more distant from the center. In addition, as also expected, around the center frequency capacity is higher for

the system with DMNs than for the system without DMN.

Nonetheless, capacity of the system without DMNs actually monotonically decreases as the frequency increases in the band, presenting better performance on frequencies lower than the center frequency. Albeit the bell-shaped like curves of the system with DMNs exposing the performance degradation at bins farther from the center, the ergodic capacity is also higher at lower frequencies than at higher frequencies.

The reason for this is that waves with lower frequencies have larger wavelength while waves with higher frequencies have smaller. For the former, then, the antenna spacing of the uniform circular arrays is relatively smaller than it is for the latter. The array is more compact at lower frequencies and, consequently, the antenna elements are more coupled electromagnetically, causing the systems at lower frequencies to have better ergodic capacity.

As it was the case for the losses in the narrowband simulations, the losses from the DMNs are larger and more prominent than the losses due to the antenna elements, causing more pronounced capacity reduction. This can be verified, as was also done in the narrowband case, in the system without DMNs that practically has its two curves overlapping, and in which the only source of losses are the antenna elements.

Similarly to the capacity values, the stronger coupling at lower frequencies also enhances the impact of the losses in the capacity, making the lossless and lossy curves of each system more different at lower frequencies than at higher frequencies.

Even with losses, the system with DMNs provides the largest capacity values around the center frequency. This demonstrates the impact optimal and even suboptimal decoupling and matching effects have in enhancing the performance of the system and, thus, in increasing the ergodic rates. Decoupling and matching are considered suboptimal at the bins around the center frequency at which capacity is larger than in the system without DMNs.

The following simulation plots the curves of the SU-SIMO scenario in Fig. 20. In the wideband, the simulations in this scenario produce the same effect as that produced in the narrowband case: the ergodic capacity is larger at every frequency bin for single antenna transmitters and multi-antenna receivers than it is in the SU-MISO scenario.

The possible causes for this are the same as those presented in the narrowband case, namely the larger sensibility of capacity to coupled transmit ports and power mismatches, the influence of precoding the channel in the available and transmit power ratios.

In addition, the effects mentioned above for the SU-MISO scenario are also valid

Figure 20 – SU-SIMO ergodic capacity and frequency

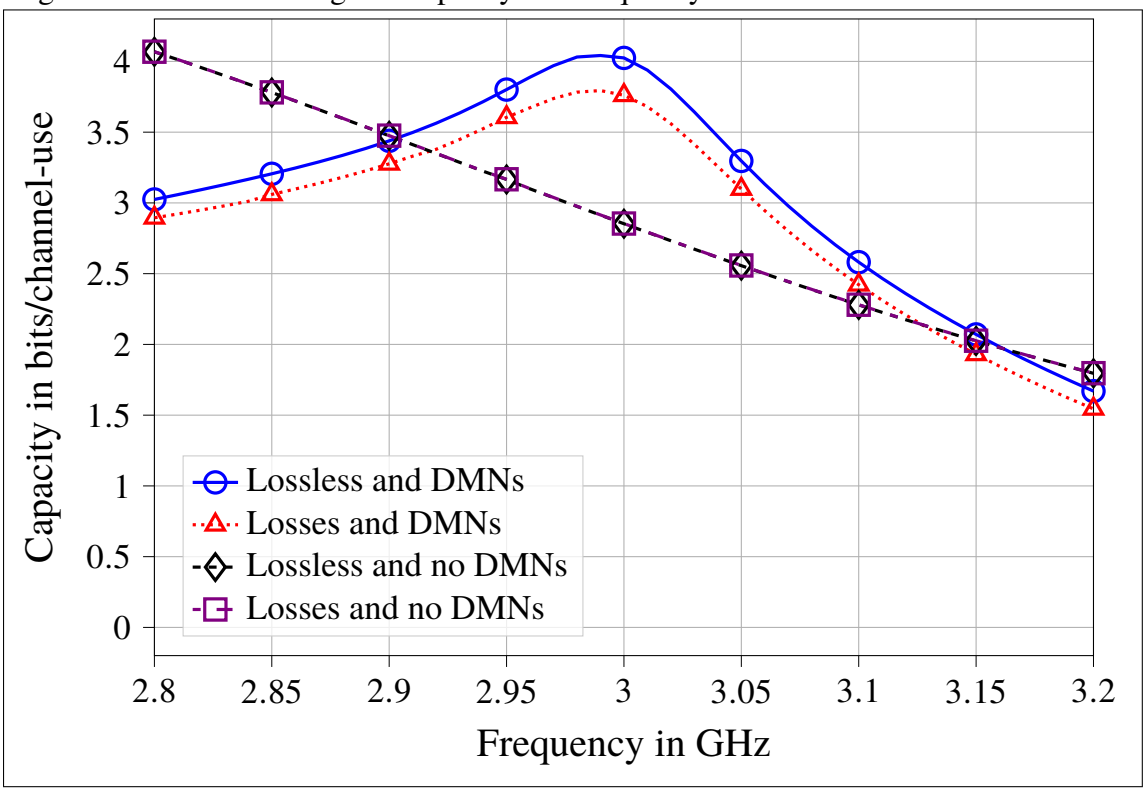

Source: The author.

here, after all, the curves have similar shapes, only less accentuated. It is possible to conclude that the systems behave similarly regarding the impact of frequencies distant and close to the center and the comparisons between the ergodic rates in lower and in higher frequencies.

In the single-user MIMO case, the mobile-user is equipped with 3 antennas in an UCA and the downlink is observed, whose simulations results are featured in Fig. 21. With the presence of antenna arrays in both sides of the link, capacity considerably increases around the center frequency in the system with DMNs and at the lower frequencies in the system without.

The larger number of antennas and of reactive DMNs' elements in the whole system with DMNs makes it achieve very large ergodic rates, but at the cost of increasing the susceptibility of the system to losses and to frequency changes, as it can be observed even on the lossless curve with DMNs. The range of the capacity variation in both systems is accentuated with the curves presenting faster decays and rises.

Finally, multiuser simulations are run to provide the results for both scenarios MU-MISO and MU-MIMO in Figs. 22 and 23, in which the same effects explained before are applicable. Again, for the multiuser scenarios, the weighted sum-rate maximization algorithm is required due to the necessity of the non-collaborative users' interference mitigation and optimal power distribution among the channels.

Figure 21 – SU-MIMO ergodic capacity and frequency

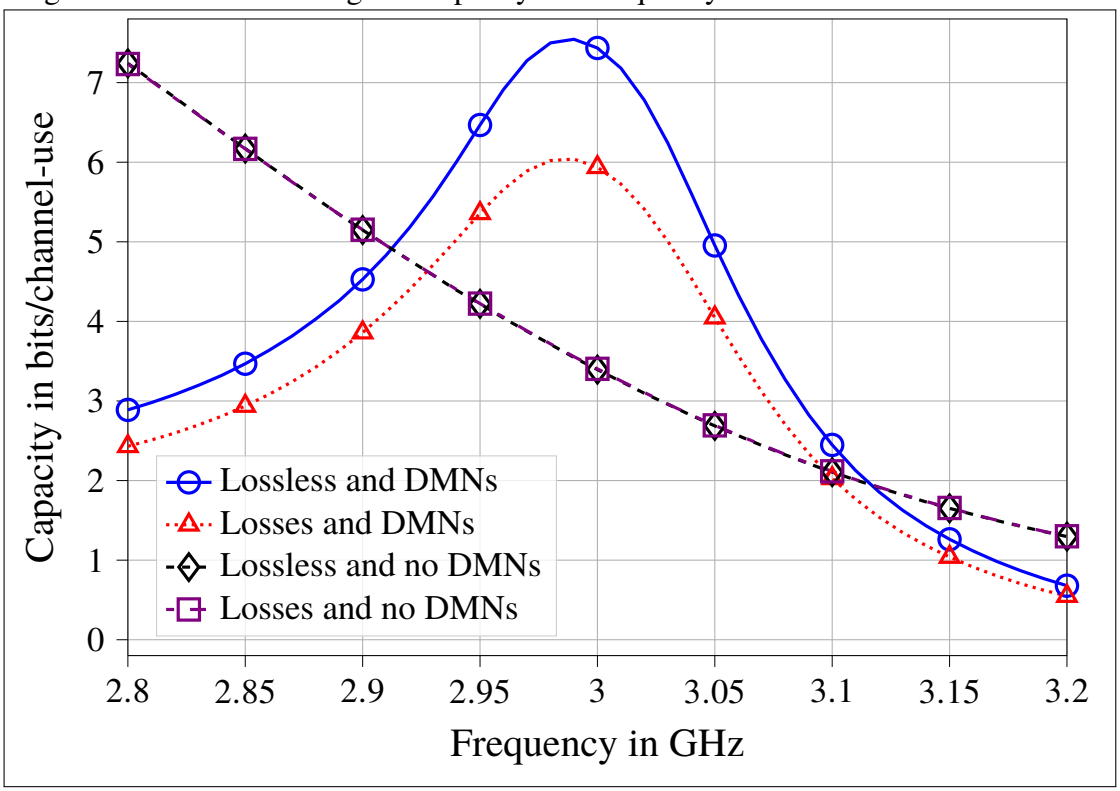

Source: The author.

Figure 22 – MU-MISO ergodic rates and frequency

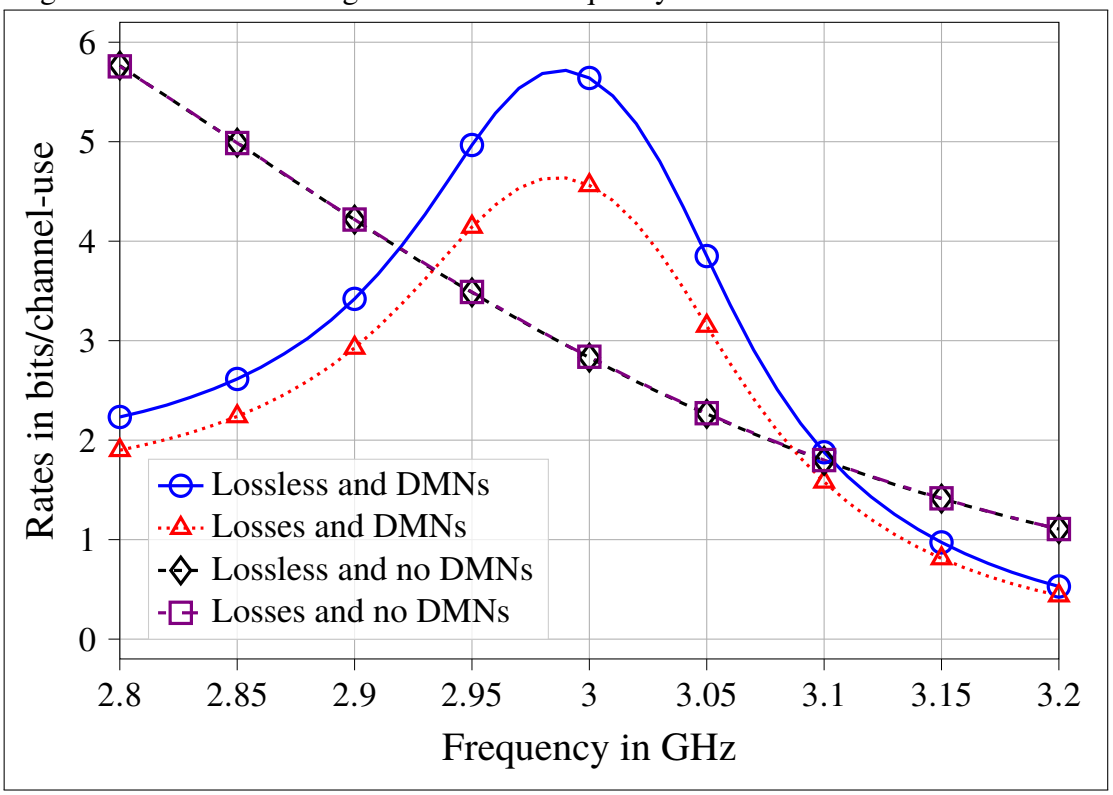

Source: The author.

The MU-MIMO in Fig. 23 scenario presents a similar scaling, in terms of rapid

Figure 23 – MU-MIMO ergodic rates and frequency

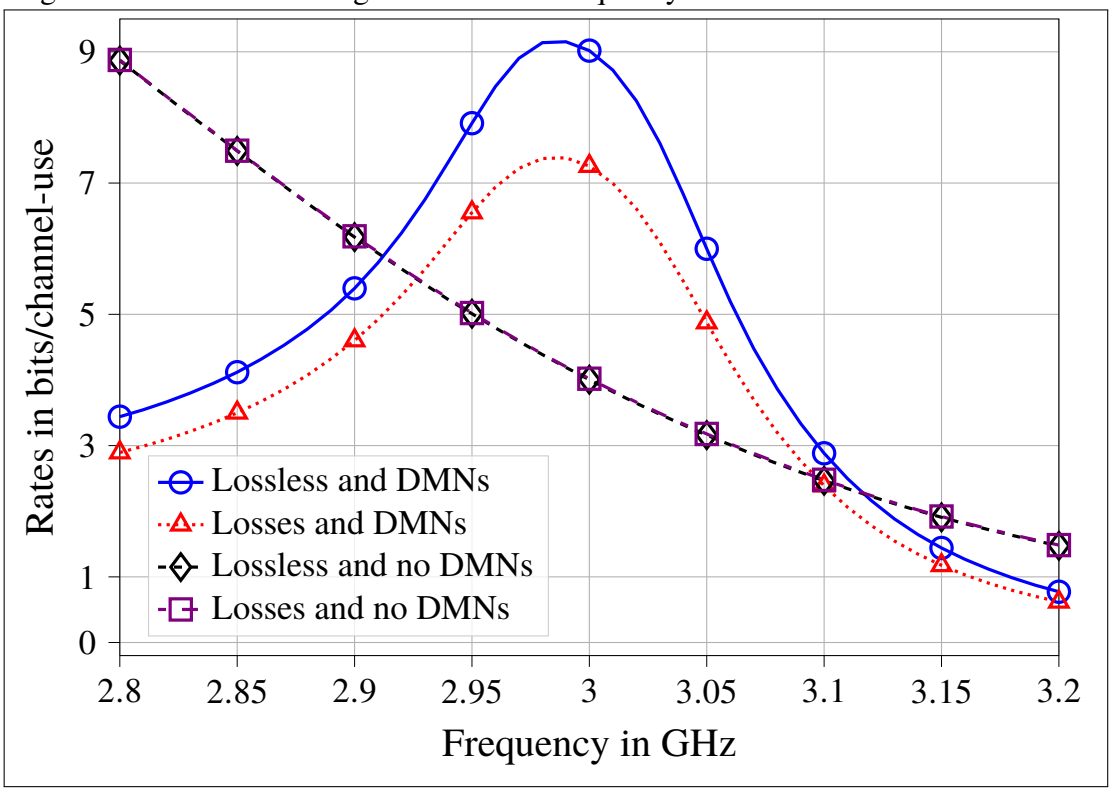

Source: The author.

variations of the curves, from the MU-MISO scenarios' results as the scaling from MISO to MIMO in single-user.

After the presentation of the ergodic capacity in bpcu as a function of frequency, the next step is to compute the total rates in b/s in a certain bandwidth.

4.3.1 Critical and Optimal Bandwidths

In all of the scenarios, the bell-shaped curves of the system with DMNs display limited bandwidths in which the system has better capacity than the system without. Depending on the scenario and the presence or absence of losses, this bandwidth can be wider or narrower. For example, the lossy curves of the system with DMNs in the MU-MISO scenario ··△·· is only of, approximately, 150 MHz, whereas in the SU-SIMO scenario ··△·· it is of 220 MHz.

Albeit allowing for drawing some conclusions, it is not a robust measure of efficiency for the decoupling and matching strategies in optimal and suboptimal states. After all, even in regions of higher and lower frequencies, in which the system with DMNs has worse rates at some bins than the system without, the sum of the rates values in the band, referenced to as total rates, might be higher.

Therefore, simulations to compute the total rates of the systems in some scenarios are carried out in terms of crescent windows of frequency band. The step of the windows' width is of 20 MHz, starting with a 20 MHz width and widening the windows until 400 MHz, i.e. the whole wideband considered in the thesis.

For this matter, the total rates are computed employing the trapezoidal rule to execute numerical integrations of the capacity values inside the windows with pairs of trapezoids 10 MHz "tall" around the center frequency. The total rates, since being computed in bandwidths in the order of 100 MHz, reach the orders of Gigabit per second by integrating capacity in bpcu.

The lossy MU-MIMO system has been chosen as an example.

Figure 24 – MU-MIMO total ergodic capacity in crescent frequency bands

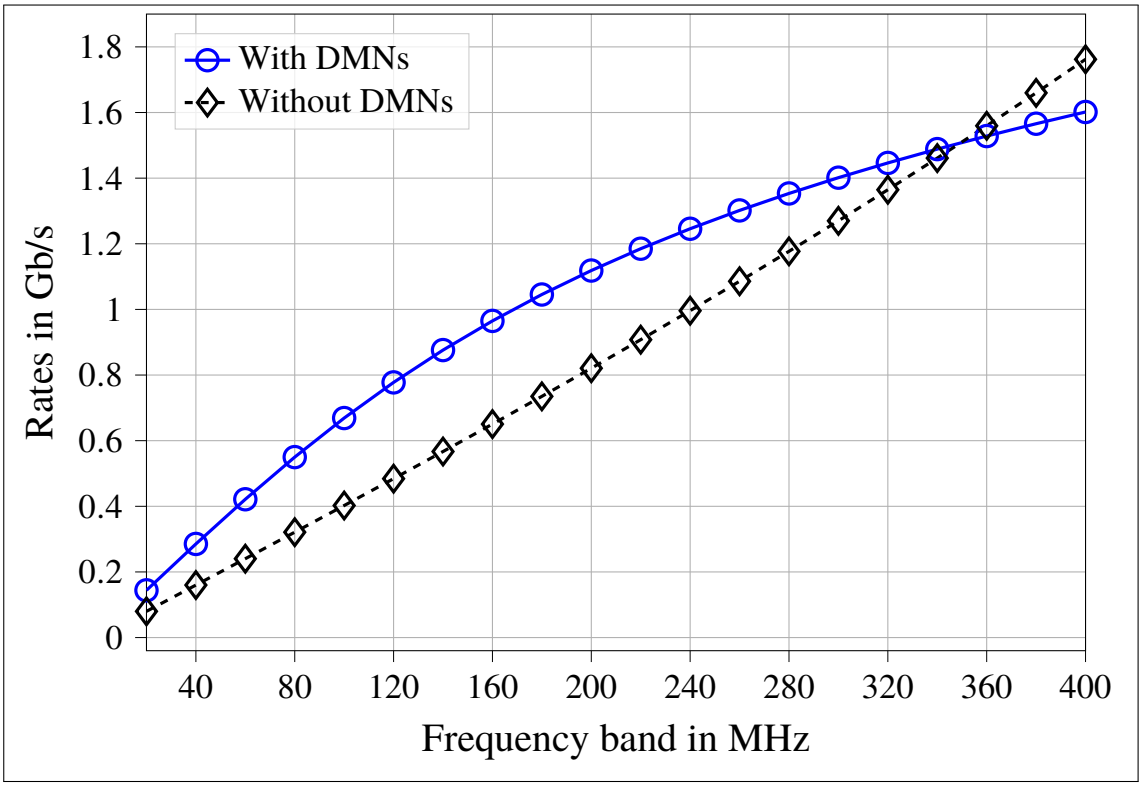

Source: The author.

As it can be seen in Fig. 24, the system with DMNs has superior total rates in a bandwidth of, approximately, 350 MHz. The positive difference between the total capacities start already in the 20 MHz, reach its maximum in a window 160 MHz wide and become zero in a bandwidth of 350 MHz. For the lossy MU-MIMO scenario, this is the critical bandwidth and the band of maximum difference is the optimal bandwidth.

In order to proceed with the investigation of these two bandwidths, the same simulation is done for the total rates in terms of the crescent bands is repeatedly carried out in every lossy

scenario with different values of the Q-factor equal to 150, 125, 100, 75 and 50. In this manner, the critical and optimal bandwidths usability criteria become functions of the Q-factor, consecutively, the decoupling and matching effectiveness become a function of the networks' components quality.

The critical bandwidth is a good measure of the limits of the decoupling and matching strategies to consider until which point to employ it is worth the complex DMNs' design and implementation and starting a which frequency band's width systems without DMNs are better choices due to their more simplified and straight-forward design and the total ergodic rates they deliver. The simulations' results are depicted in Fig. 25.

Figure 25 – Critical bandwidths and Q-factors in every lossy scenario

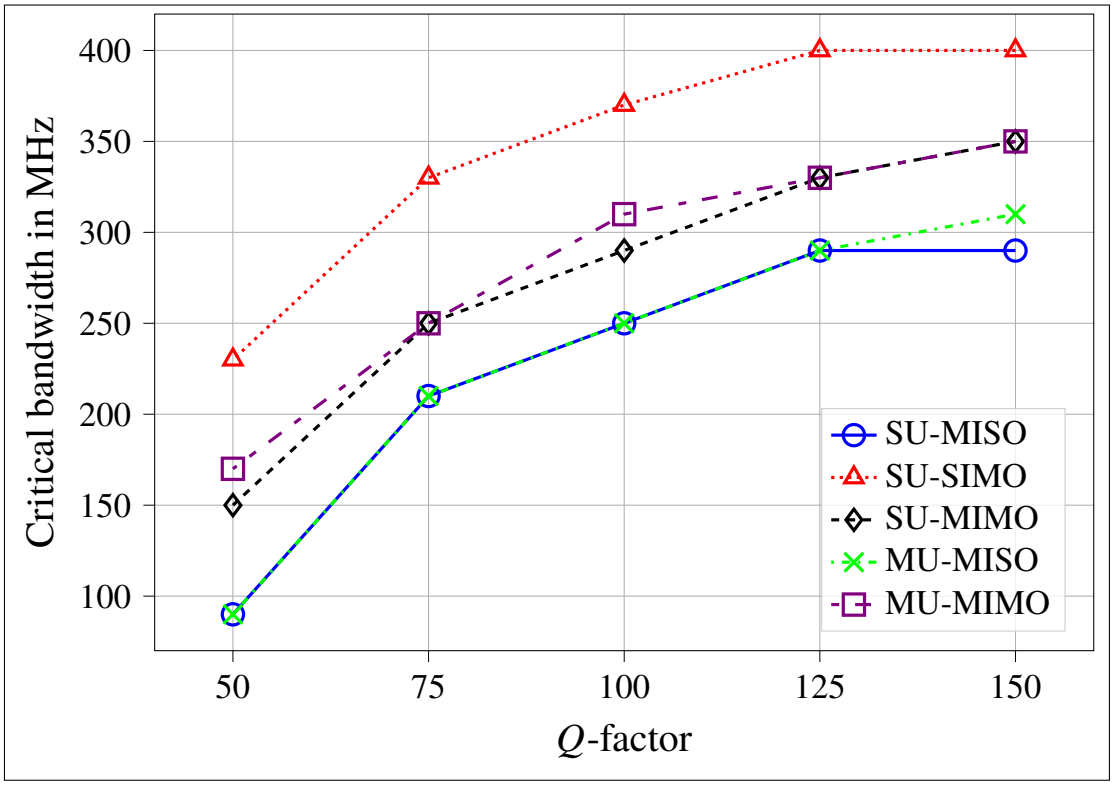

Source: The author.

The optimal bandwidth might serve as an appropriate figure of merit to justify the use of the decoupling and matching networks, considering that, for bands approximately as wide as that, the system with DMNs delivers the best total rates compared to the system without.

These two simulations are important to raise awareness on how much can the quality of the decoupling and matching networks' components reduce or improve the performance of the system. It is important to acknowledge that the simulations in wideband considered very high-quality components, whose Q-factor equal to 150, a value not common in industry. Hence,

Figure 26 – Optimal bandwidths and Q-factors in every lossy scenario

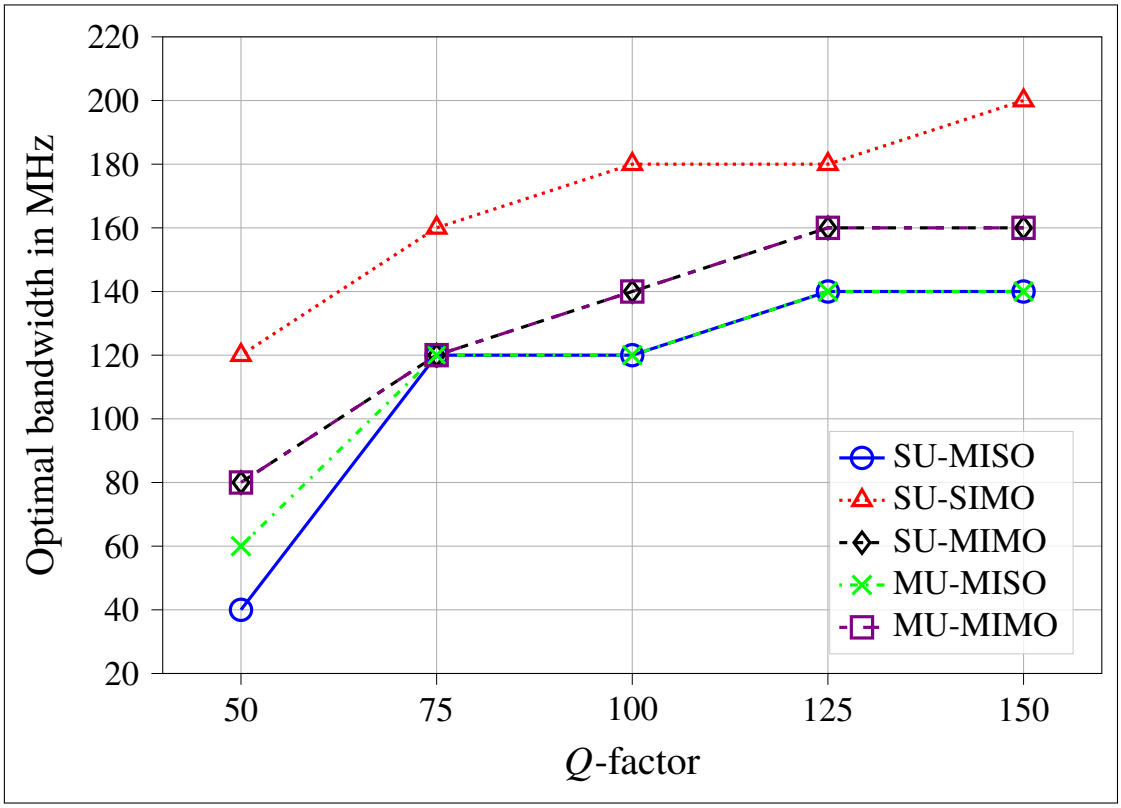

Source: The author.

more Q-factors were necessary to address the usability of the DMNs.

Still, the critical and the optimal bandwidths cannot be considered as sufficient figures of merit to fully decide on whether or not to use decoupling and matching strategies. First, even in bands a little narrower than the critical bandwidth, it might not be justifiable the complexity of the DMNs, as the system without them may already deliver high enough total ergodic rates.

Second, the optimal bandwidth does not make clear on how large the difference in capacity between the two systems is to, again, justify the complexity of decoupling and matching networks.

These hidden trade-off aspects not directly approached by the analysis of the critical and optimal bandwidths do not rule out referring to them as figures of merit, as they are valid for, at least, initial considerations, such as discarding or not the investigation of the DMNs' effects in communication systems, based on whether the desired bandwidth of operation is more similar to the critical or to the optimal bandwidth.

5 CONCLUSIONS

Optimal decoupling and matching strategies were designed for and employed in a communication system model to achieve the rates which are predicted in information theory as commonly done in the literature. However, the various simulations' results have shown these optimal effects to be restricted to very strict conditions.

The system for which the DMNs were specifically designed, considering the necessary parameters, could only attain optimal decoupling and matching of its ports when the system was operating only over a very narrow frequency band around the center frequency and when the antenna elements and the DMNs' reactances were considered lossless.

The first condition was actually relaxed to comprehend relative bands of 1%, which brought forth the narrowband results. But even so, the presence of losses in the antennas and in the DMNs considerably deteriorated the performance of the system, because of power dissipation and of the unbalance in the equations created by modifying the impedance matrices, whose original values were part of the decoupling and matching strategies' designs.

Still, the narrowband simulations showed that the lossy system with DMNs has better ergodic rates and capacity and good scaling from single to multi-antenna receivers than the system without.

When considering the wideband communication case, the two systems were deeply affected by frequency variations in the antennas' and multiport networks' impedances. The system with DMNs reflected the frequency influence in its bell-shaped curves peaked at the center frequency while the system without DMNs displayed the rather unexpected, approximately monotonic descending rates and capacity curves following the frequency augmentation.

Mutual coupling, at this point, was not only visible in how it can deteriorate capacity when not taken into account, but also in how both systems in the wideband case demonstrated the similar behavior of having larger rates and capacity at lower frequencies than at higher frequencies, due to the longer waves at lower frequencies perceiving the antenna spacing in the arrays smaller, thus with stronger coupling between the antennas.

Although mutual coupling is often understood as an effect that must be confronted and wiped out of the multi-antenna systems, the simulations show that the best strategy is to make use of this intrinsically present phenomenon as an additional source for harvesting more capacity from the antenna elements. Besides, ultimately, mutual coupling cannot be nullified, but, at best, only its effects in the transmit and receive ports can, observing the appropriate conditions.

The understanding of the underlying phenomenon of mutual coupling in multi-antenna systems allow to predict which impacts, positives or negatives, it may cause in the systems' operations and how it may do so. Hence, good measures to advantageously use this electromagnetic interaction should always be aimed for. For this end, the optimal decoupling and matching strategies might seem the best decision.

Unfortunately, as already noticed in the simulations of rates and capacity in terms of frequency, the DMNs actually introduce considerable bandwidth limitations. Nonetheless, with the concept and demonstration of the critical and optimal bandwidths, it is confirmed that DMNs are more efficient in narrow and moderately wide frequency bands, making more sense not to use them in widebands such as the considered for the simulations (400 MHz).

Overall, for very large number of antenna elements, to design and implement DMNs is, before anything, unfeasible due to the immense number of reactive elements required to produce it and the complexity naturally involved in laying them connected. In addition, the more elements, the higher the losses and the more sensible the DMNs become to frequency changes. Consequently, the system with DMNs become even more band limited.

So, for a small or moderate number of antennas, the question of whether or not using optimal decoupling and matching strategies becomes the matter of a trade-off between the complexity of the DMNs' realization and of the possible amount of gain in ergodic rates, always considering the width of the desired frequency band. For the latter consideration, the critical and optimal bandwidths become helpful figures of merit.

Finally, the most important message is that mutual coupling should always be taken into account. The strategy chosen to deal with this effect bring along with its advantages also disadvantages and limitations. Having complete knowledge on the strengths and weaknesses of the decoupling and matching strategies in multi-antenna arrays lead to physically consistent designs of multi-antenna models for practical realizations.

As possible future works, many open points can be considered as valuable candidates. Some include: designing suboptimal decoupling and matching strategies and networks such that the rates curves are flatter in widebands; investigating the increasing ergodic rates values at lower frequencies in the system without DMNs; and implementing water-filling solution to optimally distribute the total available power in the wideband, i.e. among the frequency bins.

In general, research involving the Multiport Communication Theory has much potential in terms of a wide range of rich topics available.

BIBLIOGRAPHY

ALLEN, J. L.; DIAMOND, B. **Mutual coupling in array antennas**. [S.l.], 1966.

BALANIS, C. A. **Antenna Theory**. 1. ed. [S.l.]: John Wiley & Sons, 1982.

Costa, M. Writing on dirty paper (corresp.). **IEEE Transactions on Information Theory**, v. 29, n. 3, p. 439–441, 1983.

FRIIS, H. T. Noise figures of radio receivers. **Proceedings of the IRE**, v. 32, n. 7, p. 419–422, 1944.

GUTHY, C.; UTSCHICK, W.; DIETL, G. Low-complexity linear zero-forcing for the mimo broadcast channel. **IEEE Journal of Selected Topics in Signal Processing**, IEEE, v. 3, n. 6, p. 1106–1117, 2009.

GUTHY, C.; UTSCHICK, W.; HUNGER, R.; JOHAM, M. Efficient weighted sum rate maximization with linear precoding. **IEEE Transactions on Signal Processing**, IEEE, v. 58, n. 4, p. 2284–2297, 2010.

HAUS, H.; ATKINSON, W.; BRANCH, G.; DAVENPORT, W.; FONGER, W.; HARRIS, W.; HARRISON, S.; MCLEOD, W.; STODOLA, E.; TALPEY, T. Representation of noise in linear twoports. **Proceedings of the IRE**, IEEE, v. 48, n. 1, p. 69–74, 1960.

IOANNIDES, P.; BALANIS, C. A. Uniform circular arrays for smart antennas. **IEEE Antennas and propagation magazine**, IEEE, v. 47, n. 4, p. 192–206, 2005.

IVRLAČ, M. T. **Circuit Theory and Communications**. [S.l.]: Shaker Verlag, 2017. 304 p.

IVRLAČ, M. T.; NOSSEK, J. A. Toward a circuit theory of communication. **IEEE Transactions on Circuits and Systems I: Regular Papers**, IEEE, v. 57, n. 7, p. 1663–1683, 2010.

IVRLAČ, M. T.; NOSSEK, J. A. The multiport communication theory. **IEEE Circuits and Systems Magazine**, IEEE, v. 14, n. 3, p. 27–44, 2014.

IVRLAČ, M. T.; NOSSEK, J. A. On physical limits of massive MISO systems. In: **Proc. 20th Int. ITG Workshop Smart Antennas (WSA)**. Munich, Germany: [s.n.], 2016.

JAECKEL, S.; RASCHKOWSKI, L.; BÖRNER, K.; THIELE, L. Quadriga: A 3-d multi-cell channel model with time evolution for enabling virtual field trials. **IEEE Transactions on Antennas and Propagation**, IEEE, v. 62, n. 6, p. 3242–3256, 2014.

JOHNSON, D. H. Origins of the equivalent circuit concept: the current-source equivalent. **Proceedings of the IEEE**, IEEE, v. 91, n. 5, p. 817–821, 2003.

JOHNSON, J. B. Thermal agitation of electricity in conductors. **Physical review**, APS, v. 32, n. 1, p. 97, 1928.

KAHN, W. K.; KURSS, H. Minimum-scattering antennas. **IEEE Transactions on Antennas and Propagation**, IEEE, v. 13, n. 5, p. 671–675, 1965.

LAAS, T.; NOSSEK, J.; BAZZI, S.; XU, W. On reciprocity of physically consistent tdd systems with coupled antennas. In: VDE. **WSA 2017; 21th International ITG Workshop on Smart Antennas**. [S.l.], 2017. p. 1–6.

LAAS, T.; NOSSEK, J. A.; BAZZI, S.; XU, W. On the impact of the mutual reactance on the radiated power and on the achievable rates. **IEEE Transactions on Circuits and Systems II: Express Briefs**, IEEE, v. 65, n. 9, p. 1179–1183, 2018.

LARSSON, E. G.; EDFORS, O.; TUFVESSON, F.; MARZETTA, T. L. Massive MIMO for next generation wireless systems. **IEEE Communications Magazine**, IEEE, v. 52, n. 2, p. 186–195, 2014.

LEHMEYER, B.; IVRLAČ, M. T.; NOSSEK, J. A. Lna characterization methodologies. **International Journal of Circuit Theory and Applications**, Wiley Online Library, v. 45, n. 9, p. 1185–1202, 2017.

MARZETTA, T. L. Noncooperative cellular wireless with unlimited numbers of base station antennas. **IEEE Transactions on Wireless Communications**, IEEE, v. 9, n. 11, p. 3590–3600, 2010.

NIE, D.; HOCHWALD, B.; STAUFFER, E. Electromagnetic decoupling and complexity. In: IEEE. **2014 Information Theory and Applications Workshop (ITA)**. [S.l.], 2014. p. 1–6.

NYQUIST, H. Thermal agitation of electric charge in conductors. **Physical review**, APS, v. 32, n. 1, p. 110, 1928.

ROTHE, H.; DAHLKE, W. Theory of noisy fourpoles. **Proceedings of the IRE**, IEEE, v. 44, n. 6, p. 811–818, 1956.

RUSEK, F.; PERSSON, D.; LAU, B. K.; LARSSON, E. G.; MARZETTA, T. L.; TUFVESSON, F. Scaling up MIMO: Opportunities and challenges with very large arrays. **IEEE Signal Processing Magazine**, Institute of Electrical and Electronics Engineers (IEEE), v. 30, n. 1, p. 40–60, Jan 2013. ISSN 1053-5888. Disponível em: <http://dx.doi.org/10.1109/MSP.2011.2178495>.

RUSSER, P. Antennas. In: ____. **Electromagnetics, microwave circuit and antenna design for communications engineering**. 2. ed. [S.l.]: Artech House, 2006. cap. 13.

SCHELKUNOFF, S. A.; FRIIS, H. T. Impedance of dipole antennas. In: ____. **Antennas: theory and practice**. [S.l.]: Wiley New York, 1952. v. 639, cap. 13, p. 403–412.

TELATAR, E. Capacity of multi-antenna gaussian channels. **European Transactions on Telecommunications**, Wiley Online Library, v. 10, n. 6, p. 585–595, 1999.

VASCONCELOS, T. A. de; ALMEIDA, A. L. F. de; NOSSEK, J. A. Matching strategies for multiantenna arrays. In: **Proc. 24th Int. ITG Workshop Smart Antennas (WSA)**. Hamburg, Germany: [s.n.], 2020.

WALLACE, J. W.; JENSEN, M. A. Mutual coupling in mimo wireless systems: A rigorous network theory analysis. **IEEE transactions on wireless communications**, IEEE, v. 3, n. 4, p. 1317–1325, 2004.

WARNICK, K. F.; JENSEN, M. A. Optimal noise matching for mutually coupled arrays. **IEEE transactions on antennas and propagation**, IEEE, v. 55, n. 6, p. 1726–1731, 2007.

WASYLKIWSKYJ, W.; KAHN, W. K. Scattering properties and mutual coupling of antennas with prescribed radiation pattern. **IEEE Transactions on Antennas and Propagation**, v. 18, n. 6, p. 741–752, 1970.

WASYLKIWSKYJ, W.; KAHN, W. K. Theory of mutual coupling among minimum-scattering antennas. **IEEE Transactions on Antennas and Propagation**, IEEE, v. 18, n. 2, p. 204–216, 1970.